
Hepatectomy-induced alterations in hepatic perfusion and function - Towards multi-scale modeling for a better risk assessment in liver surgery

Bruno Christ^{1,*†}, Maximilian Collatz^{2,3,4}, Uta Dahmen^{5,†}, Karl-Heinz Herrmann^{6,†}, Sebastian Höpfl⁷, Matthias König^{8,†}, Lena Lambers^{9,†}, Manja Marz^{2,†}, Daria Meyer², Nicole Radde^{7,†}, Jürgen R. Reichenbach^{6,†}, Tim Ricken^{9,†}, and Hans-Michael Tautenhahn^{5,10,†}

¹Cell Transplantation/Molecular Hepatology Lab, Department of Visceral, Transplant, Thoracic and Vascular Surgery, University of Leipzig Medical Center, Leipzig, Germany

²RNA Bioinformatics and High-Throughput Analysis, Faculty of Mathematics and Computer Science, Friedrich Schiller University Jena, Jena, Germany

³Optisch-Molekulare Diagnostik und Systemtechnologie, Leibniz Institute of Photonic Technology (IPHT), Jena, Germany

⁴InfectoGnostics Research Campus Jena, Jena, Germany

⁵Experimental Transplantation Surgery, Department of General, Visceral and Vascular Surgery, Jena University Hospital, Jena, Germany

⁶Medical Physics Group, Institute of Diagnostic and Interventional Radiology, Jena University Hospital, Jena, Germany

⁷Institute for Systems Theory and Automatic Control, Faculty of Engineering Design, Production Engineering and Automotive Engineering, University of Stuttgart, Stuttgart, Germany

⁸Systems Medicine of the Liver Lab, Institute for Theoretical Biology, Humboldt-University Berlin, Berlin, Germany

⁹Institute of Mechanics, Structural Analysis and Dynamics, Faculty of Aerospace Engineering and Geodesy, University of Stuttgart, Stuttgart, Germany

¹⁰Department of General, Visceral and Vascular Surgery, Jena University Hospital, Jena, Germany

† These authors have contributed equally to this work and share first authorship.

word count: 11500

number of figures: 6

Correspondence*:

Prof. Dr. rer nat. Bruno Christ
Bruno.Christ@medizin.uni-leipzig.de

2 ABSTRACT

3 Liver resection causes marked perfusion alterations in the liver remnant both on the organ scale
4 (vascular anatomy) and on the microscale (sinusoidal blood flow on tissue level). These changes
5 in perfusion affect hepatic functions via direct alterations in blood supply and drainage, followed
6 by indirect changes of biomechanical tissue properties and cellular function.

7 Changes in blood flow impose compression, tension and shear forces on the liver tissue. These
8 forces are perceived by mechanosensors on parenchymal and non-parenchymal cells of the liver
9 and regulate cell-cell and cell-matrix interactions as well as cellular signaling and metabolism.
10 These interactions are key players in tissue growth and remodeling, a prerequisite to restore tissue
11 function after partial hepatectomy. Their dysregulation is associated with metabolic impairment
12 of the liver eventually leading to liver failure, a serious post-hepatectomy complication with high
13 morbidity and mortality. Though certain links are known, the overall functional change after liver
14 surgery is not understood due to complex feedback loops, non-linearities, spatial heterogeneities
15 and different time-scales of events.

16 Computational modeling is a unique approach to gain a better understanding of complex
17 biomedical systems. This approach allows (i) integration of heterogeneous data and knowledge
18 on multiple scales into a consistent view of how perfusion relates to hepatic function; (ii) testing
19 and generating hypotheses based on predictive models, which must be validated experimentally
20 and clinically. In the long term, computational modeling will (iii) support surgical planning by
21 predicting surgery-induced perfusion perturbations and their functional (metabolic) consequences;
22 and thereby (iv) allow minimizing surgical risks for the individual patient.

23 Here, we review the alterations of hepatic perfusion, biomechanical properties and function
24 associated with hepatectomy. Specifically, we provide an overview over the clinical problem,
25 preoperative diagnostics, functional imaging approaches, experimental approaches in animal
26 models, mechanoperception in the liver and impact on cellular metabolism, omics approaches
27 with a focus on transcriptomics, data integration and uncertainty analysis, and computational
28 modeling on multiple scales.

29 Finally, we provide a perspective on how multi-scale computational models, which couple
30 perfusion changes to hepatic function, could become part of clinical workflows to predict and
31 optimize patient outcome after complex liver surgery.

32 **Keywords:** liver surgery, perfusion, hepatic function, multi-scale modeling, regeneration

1 INTRODUCTION

33 Liver resection, i.e., removal of part of the liver, is the most important procedure in liver surgery. In Germany,
34 more than 20,000 liver resections are performed annually (Filmann et al., 2019). Due to demographic
35 changes, the incidence of primary and secondary liver tumors increases as patient's age. In parallel, the risk
36 of liver surgery increases due to age-associated preexisting liver disease and other comorbidities that affect
37 blood flow to the liver, such as cardiovascular disease.

38 Extended liver resection remains a high risk procedure, as potential postoperative hepatic dysfunction
39 and eventual liver failure can lead to patient morbidity and even mortality. Removal of large parts of the
40 liver not only poses a high regenerative challenge but also imposes a high metabolic load on the liver
41 remnant (Ray et al., 2018). First, the loss of liver mass impairs the function of the remnant liver through
42 portal hypertension (increase of pressure in the portal venous system) and hyperperfusion (increased
43 perfusion). Both are unavoidable consequences of removing not only hepatic parenchyma but also the
44 vascular bed. Second, extended liver resection compromises hepatic perfusion because of the mismatch
45 between the two supplying portal veins and three draining hepatic veins. Transection of hepatic parenchyma
46 inevitably leads to an impairment of either supply or drainage in the corresponding hepatic region. In
47 addition, the surgical procedure itself carries functional risks (e.g. ischemia-reperfusion injury).

48 Current preoperative diagnostics allows a detailed anatomical and functional assessment of the liver. As part
49 of the clinical routine, the location of the tumor to be resected is visualized in the context of the patient's
50 vascular anatomy. In case of extended resection, hepatic hemodynamics, consisting of measurement of
51 portal venous flow and pressure is assessed additionally. Furthermore, selected metabolic functions of the
52 liver indicative of the overall function of the liver (e.g. LiMAX or indocyanine green (ICG) clearance) are
53 usually quantified.

54 However, current preoperative diagnostics have distinct limitations. Despite high-quality imaging, precise
55 determination of hepatic hemodynamics and sophisticated functional assays, the spatial resolution of
56 specific hepatic functions is still rather low. Although it is known that liver perfusion and function are
57 closely related (Takahashi et al., 2014), it is currently not possible to quantify this relationship, neither for
58 the whole liver nor for a defined liver lobe.

59 Changes in blood flow affect transport to and from regions of the liver (macroscale), in turn changing
60 gradients of oxygen and nutrients in the lobulus and sinusoid (micro-scale), and thus directly impacting
61 metabolic functions. Furthermore, changes in blood flow impose traction, tension and shear forces on
62 liver tissue. Metabolic consequences of those mechanical forces cannot yet be determined, because the
63 molecular links between perfusion and function are unknown. Although perfusion changes are likely sensed
64 via mechanosensors that transmit mechanical forces into the cell, the link to hepatic metabolism is largely
65 elusive.

66 The liver is the only parenchymal organ capable of near complete regeneration in response to tissue loss.
67 Loss of liver mass by liver resection initiates liver regeneration and tissue remodeling, both necessary
68 to restore tissue homeostasis and volume. Although the physiology and molecular mechanisms involved
69 in liver regeneration have been studied for many years, prediction of the course and outcome of liver
70 regeneration for individual patients is still not possible.

71 The perfusion-associated mechanical forces are crucial for tissue regeneration and remodeling. Both,
72 regeneration and remodeling, are ultimate prerequisites for restoring tissue homeostasis after partial
73 hepatectomy. The molecular basis of functional changes after liver surgery is not well understood because

74 of complex feedback loops, non-linearities, spatial heterogeneities, and different time-scales of events. This
75 complexity requires novel approaches to relate surgically induced alterations in liver perfusion to hepatic
76 metabolic functions. A better understanding of perfusion-function relationships hence is needed to improve
77 preoperative diagnostic and risk assessment. This would allow us to identify patients who benefit most
78 from surgery and those at increased risk for complications.

79 Systems medicine using multi-scale computational modeling is a unique approach to gain a better
80 understanding of complex biomedical systems, such as the perfusion-function relationship after
81 hepatectomy.

82 To improve patient-specific risk assessment in the context of liver surgery, computational modeling aims to
83 (i) integrate heterogeneous data and knowledge at multiple scales about how perfusion connects to hepatic
84 function, (ii) generate hypotheses based on integrated models (which need to be validated experimentally
85 and related to clinical data), (iii) support surgical planning by predicting surgically induced perfusion
86 perturbations and their functional (metabolic) consequences, and (iv) minimize surgical risk for the patient.

87 In this review, we will delineate the relationships between alterations in hepatic perfusion and their
88 consequences for hepatic functions in the context of liver surgery, using hepatectomy as an example. First,
89 we provide an overview of the current knowledge and available tools in clinical and experimental settings.
90 Second, we will discuss how computational models and systems medicine approaches can contribute to a
91 better understanding of the complex perfusion-function interactions. We end with a perspective on how
92 such a systems medicine approach based on multiscale predictive models can be incorporated into the
93 clinical decision-making process.

2 CLINICAL AND EXPERIMENTAL PART

94 2.1 Clinical problem

95 The term liver resection does not refer to a single surgical procedure, but comprises a wide spectrum of
96 procedures that differ in their respective surgical strategy and technique. Two key surgical strategies are
97 currently in use: Conventional (single-stage) hepatectomies and, for critical extended liver resections,
98 multiple two-stage procedures.

99 Conventional liver resections involve the removal of one or more anatomically defined liver segments,
100 defined as the hepatic territory supplied by the corresponding portal venous branch. Removal of liver
101 segments requires transection of the hepatic parenchyma. Surgical techniques have been developed to
102 minimize the tissue and vascular damage associated with transection in order to preserve the viability and
103 perfusion of the adjacent liver tissue.

104 Two-stage hepatectomy is performed when the volume and expected function of the future liver remnant is
105 considered too small to maintain vital metabolic functions for the patient. In the first step, the portal vein
106 branches of the tumor-bearing liver lobe are occluded. Occlusion causes atrophy of the corresponding liver
107 lobe. To compensate for this reduction in functional liver tissue, the volume of the non-ligated liver lobule
108 increases substantially. Once compensatory hypertrophy of the future remnant liver is deemed sufficient to
109 maintain the life-saving functions, the atrophied tumor bearing lobe is resected during the second step.

110 However, frequently the liver does not regenerate sufficiently because preexisting liver conditions such
111 as steatosis, fibrosis or cholestasis impair the course of regeneration. Furthermore, simple portal vein
112 occlusion without parenchymal transection often leads to a compensatory flow redistribution via existing
113 porto-portal shunts, which reduces the efficacy of this strategy (Deal et al., 2018).

114 To prevent collateral formation, a novel procedure called associating liver partition and portal vein ligation
115 for staged hepatectomy (ALPPS) has been developed (Schnitzbauer et al., 2012). Here, portal vein occlusion
116 is combined with transection of the hepatic parenchyma in the first step, followed by removal of the already
117 mobilized and transected portally deprived liver lobe in the second step. However, in two-stage hepatectomy,
118 the patient must undergo two major operations within a short time period of 7 to 10 days. Therefore, the
119 indication for this complex procedure is taken with even greater caution.

120 2.2 Preoperative diagnostics

121 Currently, there is no generally accepted standard for preoperative diagnostics prior to partial liver resection
122 regarding liver anatomy, technical operability, liver volume and function.

123 2.2.1 Liver anatomy, technical aspects and volume assessment

124 The minimum requirements are defined in national guidelines. For Germany, the S3 guideline recommends
125 ultrasound of the liver and multiphase contrast-enhanced computed tomography (CT) to assess technical
126 operability and to evaluate the expected remnant liver volume and overall parenchymal quality. If there
127 is doubt about the technical operability, more detailed imaging such as additional magnetic resonance
128 imaging (MRI) with liver-specific contrast agent (Wang et al., 2021a; Geisel et al., 2017; Barth et al., 2016)
129 is recommended. However, all contrast-enhanced techniques (CT, MRI and ultrasound (US)) represent
130 volume-based procedures and are limited in their predictive power of postoperative organ function.

131 2.2.2 Liver function assessment

132 In daily clinical routine, most centers rely on standard laboratory parameters covering different aspects
133 of hepatic function to assess overall liver function. Liver enzyme release is taken as an indicator of
134 hepatocellular injury, bilirubin as a marker of excretory function, and serum cholinesterase (cHE), albumin
135 and clotting factors as parameters of hepatic protein synthesis. However, this approach has some pitfalls.
136 Although these parameters indicate the condition and main functions of the liver (injury, detoxification,
137 protein synthesis), none of them is considered a reliable marker to quantify either functional hepatic reserve
138 or liver dysfunction in critically ill patients (Nista et al., 2004; Bonfrate et al., 2015). Furthermore, these
139 parameters provide only a static snapshot of liver function.

140 Currently, additional liver function tests are used in selected hepatobiliary centers prior to complex
141 resections: global liver function assays such as ICG-clearance and the LiMAX-Assay as well as spatially
142 resolved imaging technologies such as scintigraphy with radiolabeled tracers (e.g. mebrofenin-scintigraphy)
143 and contrast-enhanced MRI. All four provide more detailed insight into liver function (metabolism and/or
144 excretion) by reflecting the dynamic elimination of the test substance from the body.

145 ICG based liver function testing such as Indocyanine green plasma disappearance rate (ICG-PDR) and
146 ICG-R15 is an established clinical tool for the assessment of liver function and perfusion. It is the most
147 commonly used dynamic liver function test performed at bedside. After intravenous injection, ICG is
148 selectively taken up by hepatocytes and excreted into bile. The test is performed using transcutaneous
149 pulse-densitometry, a non-invasive fingertip method, and provides results within 6–8 min. ICG kinetics can
150 be a reliable indicator in the context of liver surgery. ICG-clearance successfully predicted postoperative
151 mortality in cirrhotic patients undergoing hepatic resection unlike other parameters (Hemming et al.,
152 1992) and is a very good prognostic marker for liver failure after hepatectomy (Nonami et al., 1999).
153 Preoperatively impaired ICG results are significantly associated with postoperative liver dysfunction and
154 may predict poor outcome on postoperative day 1 (Haegele et al., 2016).

155 The LiMAX test is based on the indirect determination of cytochrome P450 (CYP) 1A2 activity in
156 hepatocytes. After i.v. injection of ^{13}C -methacetin, the CYP1A2 system metabolizes the substance into
157 paracetamol and $^{13}\text{CO}_2$. Using the spectral laser technique, the ratio of $^{13}\text{CO}_2/^{12}\text{CO}_2$ can be determined
158 via a breath test. The kinetics of $^{13}\text{CO}_2$ appearance in the expired air thereby indicates the relative liver
159 function (Rubin et al., 2017). The LiMAX test has been applied to predict postoperative outcome after
160 hepatectomy (Stockmann et al., 2009). Post-hepatectomy liver failure and related mortality could be
161 reduced after implementation of a preoperative LiMAX-based patient selection algorithm (Jara et al.,
162 2015). Furthermore, LiMAX has been applied to follow restoration of functional capacity after partial
163 liver resection (Bednarsch et al., 2016; Lock et al., 2012). The prediction of future liver remnant function
164 via LiMAX highly correlated with future liver volume, and can thus be used to estimate postoperative
165 morbidity (Blüthner et al., 2020).

166 Scintigraphy-based imaging techniques exploit the specific properties of different tracers. Hepatobiliary
167 mebrofenin scintigraphy (HBS) allows determination of the specific hepatic extraction fraction
168 (HEF) (Gupta et al., 2018). For this purpose, technetium ($^{99\text{m}}\text{Tc}$) mebrofenin is applied intravenously
169 before liver scintigraphy is performed. Mebrofenin is transported into hepatocytes via specific transporter
170 proteins (OATP1B1 and OATP1B3) (Ghibellini et al., 2008) and excreted into the bile canaliculi by
171 multidrug resistance protein 2 (MDRP2) (Hendrikse et al., 2004). In liver areas with high HEF, a stronger
172 signal can be detected than in areas with low HEF. The advantage of this method compared to ICG and
173 LiMAX is the spatial resolution, albeit very coarse. Mebrofenin HBS has shown a strong correlation
174 with 15 min ICG clearance (Erdogan et al., 2004). Mebrofenin HBS has been applied to evaluate liver
175 function in hepatectomy (Dinant et al., 2007; de Graaf et al., 2010; Bennink et al., 2004) and showed a
176 strong correlation between preoperative remnant liver function and the actual 1-day post-hepatectomy
177 measurement (Bennink et al., 2004).

178 Other functional tracer-based imaging technologies used to quantify liver function include single-photon
179 emission-computed tomography (SPECT) and positron emission tomography (PET). SPECT is a nuclear
180 imaging scan that integrates CT and a radioactive tracer such as sulfur colloid. Uptake of the tracer by the
181 liver is an indicator of hepatic function. PET also estimates liver function based on the uptake and clearance
182 of different radioactive positron-emitting tracers (e.g., FDGal) (Keiding et al., 2018; Bak-Fredslund et al.,
183 2017) and has been applied to predict postoperative liver function (Cho et al., 2017).

184 MRI is a non-ionizing imaging technique routinely used to detect hepatic tumors (Liu et al., 2017). More
185 detailed analysis of the time course of the liver-specific contrast agent Gd-EOB-DTPA also allows to assess
186 liver function by imaging its spatially resolved uptake and excretion into the bile by the hepatocytes (Wang
187 et al., 2021a). Dynamic Gd-EOB-DTPA imaging has been applied to evaluate preoperative remnant liver
188 function and post-hepatectomy outcome (Wang et al., 2021b; Yoon et al., 2016; Araki et al., 2020; Kim
189 et al., 2018; Chuang et al., 2018; Itoh et al., 2017; Asenbaum et al., 2018).

190 2.3 Surrogate approaches to assess liver function

191 2.3.1 Assessment of liver stiffness

192 Liver diseases not only affect hepatic function, but also lead to morphological changes, which in turn
193 alter the mechanical properties of the tissue. Most diseases lead to increased stiffness of the tissue, e.g.,
194 liver fibrosis results in enhanced stiffness due to an increased extracellular matrix (ECM) (Wells, 2005;
195 Li et al., 2020b). Recently, hepatic elastography has gained attention, a medical imaging modality that
196 relies on sound waves or forced tissue vibrations to measure tissue elastic properties and stiffness. It can be

197 performed in combination with US or MRI. Correlations exist between liver elasticity and liver functional
198 reserve, as demonstrated with ICG (Sugiura et al., 2019) or LiMAX (Heucke et al., 2019).

199 Clinically, a variety of US elastography methods have been developed. Shear wave elastography (SWE)
200 and acoustic radiation force impulse (ARFI) are the dominant methods in clinics today, offering integration
201 with other advanced US imaging modalities (Ferraioli, 2019).

202 Alternatively, by using an external vibration generator, elastography can be performed with MRI. Current
203 literature generally attributes higher diagnostic performance and fewer technical failures to MRI compared
204 to US methods (Yin and Venkatesh, 2018). Magnetic resonance (MR) elastography also has great potential
205 to further develop new multiparametric methods to distinguish processes like inflammation, fibrosis, venous
206 congestion and portal hypertension (Frydrychowicz et al., 2017; Leung et al., 2018; Palaniyappan et al.,
207 2016; Roldán-Alzate et al., 2015; Yin et al., 2017). In the evaluation of non-alcoholic fatty liver disease
208 (NAFLD), MRI has the added advantage of providing an independent method for fat quantification (Zhang
209 et al., 2018). MR elastography has successfully been used to predict outcome after hepatectomy (Sato et al.,
210 2018; Lee et al., 2017) and regeneration capacity (Jang et al., 2017).

211 2.3.2 Quantification of intrahepatic fat

212 A clinically frequently observed pathological liver condition that affects liver perfusion, function, and
213 recovery is hepatic steatosis. Hepatic steatosis as assessed by routine preoperative MRI has been shown to
214 be an independent risk factor of severe postoperative complications after major liver resection (d'Assignies
215 et al., 2016).

216 While US, CT and MRI can be used to assess hepatic steatosis *in vivo*, proton-density fat fraction (PDFF)
217 determination with MRI is currently the most accurate imaging modality for quantification (Zhang et al.,
218 2018; Troelstra et al., 2021).

219 2.3.3 Assessment of hemodynamics and perfusion

220 Preoperative assessment of hemodynamics and perfusion relies mainly on noninvasive technologies,
221 whereas intraoperative assessment is also performed with direct invasive techniques. The two main
222 noninvasive technologies, US and MRI, can quantify blood flow in the major supplying and draining
223 vessels of the liver (Yzet et al., 2010; Chouhan et al., 2017). Doppler US typically provides localized,
224 dynamic flow measurements.

225 Similar to water-fat quantification, the evaluation and quantification of tissue perfusion with MRI has a
226 long history (Rinck et al., 1984; Rosen et al., 1990). Perfusion is defined here as blood delivery at the
227 capillary level. Over the years, two main perfusion MRI approaches have been developed. The first uses an
228 exogenous contrast agent (Jahng et al., 2014) and includes dynamic susceptibility contrast MRI (DSC-MRI)
229 and dynamic contrast-enhanced MRI (DCE-MRI) (Leporq et al., 2018; Weiss et al., 2019). DCE-MRI
230 techniques allows quantitative characterization of parenchymal and (lesion) microcirculatory changes (Thng
231 et al., 2010) and investigation of liver damage (Byk et al., 2016; Lu et al., 2017). The second group refers
232 to arterial spin-labeling (ASL) (Williams et al., 1992), which uses magnetically labeled blood itself as an
233 endogenous tracer and measures its tissue accumulation (Johnson et al., 2016), and, by applying different,
234 carefully placed labeling planes, arterial and portal perfusion can be assessed separately (Martirosian et al.,
235 2019).

236 Invasive assessment of hepatic hemodynamics involves direct measurement of portal and hepatic arterial
237 flow rates using the US Doppler technology. Determination of portal pressure requires placement of

238 a pressure sensor in the vessel of interest. Another valuable parameter is the hepatic vein pressure
239 gradient (HVPG) usually measured by inserting a balloon catheter into a branch of the hepatic vein via the
240 jugular vein. HVPG has been applied in the context of hepatectomy showing an association of outcome with
241 preoperative HVPG and a cutoff of HVPG < 10 mmHg was proposed (Boleslawski et al., 2012; Cucchetti
242 et al., 2016). While progress has been made in noninvasive assessment of portal hypertension (Gouya et al.,
243 2016) it remains a clinical challenge (Wan et al., 2021).

244 2.3.4 Assessment of tissue density by DWI

245 Diffusion weighted imaging (DWI) is an MRI technique, which is sensitive to the mobility of water
246 molecules in tissue and therefore can provide insight into local tissue changes. Sheng et al. demonstrated that
247 DWI can detect and distinguish microstructural tissue changes during ALPPS and portal vein ligation (PVL)
248 procedures (Sheng et al., 2018). DWI has been applied to assess hepatic ischemia and reperfusion injury (Lu
249 et al., 2017) and to predict survival after partial hepatectomy (Muhi et al., 2013).

250 In summary, the selection of a particular procedure for an individual patient is based on the results of the
251 extensive preoperative assessment. The diagnostic strategy in preoperative assessment is tailored to the
252 needs of the patient and follows the standards of the individual center. However, current approaches are
253 limited since they do not allow for detailed spatially resolved assessment of liver function.

254 2.4 Experimental approaches in animal models

255 2.4.1 Historical overview

256 A main limitation for clinical research is the availability of tissue-based data. Human liver tissues can be
257 obtained during surgical procedures and by liver biopsy. For ethical reasons, patients cannot be subjected
258 to repeated liver biopsies pre- and postoperatively. Therefore, animal experiments are important to better
259 understand the pathophysiological mechanisms and processes governing liver surgery and liver regeneration
260 (see Figure 1).

261 Experimental liver resection in small animals was first performed by Higgins (1931). Originally, 70%
262 of the liver mass was removed after mass ligation of the wide stump of the median and left lateral
263 lobe of the rodent liver, resulting in impaired hepatic outflow and congestion of the remnant liver. With
264 refinement of the surgical techniques (see Table 1), the parenchyma-preserving vessel-oriented technique
265 was established (Madrahimov et al., 2006). Avoidance of congestion and necrosis of the stumps allowed
266 survival of the rats even after extended 90% resection, which is lethal when using the mass ligation
267 technique. In contrast, additional ligation of portal vessel reduces the functional remnant liver mass and
268 prevents survival after 90% PHx.

269 A bit earlier, in 1920, the first experimental PVL was performed in rabbits by Rous and Larimore (1920).
270 Comparative studies revealed that the time course of liver regeneration after partial resection or PVL
271 followed different kinetics. After simple hepatectomy, hepatocyte proliferation peaks on day 1 in rats and
272 on day 2 in mice (see Table 1) and declines rapidly thereafter. Within a week, the original liver mass is
273 restored.

274 In both models, the regenerating liver lobes are hyperperfused. However, in case of PVL, the regenerative
275 need is initially much lower. Resection causes an immediate loss of function because a substantial amount
276 of liver tissue is removed. In contrast, PVL only compromises function, as the portally deprived lobe is still
277 perfused with arterial blood and thus can contribute to the overall liver function. Therefore, hepatocyte
278 proliferation after PVL in rats peaks later, on postoperative day 2, but lasts for several days García-Pérez

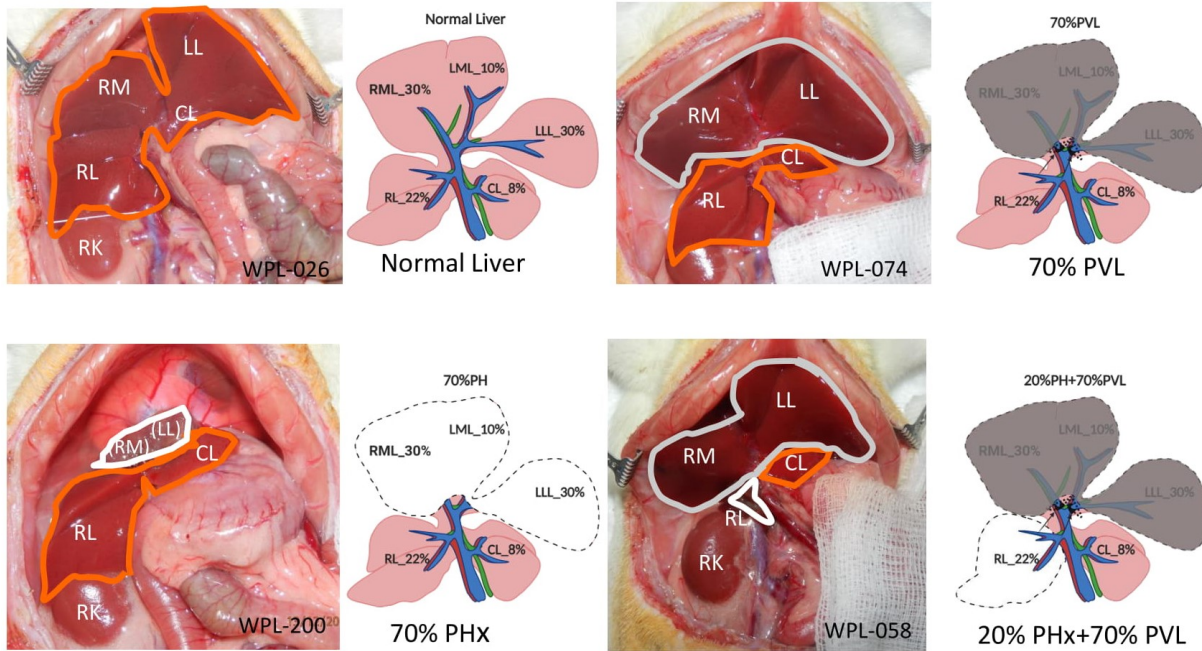


Figure 1. Surgical procedures. A: Open situs with liver (encircled in orange). B: 70% portal vein ligation. Note the slightly darker color of the ligated median and left lateral lobe (encircled in grey) compared to the fresh color of the right and upper caudate lobe (encircled in orange). C: 70% partial hepatectomy. Note the stump (encircled in white) above the right lobes (encircled in orange). D: Combined 20% partial hepatectomy with 70% portal vein ligation: Note the dark color of the portally ligated median and left lateral lobe (encircled in grey), the fresh red color of the upper caudate lobe (encircled in orange) and the stumps from the right lobes (encircled in white). LLL left lateral lobe, ML median lobe, RL right lobe, CL upper caudate lobe, RK right kidney, (LLL), (ML), (RL) stumps of the respective lobe.

279 et al. (2015); Rozga et al. (1986). Along with the development of hepatic atrophy, the regenerative need
280 increases, leading to a reduced but prolonged regenerative response (see Table 2).

281 Several combined procedures were introduced to better understand regulation of liver regeneration.
282 Sequential procedures include repeated hepatectomy and 2-stage PVL to elucidate the proliferative capacity
283 of the regenerating liver (Saito et al., 2006; Sugimoto et al., 2009). The impact of obstructive jaundice on
284 liver regeneration was studied by first performing bile duct ligation one week prior to liver resection (Li
285 2014). Different models of 2-stage hepatectomy (e.g. 70% PVL with (ALPPS) or without transection of the
286 median lobe followed by partial hepatectomy (PHx) of atrophied liver lobes) were developed to better assess
287 the impact of preventing collateral formation (García-Pérez et al., 2015; Wei et al., 2020). Here actually,
288 the development of animal model only happened after introducing the procedure into clinic (Schnitzbauer
289 et al., 2012).

290 However, liver resections and portal occlusions were also combined with other interventions to better
291 understand factors affecting hepatocyte proliferation and liver regeneration. This includes interventions
292 affecting hepatic perfusion such as right median hepatic vein ligation (Dirsch et al., 2008a; Huang et al.,
293 2014). For better understanding the impact of additional damage of the portally ligated lobe, bile duct
294 ligation was performed resulting in increased regeneration of the future remnant liver (FLR). A similar
295 effect on regeneration of the FLR was observed when inducing congestion of the portally ligated lobe
296 by performing an additional ligation of left lateral hepatic vein together with PVL. Combination of an
297 additional resection with PVL induced hepatocyte proliferation in the portally deprived liver lobe (Wei et al.,

298 2020). In conclusion, the wide spectrum of surgical models, which emerged over the years, is very useful
299 to investigate the different facets of liver regeneration and the underlying complex pathophysiological
300 mechanism, see Table 2.

301 **2.5 Regulatory molecular networks in regeneration**

302 In the past, animal models of liver resection were mainly used to study the molecular mechanism underlying
303 the course of liver regeneration (see Table 3). Many experimental studies focused on the exploration of
304 single molecular pathways governing central processes such as proliferation, inflammation, angiogenesis
305 (“vessel formation process”), and recently also autophagy (cell survival process) involved in regeneration by
306 classical interventional studies. Specific blocking and re-introducing of selected molecules was performed
307 to elucidate the relevance of the selected molecules for liver regeneration.

308 **2.6 Interaction between regeneration and metabolism**

309 Metabolic pathways regulating energy homeostasis are of key importance for regeneration. Their role was
310 investigated performing liver resection predominantly in knockout models, see Table 4. As an example,
311 lack of sirtuin and PPAR β reduced energy metabolism and inhibited regeneration (Liu et al., 2013,
312 2019). In contrast, lack of PTEN and aldolase reductase increased energy metabolism and induced liver
313 regeneration (Kachaylo et al., 2017; Li et al., 2020a).

314 **2.7 Hepatic hemodynamics and microcirculation**

315 Few studies were dedicated to exploring hepatic hemodynamics and microcirculation in small animals
316 subjected to different hepatobiliary procedures, as shown in Table 5. They are mainly of descriptive
317 nature. This might be partially due to the technical difficulty in assessing hepatic hemodynamics and
318 microcirculation in small animal models. Assessment of hepatic hemodynamics can be performed in
319 rats using standard equipment (fluid filled catheter and ultrasound flow probes). The same procedure
320 is also feasible in mice (Xie et al., 2016), but more challenging due to the small size. Both, portal
321 pressure and portal venous blood flow per liver weight in small animals are comparable to humans.
322 Resection respectively portal vein occlusion induce portal hypertension, hepatic hyperperfusion and in
323 humans also focal outflow obstruction. Some experimental studies focused on describing and modulating
324 resection-induced impairment of hepatic hemodynamics. Fewer studies aim for interfering by surgical or
325 pharmacological interventions (e.g. splenectomy, drug treatment). Good examples are the reports from
326 Huang (2014) and Arlt (2017) who both used a rat model of 70% PHx combined with right median hepatic
327 vein ligation. This combined procedure mimicks resection- associated focal outflow obstruction due to
328 transection of hepatic veins. The group around Dahmen explored the impact of several interventions (e.g.
329 application of vasoactive drugs like Molsidomine, L-NAME) on the formation of sinusoidal vascular canals
330 during the spontaneous recovery process from focal outflow obstruction (Arlt et al., 2017).

331 For assessment of hepatic microcirculation two different technologies are commonly used: intravital
332 microscopy using fluorescent labeled dyes and dark field microscopy. Intravital microscopy is frequently
333 performed in animal experiments. It allows the assessment of fluidic flow based on the injection of
334 fluorescent albumin, but also intravascular labeled blood cells labeled as well as the migration of blood
335 derived cells into the hepatic parenchyma. However, due to required injection of fluorescently labeled
336 molecules or cells, it is not applied clinically. Dark field microscopy does also allow the quantification of
337 blood flow velocity (Dahmen et al., 2007) and has occasionally been applied in clinical studies (Puhl et al.,
338 2003).

339 In summary, a multitude of experimental approaches was developed to investigate regulatory processes
340 in liver regeneration after partial hepatectomy. However, few studies were designed for a comprehensive
341 evaluation of the interplay between physical challenges, perfusion changes, their recognition by
342 mechanoperception and the impact on regeneration and metabolism.

343 2.8 Mechanoperception in the liver and impact on cellular metabolism

344 2.8.1 Hemodynamic changes after partial hepatectomy may trigger liver regeneration

345 Liver regeneration to restore tissue loss after surgical removal or toxic insult, is achieved by the proliferation
346 of both parenchymal and non-parenchymal cells of the liver. In case of loss due to PHx, proliferation of
347 hepatic cells is distributed all over the parenchyma and the factors initiating and perpetuating liver cell
348 proliferation during regeneration have been described (Michalopoulos, 2017). However, the primary trigger
349 sensing the parenchymal loss remains largely elusive.

350 Hepatectomy markedly changes blood flow in the remnant liver featuring, e.g., portal hypertension and
351 arterial hypoperfusion. Experimental evidence suggested that flow changes may regulate regeneration. As
352 an example, in pigs, the increase in total hepatic flow after partial hepatectomy preceded the increase in liver
353 regeneration. Changes in hepatic flow correlated with the degree of liver mass loss resulting in a 2-3-fold
354 increase in hepatic perfusion and a 10-30% increase in portal pressure, thus suggesting a quantitative
355 relationship (Kahn et al., 1984; Dahmen et al., 2007).

356 The surgery-induced increase in portal flow seems to be crucial for regeneration. Liver regeneration
357 was hampered in dogs when a portacaval shunt, reducing portal blood flow, was added to hepatectomy
358 (Mann et al., 1931). Patients with poor clinical outcome displayed a significant decrease of portal flow
359 during extensive hepatectomy suggesting that an adequate rise in portal flow is essential for hepatic
360 regeneration (Kawasaki et al., 1991). Similarly, post-hepatectomy outcome improved in patients featuring
361 higher portal flow postoperatively. Functional improvements like bilirubin levels and hepatic growth rate
362 correlated with mean portal flow velocity (Kin et al., 1994; Hou et al., 2018). In humans, portal blood
363 flow in the remnant portal branches after partial hepatectomy was distributed inhomogeneously as was the
364 distribution of hepatocyte proliferation, suggesting a causal relationship between heterogeneous distribution
365 of portal blood flow and regeneration (Iimuro et al., 2013).

366 Yet, there is some evidence against portal blood flow being the only regulator of liver regeneration. Minor
367 (10-30%) removal of liver mass results only in a marginal regenerative response, suggesting that a threshold
368 change in portal blood flow is needed to initiate an appropriate compensatory growth (Abshagen et al.,
369 2012a). Moreover, liver regeneration may occur even in the absence of portal flow. Despite ligation of
370 the portal branch, a moderate proliferative response was observed in the corresponding ligated liver lobe,
371 especially after an additional liver resection (Weinbren, 1955).

372 Although portal hyperperfusion might not be indispensable, the importance of flow-related mechanical
373 forces has been shown repeatedly. Mechanical inflictions induced by flow changes may play a major role
374 in both the initiation and the termination of liver regeneration (Song et al., 2017). This is corroborated
375 by the inverse quantitative correlations between the increase in portal blood flow and the remnant liver
376 volume, which is accompanied by the increase in hepatic shear stress stimulating liver mass restoration.
377 Likely, the increase of the blood flow-to-liver mass-ratio immediately after PHx and the resulting increased
378 intrahepatic shear stress stimulate and regulate liver regeneration (Nobuoka et al., 2006; Sato et al., 1999;
379 Schoen et al., 2001; Niiya et al., 1999). Conversely, reduction of shear stress in the liver by portacaval
380 shunts resulted in liver atrophy (Sato et al., 1997; Abshagen et al., 2012b).

381 2.8.2 Changes in haemodynamics may be sensed and trigger cellular responses

382 Changes in blood flow impose forces on the liver tissue. Since the hepatic sinusoids are likely the
383 first to sense changes in hepatic flow, the sinusoidal endothelium may play a major role in transducing
384 these forces (Shu et al., 2021). This is supported by the hierarchical topology of the hepatic sinusoids
385 involving cell-cell and cell-matrix interactions. Hepatocytes communicate directly with the sinusoids via
386 the ECM. The ECM is connecting the extraluminal side of endothelial cells and the sinusoidal face of
387 hepatocytes thereby bridging the space of Disse. Indirect communication connects cells in the space of
388 Disse like hepatic stellate cells (HSC) via the ECM to endothelial cells, and in turn hepatic stellate cells
389 to hepatocytes. Direct cell-cell contacts between adjacent hepatocytes maintain epithelial hepatocyte to
390 hepatocyte communication (Kang, 2020).

391 Cellular adhesion molecules, which transmit mechanical forces into cells, mediate cellular contacts to
392 the ECM or to neighbouring cells. In focal adhesion contacts, integrins connect cells and the ECM, and
393 serve as receptors for components of the ECM like fibronectin and collagens. Mechanical challenges
394 of the ECM induce conformational changes in the integrin chains, followed by integrin clustering and
395 intracellular activation of signaling pathways comprising the activation of, e.g., Focal adhesion kinase
396 (FAK), phospholipase C, and phosphoinositide 3-kinase (PI3K) and others (Alexius, 1991). Besides
397 transmission of mechanical forces imposed to the ECM, integrins transmit intrinsic properties of the
398 ECM to anchored cells. In the healthy liver, quiescent HSCs and sinusoidal endothelial cells create a
399 homeostatic ECM of relatively low stiffness in the space of Disse, which is necessary for hepatocyte
400 function linked to normal hepatocyte polarity (Musch, 2014). In the fibrotic liver, activated stellate cells
401 produce ECM featuring augmented stiffness impacting on hepatocyte polarity and function. Transforming
402 growth factor β (TGF- β), the major mediator of liver fibrosis, is activated by release from its latent
403 integrin-associated form, thus responding to any conformational change of the ECM, either triggered by
404 mechanical challenges or by changes of the ECM composition and stiffness (Hintermann and Christen,
405 2019).

406 Major cell adhesion molecules comprise E- and N-cadherin. In the rodent liver, E-cadherin is expressed in
407 periportal areas, while N-cadherin is expressed all over the parenchyma (see Figure 2). By homodimeric
408 binding of the extracellular domains of cadherins on adjacent cells, they form adherens junctions, which link
409 the junction complex to the cytoskeleton by connecting the intracellular domains of the cadherins via p120,
410 β -catenin and α -catenin to actin. Thus, physical forces as likewise induced by sinusoidal flow changes
411 impact on cellular behavior in respect to proliferation, differentiation and tissue homeostasis (Buckley et al.,
412 2014); kyoto encyclopedia of genes and genomes (KEGG) pathway entry: hsa04520. Further, changes of
413 mechanical forces outside of the cell are transmitted into the cell by the tight junction complex comprising
414 occludins, claudins and junctional adhesion molecules (JAM). These may couple to the actin filament
415 system via interactions with ZO. The tight junction complex may activate intracellular signaling pathways
416 via protein kinase C (PKC), PI3K and others impacting on cell polarity, differentiation, and paracellular
417 transport (Chiba et al., 2008); KEGG pathway entry: hsa04530].

418 Flow changes after liver surgery may thus be sensed and transmitted into the cellular interior and induce
419 responses like proliferation or cell migration. Only minimal information exists, whether flow-associated
420 metabolic changes might also involve mechano-transduction mechanisms. Yet, there is an obvious and
421 hence likely potential crosstalk between mechano-transduction and molecules involved in metabolic
422 regulation.

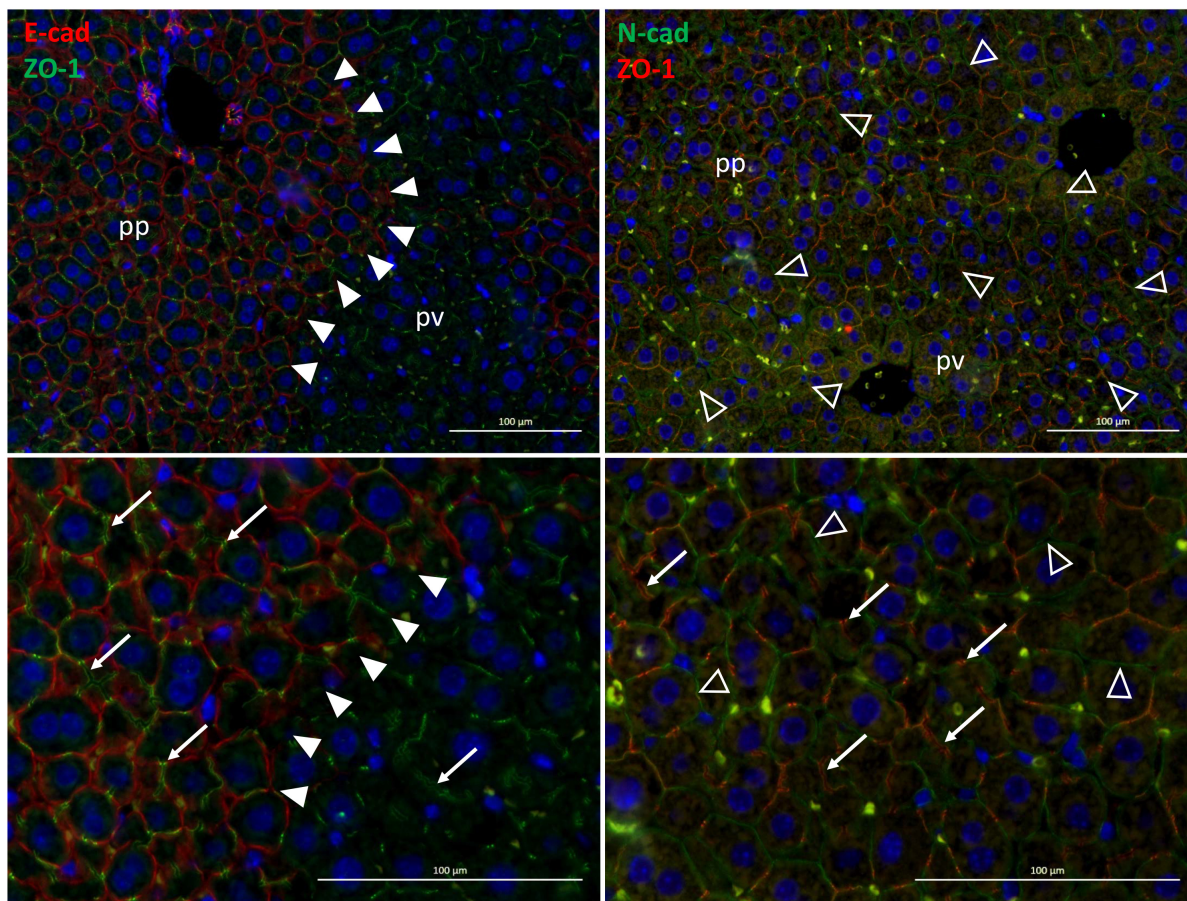


Figure 2. Zonal expression of E-cadherin (red, left panels) and of N-cadherin (green, right panels) in mouse liver sections. The exclusive periportal expression of E-cadherin demarcates the boundary between periportal and perivenous hepatocytes in the liver lobule (solid arrowheads). In contrast, N-cadherin is expressed all over the hepatic parenchyma (open arrowheads). Also, the tight junction protein zonula occludens protein (ZO)-1 (green, left panels; red, right panels) designating the bile canaliculi (white arrows) is expressed pan-parenchymally. Lower panels are digital magnifications of images shown in the upper panels. pp – periportal; pv – perivenous.

423 2.8.3 β -catenin mediates between adherens junctions and metabolic imprinting of perivenous
424 hepatocytes

425 β -catenin is part of the adherens junction complex and acts as an intracellular transducer of Wnt
426 (wingless/Int) signaling. It may be mobilized from the adhesion junction complex by tyrosine
427 phosphorylation in response to receptor activation by growth factors like hepatocyte growth factor (HGF),
428 epidermal growth factor (EGF) and TGF- β . Mobilization may lead to nuclear translocation of β -catenin,
429 activation of genes promoting mitogenesis and the dissociation of the adherens junctions complex required
430 for tissue morphogenesis during regeneration and development (Monga, 2014). Signaling through β -
431 catenin, however, plays also a major role in hepatocyte metabolic specification (Burke and Tosh, 2006;
432 Torre et al., 2011). In tumor cells, the high expression of aberrantly active forms of β -catenin coincided
433 with high glutamine synthetase (GS) expression, the key enzyme of ammonia fixation in perivenous
434 hepatocytes (Gebhardt et al., 2007). Providing further evidence, conditional disruption of β -catenin
435 expression in mice caused impairment of ammonia metabolism and perivenous expression of enzymes
436 of the CYP family (Sekine et al., 2006). Activation of Wnt/ β -catenin signaling by the glycogen synthase

437 kinase 3 beta (GSK3B) inhibitor SB-216763 or Wnt-conditioned media increased perivenous marker
438 protein expression in isolated hepatocytes (Hailfinger et al., 2006). Thus, β -catenin is involved in both
439 adhesion junctions and metabolic regulation predominantly in pericentral hepatocytes.

440 2.8.4 AMPK mediates between adherens junctions and lipid metabolism

441 The coordination of tissue homeostasis via adherens junctions and metabolic specification of hepatocytes
442 might be linked via AMP-activated protein kinase (AMPK) (Salvi and DeMali, 2018), a central regulator
443 of hepatic lipid metabolism. AMPK is activated through phosphorylation by the upstream kinase complex
444 called LKB1/STRAD-MO25 (liver kinase B1/STE20-related adapter protein-MO25). Activated AMPK
445 in turn inhibits fatty acid synthesis, lipogenesis and triglyceride synthesis while anti-lipogenic pathways
446 like fatty acid oxidation and ketogenesis are stimulated (Jansen et al., 2009; Mihaylova and Shaw, 2011).
447 In contrast, dephosphorylation and inactivation of AMPK stimulates fatty acid synthesis, lipogenesis
448 and triglyceride synthesis, which in turn causes steatosis in the chronic setting. Also cellular polarity
449 is regulated by E-cadherin via the LKB1 complex, thus creating a functional link between cell contact
450 maintenance and metabolic regulation of polarized cells such as hepatocytes. In line, the LKB1/STRAD
451 complex and AMPK localize to and thereby stabilize adherens junctions (Sebbagh et al., 2009).

452 2.8.5 YAP/TAZ signaling mediates tissue plasticity and metabolic regulation

453 Enhancement of matrix stiffness activates the YAP/TAZ pathway (Dupont et al., 2011). Changes in matrix
454 stiffness are sensed and transduced into the cell interior by the cell adhesion receptors as described above
455 and communicated to the actin cytoskeleton filaments. Actin reorganization releases cytoplasmic retention
456 of Yes-associated protein (YAP)/TAZ. This, in turn, promotes nuclear translocation and transcriptional
457 activation of target genes that are involved in processes of tissue growth like proliferation after injury,
458 embryonic development, and tumor growth in cancer (Pocaterra et al., 2020). Similarly, YAP/TAZ
459 relocation is mediated by substrate stiffness. While soft materials (~ 1 kPa) foster cytoplasmic localization,
460 stiff substrates (~ 40 kPa) force nuclear translocation (Halder et al., 2012; Dupont et al., 2011). In the liver,
461 hedgehog-dependent activation of the YAP pathway was necessary to sustain proliferation of hepatocytes
462 after partial hepatectomy in the mouse (Swiderska-Syn et al., 2016). The same mechanism also regulated
463 energy supply from glutamine during proliferation of activated HSCs. This was associated with epithelial-
464 mesenchymal transition after acute and chronic liver injury (Du et al., 2018; Choi et al., 2009; Chen et al.,
465 2019) indicating a functional relationship between regulation of tissue homeostasis, ECM mechanical
466 properties, and metabolic regulation.

467 Taken together, mechanical forces inflicted by changes in hepatic hemodynamics after e.g., PHx, seem
468 to play a prominent role in the regulation of tissue homeostasis and function during liver regeneration
469 spanning from the organ to the cellular scale.

470 2.9 Alterations in gene expression after hepatectomy

471 The state of a cell is mainly determined by its protein composition which is steadily changing due to protein
472 turnover, i.e., protein degradation and synthesis (Schoenheimer, 1942). An important method to gain
473 information about the cellular state is gene expression analysis. However, absolute quantification of gene
474 expression is difficult, therefore, mostly gene expression analysis aims for relative quantification when
475 comparing differences in transcription under various conditions (e.g., age, stress, disease, or surgery).

476 In the context of liver surgery, gene expression was mainly analyzed in tissue samples but recently more
477 and more single cell studies have become available. Even though most gene expression studies focus on

478 protein encoding transcripts, it has to be kept in mind that only a small fragment of the human genome is
 479 protein coding, and many non-protein coding RNA exist.

480 Gene expression studies may help to understand liver functions in general and liver regeneration after
 481 hepatectomy in particular. Recently, gene expression studies took advantage of microarray technology and
 482 RNA sequencing to generate novel insights into liver regeneration. Multiple studies exist that focus on
 483 differential gene expression after surgical interventions like PHx, PVL or ALPPS with the main model
 484 organisms being rat and mouse (see Table 6 for an overview).

485 2.9.1 Bioinformatical methods for differential transcriptome analysis

486 In general, the transcriptome is analyzed through RNA-Seq experiments. Figure 3 shows a state-of-the-art
 487 workflow. The raw reads, which are produced by sequencing the RNA extracted from the sample of interest
 488 can vary a lot in their quality. Thus, the first step during RNA-Seq analysis is quality control (Li et al.,
 489 2018a) and trimming, to remove sequencing remainders, e.g. sequencing adaptors. Next, the reads are
 490 mapped against the reference genome and post-processed (sorting, transforming to binary format). After
 491 counting the reads mapped per gene, the data are normalized to make the results comparable among
 492 the different replicates (Love et al., 2014). For differential expression, the normalized gene expression
 493 is compared between the different groups (e.g. PHx vs. sham). Thus, in the end a list of differentially
 494 expressed genes is returned, which can be used for further downstream analysis, like for example pathway
 495 analysis or modelling.

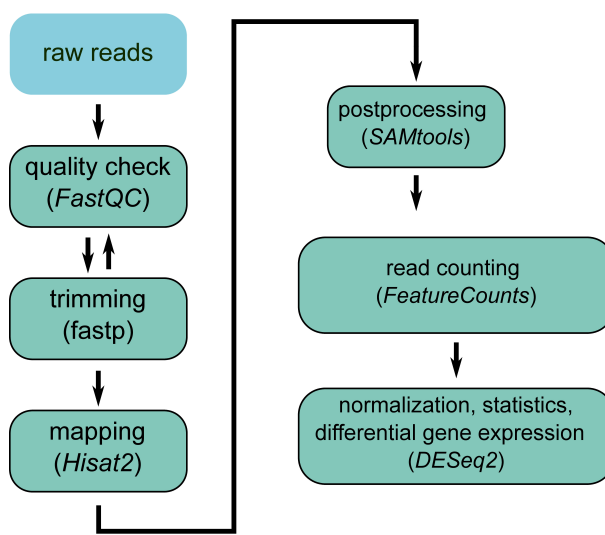


Figure 3. RNA seq analysis workflow.

496 Gene expression studies are helpful to identify signaling pathways mostly affected by a given procedure. A
 497 number of studies was performed focussing on PHx and confirmed the relevance of cell cycle associated
 498 genes in the process of liver regeneration (Colak et al., 2020; Borger et al., 2019). Pathway analyses
 499 or gene set enrichment analyses compare differentially expressed genes against pathway databases like
 500 KEGG (Kanehisa and Goto, 2000) or gene ontology (GO) (Ashburner et al., 2000), in which genes are
 501 assigned to different pathways. In this way, the enrichment of complete pathways can be inferred from
 502 a list of differentially expressed genes. Examples for liver-specific pathways in the KEGG database are
 503 for example hsa05225 (Hepatocellular carcinoma - Homo sapiens (human)), hsa04932 (on-alcoholic fatty

504 liver disease - Homo sapiens (human)) or more general ko04979 (Cholesterol metabolism) and ko01100
505 (metabolic pathways).

506 2.9.2 Differential pathways activated in different surgical regeneration models.

507 Comparative studies contribute to the molecular understanding of the different regeneration mechanisms
508 and kinetics observed in different resection models.

509 Colak et al. (Colak et al., 2020) investigated the differential gene expression patterns in rats subjected
510 to PHx, PVL and ALPPS. This study was based on RNA sequencing and provided a comprehensive
511 overview about transcriptomic changes. A similar study by Li in 2017 (Li et al., 2018a) revealed that
512 hypoxia pathways were activated in the ligated lobes undergoing atrophy. In contrast, cell proliferation and
513 cell-cycle pathways were activated in the non-ligated lobes undergoing regeneration. In 2004 Nagano et
514 al. (Nagano et al., 2004) investigated gene expression changes after PVL followed (four days later) by PHx,
515 in comparison to rats which were subjected only to PHx. The group with PVL showed a significantly higher
516 survival rate compared to the control group, which was associated with a more pronounced upregulation of
517 CCND1.

518 In 2019 Borger et al. (Borger et al., 2019) performed transcriptome profiling of two different mouse models
519 to identify pathways associated with liver regeneration. One group was subjected to an ALPPS, while in
520 the other group a PVL followed by transection was performed. After ALPPS the IGF1R signaling pathway,
521 the ILK pathway and the IL10 pathway were significantly enriched, whereas the Interferon pathway was
522 reduced. Furthermore the PAK- and ILK-associated intra cellular signaling pathways were activated at an
523 earlier time point compared to gene expression after 68% PHx only. These findings point to an accelerated
524 liver regeneration after ALPPS.

525 In 2011 Dupont (Dupont et al., 2011) already found that YAP expression changes occurred in response
526 to changes in tissue rigidity in liver cells. These changes are known to occur with age, but also after
527 hepatectomy. In 2015 Pibiri et al. (Pibiri et al., 2015) demonstrated strong changes in gene expression of
528 YAP when comparing normal and regenerating liver in young and old mice. Interestingly, YAP expression
529 was significantly upregulated when comparing young and old mouse livers, but not when comparing
530 quiescent and regenerating livers. In 2018 Pibiri (Pibiri, 2018) discussed the possibility to improve
531 the hepatic regenerative capacity in elderly through elimination of senescent cells via autophagy. This
532 hypothesis has yet to be confirmed.

533 2.9.3 Metabolism and Perfusion

534 Genome-wide expression analysis provides a good basis to identify differentially expressed pathways. The
535 impact of different surgical methods on gene expression and pathway activation, are well studied (see
536 Table 4). However, most of these studies analyze the regeneration after liver surgery in general, without
537 considering the underlying causes separately.

538 Perfusion, mechanosensing and mechanotransduction are important processes possibly affecting liver
539 regeneration and functional recovery (Song et al., 2017). Only a few studies exist that analyze the interplay
540 between these processes (Tchirikov et al., 2002; Nishii et al., 2018).

541 A comprehensive review about liver metabolism can be found (Rui, 2014). More specifically, multiple
542 genes related to metabolism are described to be induced in severe NAFLD. For genes being specifically
543 differentially expressed in the regeneration process after partial hepatectomy with and without partial portal
544 ligation, we refer to (Nobuoka et al., 2006). Notably, a minimal CYP reduction during liver regeneration
545 could be observed, with the conclusion that portal blood flow plays an important role in liver regeneration

546 and cell cycle gene expression. In another study, shear stress on murine liver progenitor cells could be
547 shown and was reflected by a significant upregulation of regeneration-associated genes, such as CFOS,
548 IP10, MKP1, ALB, WNT, VEGF, or EpCAM (Nishii et al., 2018).

549 2.9.4 Integration of omics data

550 In contrast to transcriptomics analysis, which is widely applied in the context of liver surgery, data on
551 changes in proteomics (e.g. (Guo et al., 2006a,b; Chen and Xu, 2014; Strey et al., 2005; Sun et al.,
552 2007; Kumar et al., 2013) and metabolomics (e.g. (Zhao et al., 2020; Jung et al., 2013; Samino et al.,
553 2013; Carril et al., 2020; Saito et al., 2018)) is more sparse. Almost all studies focus on a single omics
554 approach, while multi-omics seldom has been applied. An exception is the work by Caldez et al., who
555 used an integrated transcriptomic and metabolomic approach to study metabolic remodeling during liver
556 regeneration following hepatectomy (Caldez et al., 2018).

557 The information from omics studies can be used in combination with computational models to better
558 understand changes in signaling, metabolism and hepatic function. The general workflow for integration is
559 as following:

- 560 (i) Preprocessing and normalization of omics data. In this initial step data from different experimental
561 conditions and time points are made comparable (normalization of data), outliers are filtered and
562 quality control on the data is performed (e.g. removal of batch effects).
- 563 (ii) Quantification of differential changes. Most omics approaches provide reliable data for relative
564 changes between conditions, whereas absolute approaches are more complex (e.g. spike ins), often
565 challenging and rarely applied. The result of the analysis is a list of top molecular candidates based on
566 significance and/or fold change (e.g. a list of differentially expressed transcripts during regeneration
567 after hepatectomy).
- 568 (iii) Linking the experimental data to the model. This includes mapping of the experimentally determined
569 fold changes to model parameters and variables in the model. Transcriptomics data is often used as a
570 proxy for changes in protein amounts and mapped to the corresponding proteins in the model, whereas
571 proteomics and metabolomics data can be mapped more directly. Often a computational model for the
572 control condition is used as a baseline model, which is parametrized with the data to give multiple
573 model variants corresponding to the various experimental conditions.
- 574 (iv) Simulation under differential parametrization. The last step consists of performing simulations with
575 the baseline model and the different model variants and evaluating changes in model predictions.

576 Since omics data provides information on cellular components (RNA, proteins, metabolites), the
577 corresponding computational models reflect the cellular scale (see Section 3.2.1). A classical approach
578 is the parametrization of constraint-based metabolic models to generate tissue-specific or condition-
579 specific models. Examples in the context of liver metabolism are the stratification of patients with
580 hepatocellular carcinoma (HCC) based on acetate utilization (Björnson et al., 2015), a metabolic and
581 functional evaluation of NAFLD by integrating metabolic flux data and global transcriptomic data from
582 human liver biopsies (Hyötyläinen et al., 2016), or the study of metabolic pathways in NAFLD (Mardinoglu
583 et al., 2014). Metabolic network-based stratification has been used to reveal distinct tumor subtypes or
584 heterogenous redox responses in HCC using transcriptomics data (Bidkhori et al., 2018; Benfeitas et al.,
585 2019). Benefits of a carbohydrate-restricted diet on hepatic steatosis have been studied using a similar
586 multi-omics approach (Mardinoglu et al., 2018). A similar workflow is applied for kinetic pathway models,
587 for instance to study metabolic heterogeneity in HCC based on proteomics data (Berndt et al., 2021).

588 The same approach can be applied for spatially resolved data, e.g. using zonated omics. The data is hereby
589 mapped on sub-models corresponding to the respective spatial location (e.g. periportal or perivenous); An
590 example is the study of ammonia detoxification in the rodent liver (Bartl et al., 2015).

591 Whereas omics data has been measured in the context of liver surgery, the integration of these data
592 into computational models is still in its infancy. Time courses of the transcriptome in regeneration exist
593 (different conditions and different time courses), but have not yet been integrated into computational
594 models. Similarly, no approaches to predict hepatic functions after surgery-induced perfusion changes by
595 computational modeling are available so far.

3 DATA INTEGRATION AND COMPUTATIONAL MODELING

596 A vision of systems medicine in liver surgery is the development of an integrated modeling framework. This
597 framework should (i) incorporate state of the art knowledge regarding vascular anatomy, tissue architecture,
598 liver perfusion and their impact on key physiological processes, (ii) integrate clinical and experimental
599 data from all relevant measurement/assessment procedures on the different temporal and spatial scales, (iii)
600 enable to study the system in silico using model predictions, and (iv) allow for individual risk assessment.

601 Computational models can generally provide such a framework. The specific goal in the context of hepatic
602 surgery is to support pre-operative personalized diagnostic and risk assessment. This requires reliable
603 predictions of the remaining hepatic function after resection, the hepatic regeneration capacity and the
604 course of functional recovery after surgery. All three are influenced by perfusion alterations on different
605 scales and their corresponding impact on function. In this context, a consistent estimation of uncertainties
606 in model predictions is important to guide decisions regarding the surgical strategy (Saltelli et al., 2020).

607 To reach this ambitious goal, a concerted and iterative effort of clinicians, modelers, and experimenters
608 in a modeling-experiment cycle is required. Such a procedure usually starts with a first set of defined
609 experiments and a set of models. In the context of hepatic surgery, these are measurements obtained in cell
610 culture and animal experiments and from patients undergoing partial hepatectomy. Multidimensional data
611 include anatomical and morphological data such as hepatic volumetry and information regarding type and
612 severity of pre-existing disease (e.g. steatosis), liver perfusion, quantification of liver function (e.g., from
613 test compounds) and additional data such as omics, all obtained from multiple sources.

614 Based on existing modeling approaches, structure and granularity of the models have to be adapted to the
615 data and the question at hand. For example, assessing liver function on the organ level does not reflect the
616 heterogeneity of pathways in the liver parenchyma or even in individual hepatocytes, hence respective
617 models have to be coarse-grained in this respect. Likewise, liver regeneration is observed on a daily basis
618 only, assuming that the time course can be interpolated between measurements on different days. Omics
619 data is gathered from selected regions of interest (ROI), assuming these ROIs to be representative for
620 the organ. The integration of data into computational models in such an iterative cycle is generally a
621 challenging task, as is the uncertainty quantification.

622 In this section, we present specific challenges in modeling hepatic perfusion-function relations for better
623 risk assessment in the context of liver surgery (Section 3.1), followed by a review of relevant computational
624 models on the multiple scales (Section 3.2).

625 3.1 Data integration and uncertainty quantification

626 3.1.1 Lack of data integration standards

627 Currently, no standards for the integration of various data types and coupling of different spatial and
628 temporal scales exist. In the context of liver surgery, data comprise (i) imaging data on different spatial
629 scales such as CT and MRI reflecting the organ scale, and histology reflecting the lobular scale, (ii)
630 numerical data on hemodynamic information such as pressure and flow data as well as microcirculation
631 data, and (iii) numerical data regarding metabolism and proliferation reflecting organ and cellular scale (see
632 Sec. 2) and (iv) omics data representing the molecular scale in one defined region of interest. Altogether,
633 these data describe and quantify interlinked processes on the molecular, cellular, lobular and organ scale.

634 The calibration of models to experimental or clinical data requires a direct comparison between data and
635 model outputs beyond a pure qualitative agreement. The quantification of the quality of a fit in terms of
636 numerical values is necessary for a comparison of different model fits and allows to apply optimization
637 algorithms and methods for model comparison. In this procedure, appropriate data pre-processing steps
638 such as normalization, background correction, transformations, the elimination of outliers or the estimation
639 of summary statistics have to be conducted. In case of large datasets, for example omics or imaging data, in
640 addition machine learning approaches are used for feature selection and dimension reduction. Often, model
641 calibration is then formulated as an optimization problem, in which pre-processed data are incorporated as
642 numerical values. Such problems belong to the class of (non-linear) inverse problems, whose solutions
643 need efficient algorithmic schemes.

644 For example, a standard modeling approach for hepatic metabolic pathways such as the test compound
645 metabolism, or signaling pathways like YAP/TAZ induced pathways, are ordinary differential equations
646 based on chemical reaction kinetics. Time course data of key metabolites are used to estimate unknown
647 reaction rate constants. These data must be normalized and often contain information about fold changes
648 rather than absolute concentrations. This pre-processing step can be done in different ways (Degasperi et al.,
649 2014) and affects sensitivity analysis and summary statistics (Kirch et al., 2016; Thomaseseth and Radde,
650 2016). The objective function in the optimization problem can be the sum of squared differences (least-
651 squares estimate) or the likelihood function with an appropriate error model (Kreutz et al., 2007). Coupling
652 of metabolic models to models on larger scales like models of pressure and blood flow distributions in
653 liver lobules requires a definition of coupling parameters and, for model calibration, also model reduction
654 techniques.

655 Standards for the representation of pathway-based models have been established, with the systems biology
656 markup language (SBML) being the de facto standard (Keating et al., 2020; Hucka et al., 2019). Extensions
657 allow hierarchical model composition (comp package) (Smith et al., 2015), and representation of uncertainty
658 (distrib package) (Smith et al., 2020), an important requirement for multi-scale modeling approaches and
659 tracking model and data uncertainty. While mechanisms exist for the annotation of models and data with
660 meta-data (Neal et al., 2019), data-model integration standards and respective workflows are lacking, and
661 coupling of models in different mathematical frameworks is still challenging.

662 3.1.2 Sparse data setting and uncertainty quantification

663 Even if the structure of a model is defined, the data available for model calibration often does not
664 contain sufficient information to identify all model parameters uniquely. This already applies to models
665 on individual scales, such as intracellular metabolic pathways or pharmacokinetic models on the whole
666 body scale, due to a low time resolution in the measurements or because only a few model components

667 can be quantified. The problem becomes aggravated for larger and multi-scale models. Statistical methods
668 generally provide a solution to this problem. They allow for a consistent tracking of variability in input
669 data via uncertainty in model parameters to confidence bounds in model predictions. However, many of
670 those methods are computationally expensive and thus not ad hoc applicable to larger models, so that they
671 must be adjusted accordingly. Generally, uncertainty in model predictions is often underestimated, because
672 model assumptions are not questioned, the effect of unmodeled factors is neglected, or local sensitivity
673 methods are used also in cases where parameters and input variables are largely uncertain (Saltelli et al.,
674 2020). Since decisions based on model predictions, such as the selection of patients for surgery, are highly
675 dependent on uncertainties, it is important to develop methodology for the adaptation of statistical methods
676 for a consistent estimation of sensitivities and uncertainties for the specific problem at hand.

677 3.1.3 Computational costs

678 Coupled processes on different length- and time scales, as well as the need for spatial resolution to describe
679 spatial inhomogeneities in the liver, require multi-scale models. These models suffer from long forward
680 simulation times. Hence, standard methods for sensitivity analysis, uncertainty quantification, parameter
681 estimation or identifiability analysis are not ad hoc applicable for these models. For example, a single
682 forward simulation of a spatially-resolved liver lobule on a workstation with i7 processor of the 7th
683 generation, 4 cores and 8 threads needs 15 minutes for the simulation of a twelfth of a single lobule and
684 more than 900 minutes for a group of seven adjacent lobules. For a global sensitivity analysis, the number
685 of forward simulations that have to be conducted grows exponentially with the number of parameters,
686 resulting in a huge computational effort. Altogether, long forward simulation times of multi-scale models,
687 combined with difficult inverse problems for model calibration and the need for an uncertainty analysis
688 caused by sparse data, pose a great challenge towards an integrated framework supporting decisions in
689 liver surgery. On the modeling side, there is plenty of space to develop methodology that makes analysis
690 more efficient, such as model reduction techniques or the use of surrogate models to reduce simulation
691 times or efficient numerical schemes to solve optimization problems and quantify uncertainties in model
692 predictions.

693 3.1.4 Transfer of models calibrated with animal data to patients

694 A further challenge is the translation of models that have been calibrated with animal data to models
695 involving patient data. For example, computational models using hemodynamic measurements after
696 liver resections or PVLs as performed in rodents have to be adapted to the patient situation, taking into
697 account different anatomical features as well as parameters like age, gender, and pre-existing diseases. It is
698 known that animal studies are often poor direct predictors for human reactions to medical treatments or
699 exposures (Bracken, 2009; Perel et al., 2007). A modeling framework that is adapted to human parameters
700 might support this problem, but is challenging. Not only that one has to deal with different kinds of data for
701 humans and animals, human patients also show a much larger variability. Reasons for this are that hepatic
702 (dys)function, the metabolic state of the liver and function perfusion relations are subject to individual
703 lifestyle, environmental impact and nutritional habits. The effects of those factors can be controlled in
704 designed animal studies. Thus, building predictive models for patients subjected to liver surgery based
705 on models that have been fitted to animal data is a multi-layered problem. However, it is also known that
706 many physiological and mechanical parameters, such as lobulus architecture of the liver or perfusion, are
707 similar in humans and thus can be transferred (Kruepunga et al., 2019). For some parameters, such as
708 the regeneration course after resection, a transfer can be done by proper rescaling of the time scale, for
709 which comparison studies are available in the literature (Periwal et al., 2014). If a transfer of parameters is

710 not possible, models must be adapted to patients via the calibration of selected parameters to human data.
 711 Furthermore, models can be enriched by analysis methods applied to human data for extracting influential
 712 features on regeneration courses as well as risk analysis and their integration into models.

713 3.2 Computational modeling

714 Multi-scale computational models are a unique approach to gain a better understanding of liver surgery-
 715 induced alterations in hepatic perfusion, function and subsequently on regeneration. Relevant scales range
 716 from the whole-body down to the single cell (Figure 4). On the whole body scale, systemic circulation
 717 connects the liver to the rest of the body. On the organ scale the blood is distributed within the liver via a
 718 network of hepatic vessels (macroscopic perfusion), supplying the liver with oxygen-rich blood from the
 719 hepatic artery and nutrient-rich blood from the portal vein. The hexagonal liver lobules form the functional
 720 units of the liver, in which the blood is guided via sinusoids along the liver cells from the outer periportal
 721 region to the central perivenous region (microcirculation). The perivenous blood is subsequently drained via
 722 the hepatic veins from the liver to the inferior vena cava. Mechanotransduction, signaling and metabolism
 723 occur on the level of the hepatocytes, which are located along the blood vessels (sinusoids) of the liver
 724 lobules.

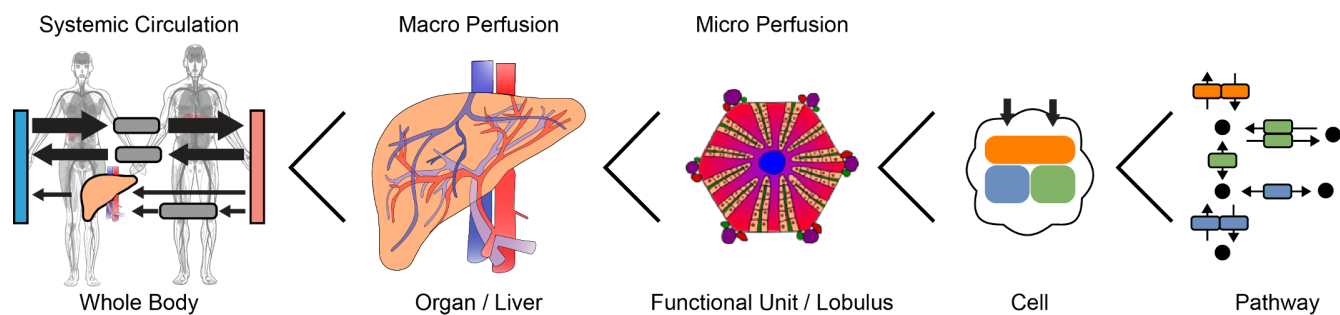


Figure 4. Multiple scales relevant for computational modeling of perfusion-function relationships. Anatomograms under CC-BY Papatheodorou et al. (2020).

725 Within this section we review relevant computational models to understand the effect of hepatectomy-
 726 induced alterations in perfusion on hepatic function on the cellular scale (Section 3.2.1), lobular scale
 727 (Section 3.2.2), organ and whole-body scale (Section 3.2.3).

728 3.2.1 Cellular scale

729 Computational models on the cellular scale can provide insights into the mechanism of how changes in
 730 tissue micro-perfusion and mechano-properties can alter hepatic function. Relevant processes include
 731 mechanotransduction, signaling, and metabolism (Figure 5) with selected computational models listed in
 732 Table 7.

733 Mechanotransduction is the process of sensing and translating changes in stiffness/elasticity and force
 734 into a cellular signal (see also section 2.8). Substantial knowledge exists on the biochemical and
 735 mechanical properties of the ECM (collagen, proteoglycans) and its interaction with the cytoskeleton
 736 (actin, intermediate filaments). Detailed computational models have been developed on these interactions
 737 (see (Elosegui-Artola et al., 2018) for a recent review). Less information and models exist on
 738 the mechanotransduction via integrins and cadherins. Examples range from a model coupling
 739 mechanotransduction to YAP/TAZ signaling (Peng et al., 2017), a model of how ECM mechanical

740 properties convert to biochemical signals via adhesion, and integrated intracellular signaling cascades
 741 associated with cytoskeleton dynamics (Sun et al., 2016) to a mathematical model of Hippo and TGF- β
 742 cross talk to YAP/TAZ signaling (Labibi et al., 2020).

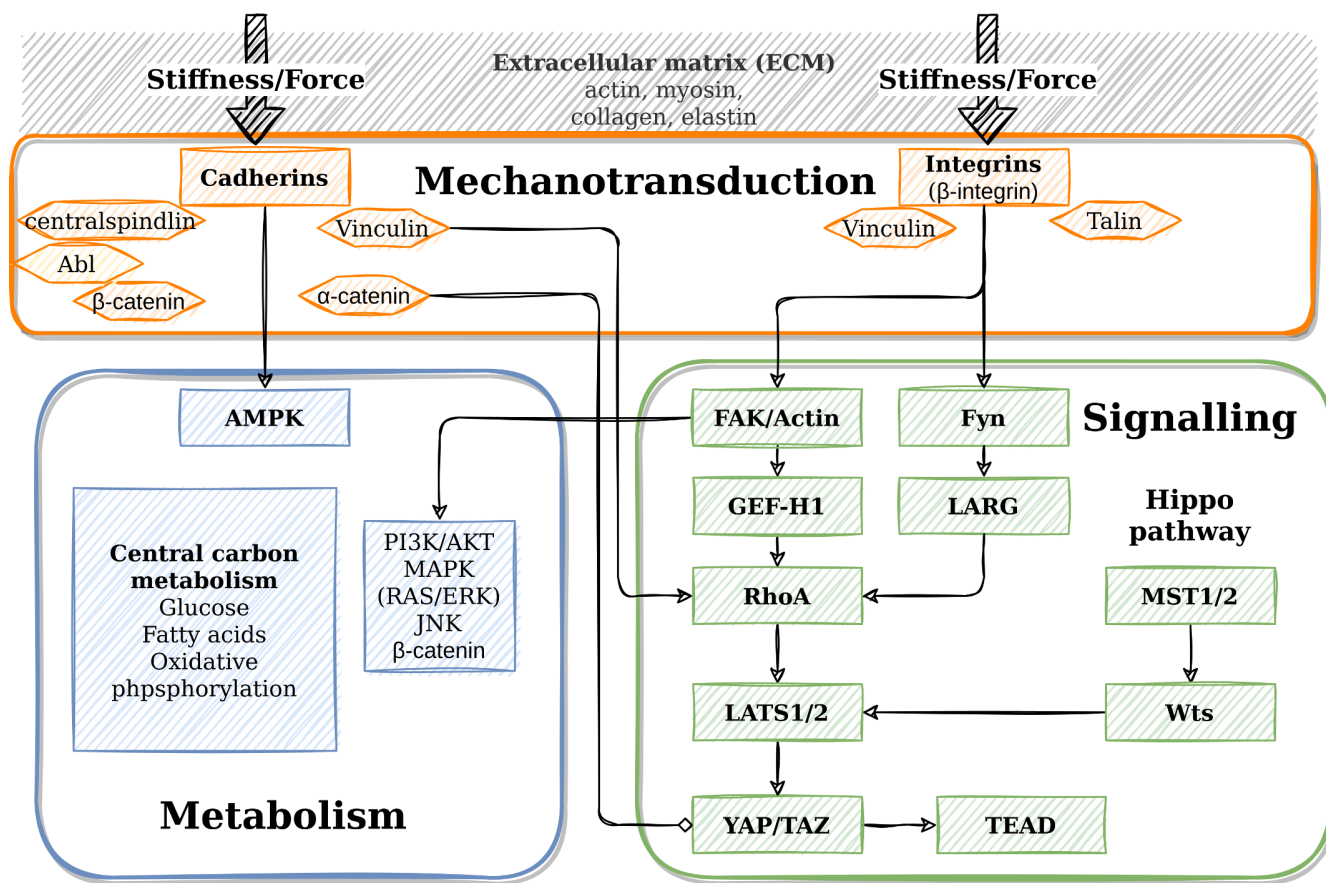


Figure 5. Cellular adaptations to changes in tissue perfusion and mechanical properties (mechanotransduction, signaling, metabolism). The extracellular matrix (collagen, proteoglycans) plays an important role in how changes in perfusion and pressure are translated to changes in stiffness and force. Changes in stiffness and force are sensed by cadherins and integrins (mechanotransduction), which transfer the information via signaling cascades. A main signaling route is the FAK to YAP/TAZ pathway, with important crosstalk from the Hippo pathway. Important signaling pathways regulating metabolism can be modified due to mechanotransduction, among them AMPK, PI3K/AKT, MAPK, JNK and β -catenin which regulate central metabolic functions. See 2.8 for details.

743 Signaling pathways translate the mechanical signals into cellular responses. Existing models
 744 representing mechanosensing and mechanotransduction mainly focus on the YAP/TAZ pathway, e.g.,
 745 YAP/TAZ mechanosensing (Sun et al., 2016) or the control of TGF- β /Smad nuclear accumulation by
 746 YAP/TAZ (Labibi et al., 2020). An important part of the YAP/TAZ signaling is shuttling of YAP/TAZ
 747 between nucleus and cytoplasm. Scott et al. modeled this nuclear translocation via a stiffness transfer
 748 function (Scott et al., 2020), Wehling et al. used 2D reaction diffusion equations (Wehling et al., 2021). In
 749 contrast, Aprupe et al. applied an ODE approach to model YAP/TAZ shuttling as a response to cell density,
 750 actin dynamics, and liver damaging drugs (Aprupe et al., 2020). Meyer et al. presented a mechanistic
 751 model predicting a switch-like activation of YAP upon mechanical stimulation during regeneration (Meyer
 752 et al., 2020). Gumberman et al. developed a boolean regulatory network model in epithelial cells that
 753 synthesizes mechanosensitive signaling, which links anchorage and matrix stiffness to proliferation and

754 migration including key signaling players such as YAP, PI3K, AKT, and mitogen-activated protein
755 kinase (MAPK) (Guberman et al., 2020). Hence, YAP/TAZ has been the focus of multiple modeling
756 approaches, but the linking and crosstalk to other signaling cascades is still in its infancy. One such example
757 is a model of cyclin-dependent kinases (CDKs) with phenomenological effect of ECM via FAK and cell
758 density (contact inhibition mediated via Hippo/YAP pathway) (Gérard and Goldbeter, 2014).

759 Metabolism encompasses the set of chemical reactions, with the liver being the metabolic hub of the body.
760 The activity of a key regulator of cell metabolism, the AMPK, has been shown to be mechanoresponsive,
761 and thus can bridge adhesion mechanotransduction and energy homeostasis (Isogai et al., 2017).

762 As a consequence, key hepatic pathways such as glucose metabolism, fatty acid metabolism, or oxidative
763 phosphorylation can be affected by changes in perfusion. Similarly, many of the pathways relevant for
764 evaluating liver function via test compounds, such as Cytochrome P450 detoxification (e.g. LiMAX
765 via CYP1A2) or transport and secretory activity (e.g. ICG) could be mechanosensitive and be affected
766 by perfusion changes following hepatectomy. Metabolic models of many of these pathways have been
767 established in recent years. Genome-scale models of hepatic metabolism using a constraint-based approach
768 exist (Gille et al., 2010; Mardinoglu et al., 2014) as do detailed kinetic models of central carbon
769 metabolism (Berndt et al., 2018) or glycolysis (König and Holzhütter, 2012; König et al., 2012). Small
770 metabolic pathway models are often included in lobular and organ scale models, e.g., acetaminophen
771 detoxification (Means and Ho, 2019; Sluka et al., 2016; Fu et al., 2018) or glucose metabolism (Ricken et al.,
772 2015). However, the link of metabolic pathway models to mechanotransduction and mechano-signaling
773 was only established rarely. One such example is a mechanobiological model to study the effect of shear
774 stress on urea and albumin synthesis (Nikmaneshi et al., 2020).

775 In summary, models for key signaling pathways involved in mechanotransduction as well as metabolic
776 models for pathways important for liver function, such as central carbon metabolism or detoxification
777 have been established. However, models integrating mechanosensing/mechanotransduction with these
778 signaling pathways and subsequent changes in hepatic metabolism are lacking so far. Furthermore, most of
779 the existing models on mechanotransduction and signaling are not liver-specific.

780 3.2.2 Lobular scale

781 In recent years, a wide range of computational models have been presented to simulate hepatic perfusion
782 on the liver lobule scale (Table 8). These models differ both in the selection of the method and in the
783 consideration of perfusion processes. An overview of computational models for hepatic processes can be
784 found in Christ et al. (Christ et al., 2017) or Ricken and Lambers (Ricken and Lambers, 2019). A common
785 method to describe hepatic microcirculation on the lobular scale is computational fluid dynamics (CFD).
786 Using this method, simulations of hemodynamics in a part of a lobule e.g. (Rani et al., 2006) or one
787 respective sinusoid e.g. (Ma et al., 2020) have been presented. The extension of the geometry to a
788 hexagonal shaped liver lobule e.g. (Debbaut et al., 2014) using CFD has provided insights into spatial
789 distribution of lobular perfusion and microcirculation.

790 The porous structure of the liver and the resulting effects are captured by porous media approaches. Various
791 models for the simulation of lobular perfusion (Antonov et al., 2017) after liver resection (Bonfiglio et al.,
792 2010) or in fibrotic and cirrhotic liver (Hu et al., 2017) were developed.

793 However, these models do not take into consideration hepatic function and its coupling with perfusion.
794 Several multiscale models combine processes on organ, lobular and cellular scale using physiologically

795 based pharmacokinetic (PBPK) equations (Sluka et al., 2016; Diaz Ochoa et al., 2012) or PDE-ODE
796 coupling (Ricken et al., 2015).

797 To mimic the behavior of hepatic processes on the lobular scale, a detailed knowledge about the organ
798 physiology as well as the sensitivity to changes in boundary conditions is required. A suitable simulation
799 of function-perfusion-coupling depends on material parameters as well as boundary conditions used as
800 initial values for the lobular model. Since the model quality is directly related to the quality of the available
801 data, a detailed observation of hepatic conditions and their measurements are necessary. Information on
802 liver geometry, heterogeneity of liver lobules, damage such as the degree of fatty tissue, hyperperfusion,
803 growth and remodeling (Ateshian and Ricken, 2010; Ricken and Bluhm, 2010; Ricken et al., 2007) and the
804 degree of resection must be determined in experiments or clinical procedures and then integrated into the
805 computational framework.

806 For example, computational modeling on the lobular scale requires information on tissue elasticity to
807 capture the poro-elastic behavior. Information on the mechanical behavior of liver tissue can be determined
808 e.g., by using indentation methods or multiparametric MR elastography. The elasticity modulus can be
809 obtained non-invasively via various methods described in Section 2.3.1. To capture the realistic geometry
810 of liver lobules with the respective inflow and outflow conditions, the geometry can be determined via
811 image segmentation from histological slices (Ahmadi-Badejani et al., 2020). Hepatic blood flow can
812 be measured using Doppler-US or functional MRI for macroscopic blood flow as well as orthogonal
813 polarization spectroscopy (OPS) for microcirculation (Ricken et al., 2010).

814 The development of a robust and efficient multiscale model must integrate data provided by cellular
815 models via appropriate coupling parameters. To reduce computational costs, model order reduction (MOR)
816 techniques (Armiti-Juber and Ricken, 2021) can be implemented. To get an initial intuition of the model
817 properties, surrogate models of parts of the simulation are compiled for a quick analysis of the component
818 behavior.

819 3.2.3 Organ and whole-body scale

820 Computational models on the whole-body scale can provide important information on the systemic
821 circulation and hepatic blood flow, as well as whole-body function. pharmacokinetic (PK) models can
822 provide an accurate description of total liver clearance or metabolism/function (Willmann et al., 2003).
823 An important class are PBPK models describing the whole body (Jones and Rowland-Yeo, 2013) (Figure 6).
824 PBPK models include the systemic circulation between organs and are therefore uniquely suited to evaluate
825 the effect of blood flow changes on hepatic function. PBPK models integrate information from multiple
826 sources, including drug-dependent, physiological, and biological parameters and their variation between
827 species, subjects, or with age and disease state. The biological and mechanistic bases of PBPK models
828 allow the extrapolation of kinetic behavior between species (Espié et al., 2009).

829 Various hepatic clearance models have been developed to integrate the factors of blood flow, binding,
830 transport and metabolism on whole-body scale to predict clearance of substances by the liver (Ho and Zhang,
831 2020). The simplest model is the well-stirred model, which describes the liver as a single compartment with
832 concentration of drug in the liver being in equilibrium with that in the emergent blood, and the concentration
833 of substances being identical throughout the liver (Rowland et al., 1973; Pang and Rowland, 1977).
834 Approaches to describe heterogeneity within the liver are the parallel tube model (Winkler et al., 1973),
835 the distributed-model (Bass et al., 1978), the series-compartment model (Gray and Tam, 1987), and the
836 variable transit-time or dispersion model with mixing between sinusoidal blood and hepatocytes (Goresky
837 et al., 1973).

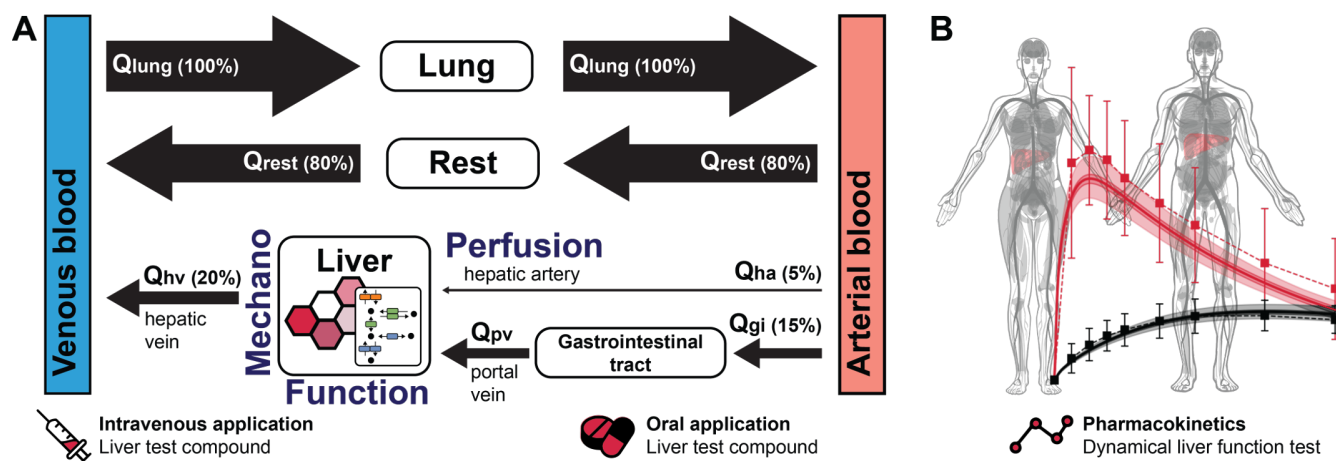


Figure 6. Physiological based pharmacokinetic (PBPK) model for liver function on the whole-body scale. (A) PBPK models include organs and the systemic circulation between these organs. The liver receives around 20% of the cardiac output as blood flow with one quarter coming from the hepatic artery and the remainder from the portal vein. Liver function depends on hepatic perfusion and metabolism as well as the mechanical tissue properties, which can influence hepatic function either directly via changes in blood flow or indirectly by changes in metabolism following mechanotransduction. In the example, all organs besides the liver and the lung have been pooled in the Rest compartment for simplification. Q_{lung} - blood flow lung, Q_{ha} - blood flow hepatic artery, Q_{gi} - blood flow gastrointestinal tract, Q_{pv} - portal vein blood flow, Q_{hv} - hepatic vein blood flow; Q_{rest} - blood flow rest of body. (B) The pharmacokinetics of liver test compounds as measured in dynamical liver function tests such as ICG elimination or LiMAX allows the evaluation of liver function on the whole body scale. Here, in red caffeine (test compound) and black paraxanthine (main product) in an example liver function test based on caffeine. PBPK models are uniquely suited to model these tests. Anatomograms under CC-BY Papatheodorou et al. (2020).

838 Whereas PBPK models are routinely applied to predict the detoxification of drugs under healthy and
 839 disease conditions (e.g. liver cirrhosis (Edginton and Willmann, 2008)), their application in the context of
 840 liver surgery and hepatectomy is still in its infancy (Table 9). The existing models account for the loss of
 841 liver volume in hepatectomy via reducing the liver volume in silico (Lu et al., 2006; Lagneau et al., 2005;
 842 Köller et al., 2021) and allow to simulate the effect of various resection rates on the pharmacokinetics
 843 (e.g. on liver function measured via ICG (Köller et al., 2021)). The model by Lagneau et al. considered
 844 changes in perfusion or hemodynamics due to liver surgery, i.e., intraoperative liver pedicular triad
 845 clamping, intraoperative blood loss and the associated changes in cardiac output in addition to the volume
 846 loss (Lagneau et al., 2005)).

847 Hemodynamics is included in PBPK models in the form of blood flows between compartments and tissues,
 848 but important information such as pressure, pressure gradients, or tissue resistance are lacking. In contrast,
 849 approaches simulating CFD allow to capture the postoperative hepatic hemodynamics in reconstructed
 850 vessel geometries in detail. CFD models have been applied to study the changes in hemodynamics following
 851 hepatectomy in humans (Ho et al., 2010; Ma et al., 2020; Lin et al., 2021; Ho et al., 2012). CFD approaches
 852 can be very computation intensive (Lin et al., 2021). Furthermore, the existing examples only cover the
 853 respective reconstructed vessel structures of the liver, without any information on the systemic circulation.
 854 Closed loop 0D models (a lumped parameter model of the entire circulation without any spatial dimensions)
 855 allow to model cardiac output and systemic circulation in detail (Shi et al., 2011). Depending on their
 856 resolution, the liver can either be modeled as a single unit or the structure of the lobes can be resolved.
 857 Closed loop 0D models can be efficiently solved and can reflect physiology and be applied to model surgical
 858 interventions. Such models have been applied to study the impact of partial hepatectomy on the hepatic

859 hemodynamics in rat (Debbaut et al., 2012), pig (Audebert et al., 2017) and human (Golse et al., 2021). 0D
860 models can easily be coupled with 1D, 2D or 3D models of vessels or tissues and contain information on
861 pressure and flows, both important requirements for multi-scale approaches. Systemic circulation has been
862 studied in detail with 0D models, but to our knowledge the coupling to PBPK models to describe clearance
863 of substances by the liver has not been performed so far.

864 An important step would be to couple models of hemodynamics (0D closed loop) and function (PBPK) on
865 a whole-body scale with spatially resolved 1D/2D/3D approaches on the sinusoid/lobule scale. Application
866 of such multi-scale models to dynamic liver function tests (such as ICG or LiMAX) could provide important
867 insights in how alterations in hepatic hemodynamics after hepatectomy affects liver function.

4 PERSPECTIVE

868 Within this review, we have delineated current knowledge on the relationships between alterations in hepatic
869 perfusion and their consequences for hepatic function in the context of liver surgery, using hepatectomy as
870 an example.

871 Computational models and systems medicine approaches can contribute to a better understanding of the
872 complex perfusion-function interactions after hepatectomy at all relevant spatial and temporal scales, from
873 the single cell to the complete liver, and from the immediate changes after surgery to long-term regeneration.
874 Multi-scale models provide a unique opportunity to integrate heterogeneous experimental and clinical data.
875 But despite a wide array of available tools in clinical and experimental settings, data generated with these
876 methods has not yet been systematically integrated with multi-scale computational models in the context of
877 liver surgery. Major challenges remain, such as lack of data integration standards, sparse data setting and
878 uncertainty quantification (Pivovarov et al., 2019), computational cost of multi-scale models, and transfer
879 of models calibrated with animal data to patients. Key requirements for success are tight cooperations
880 between animal, clinical, and modelling research in an iterative cycle. Especially important in this context
881 is the generation of animal data orthogonal to the patient data for model calibration, complemented with
882 data featuring sufficient overlap between animals and patients to allow for translation.

883 Current computational tools applied in the clinics are limited to the visualization of tumor localization in
884 respect to the individual vascular anatomy and the virtual planning of the resection plane. Virtual resection
885 allows to visualize and quantify the volume of the territories at risk. However, the current visualization
886 tools cannot determine the impact of impaired hepatic venous drainage on hepatic function. They do not
887 take into account the impact of surgery-induced perfusion perturbation on hepatic function after resection.
888 A key challenge is to develop multi-scale computational models for the liver function diagnostics applied
889 in liver surgery, such as the dynamical liver function tests based on ICG or LiMAX. At this moment, no
890 integrated scale spanning computational model exists, integrating functional aspects on the molecular and
891 cellular scale as well as hepatic perfusion on the lobular level resulting in a prediction of global function
892 on the organ level. Therefore predictions taking any spatial inhomogeneity into account are not possible.
893 Multidimensional modeling is needed to close the gap between the current possibilities to assess hepatic
894 perfusion, metabolism and regeneration and the need for reliable predictions for individual patients.

895 A systems medicine approach based on multiscale predictive models incorporated into the clinical decision
896 process could provide actionable information. In the context of liver surgery, utilizing these techniques will
897 improve prediction of the outcome after extended liver resection. This may help to prevent operations in
898 patients at risk and allow a personalized approach to advanced hepatic surgery. Based on the models and

899 the resulting predictions, individual pre-rehabilitation measures can be initiated to reduce perioperative
900 morbidity and mortality after extensive liver resections.
901 To be successful, two major gaps have to be filled: (i) the application of multi-scale models in the context
902 of liver surgery and (ii) accounting for the complex perfusion-mechano-function interactions on micro- and
903 macro-scale using such a systems medicine approach. Our long-term vision is an application, integrated in
904 the hospital information system, which allows an accurate estimate of liver regeneration and post-surgical
905 morbidity and mortality already when virtually planning the surgery.

5 LIST OF ABBREVIATIONS

906 ALPPS	associating liver partition and portal vein ligation for staged hepatectomy
907 AMPK	AMP-activated protein kinase
908 ARFI	acoustic radiation force impulse
909 ASL	arterial spin-labeling
910 CDK	cyclin-dependent kinase
911 CFD	computational fluid dynamics
912 cHE	cholinesterase
913 CT	computed tomography
914 CYP	cytochrome P450
915 DCE-MRI	dynamic contrast-enhanced MRI
916 DSC-MRI	dynamic susceptibility contrast MRI
917 DWI	diffusion weighted imaging
918 ECM	extracellular matrix
919 EGF	epidermal growth factor
920 FAK	Focal adhesion kinase
921 FLR	future remnant liver
922 FOO	focal outflow obstruction
923 GO	gene ontology
924 GS	glutamine synthetase
925 GSK3B	glycogen synthase kinase 3 beta
926 HBS	hepatobiliary mebrofenin scintigraphy
927 HCC	hepatocellular carcinoma
928 HEF	hepatic extraction fraction
929 HGF	hepatocyte growth factor
930 HSC	hepatic stellate cells
931 HVPG	hepatic vein pressure gradient
932 ICG	indocyanine green
933 ICG-PDR	indocyanine green plasma disappearance rate
934 JAM	junctional adhesion molecules
935 KEGG	kyoto encyclopedia of genes and genomes
936 MAPK	mitogen-activated protein kinase
937 MDRP2	multidrug resistance protein 2
938 MOR	model order reduction
939 MRI	magnetic resonance imaging
940 MR	magnetic resonance

941	NAFLD	non-alcoholic fatty liver disease
942	OPS	orthogonal polarization spectroscopy
943	PBPK	physiologically based pharmacokinetic
944	PDFF	proton-density fat fraction
945	PET	positron emission tomography
946	PHx	partial hepatectomy
947	PI3K	phosphoinositide 3-kinase
948	PKC	protein kinase C
949	PK	pharmacokinetic
950	PVL	portal vein ligation
951	ROI	regions of interest
952	SBML	systems biology markup language
953	SPECT	single-photon emission-computed tomography
954	SWE	shear wave elastography
955	TAZ	WW domain-containing transcription regulator protein 1
956	TGF-β	transforming growth factor β
957	US	ultrasound
958	YAP	Yes-associated protein
959	ZO	zonula occludens proteins

CONFLICT OF INTEREST STATEMENT

960 The authors declare that the research was conducted in the absence of any commercial or financial
961 relationships that could be construed as a potential conflict of interest.

AUTHOR CONTRIBUTIONS

962 BC, UD, KH, MK, LL, MM, NR, JR, TR, HT were involved in designing, writing and revising the
963 manuscript. MC, SH, DM wrote sections of the manuscript. All authors contributed to manuscript revision,
964 read, and approved the submitted version.

FUNDING

965 This work was supported by the German Research Foundation (DFG) within the Research Unit Programme
966 FOR 5151 "QuaLiPerF (Quantifying Liver Perfusion–Function Relationship in Complex Resection—A
967 Systems Medicine Approach)" by grant number 436883643.
968 Funded by Deutsche Forschungsgemeinschaft (DFG, German Research Foundation) under Germany's
969 Excellence Strategy – EXC 2075 – 390740016.
970 Funded by Deutsche Forschungsgemeinschaft (DFG, German Research Foundation) by grant number
971 312860381 (Priority Programme SPP 1886, Subproject 12)
972 MK is supported by the Federal Ministry of Education and Research (BMBF, Germany) within the research
973 network Systems Medicine of the Liver (LiSyM, grant number 031L0054).
974 BC and HMT are supported by the Deutsche Forschungsgemeinschaft (DFG, German Research Foundation)
975 in a joint research project (CH 109/25, TA 1583/1).

TABLES

Table 1. Overview of different liver resection techniques, differing in how the vascular structures (portal triad and hepatic vein) are ligated respectively transected.

Reference	Species	Incision	Extent of resection	Resected liver lobule	Ligation of portal triad	Ligation of hepatic vein
Liver resection						
Higgins (1931)	Mouse	Midline	70% PHx	LL, ML	Not done	Parenchymal mass ligation
Weinbren and Woodward (1964)	Rat	Midline	90% PHx	LL, ML, RSL, CL	Not done	Mass ligation
Gaub and Iversen (1984)	Rat	Midline	90% PHx	LL, ML, RSL, RIL	Not done	Parenchymal mass ligation Mass ligation
Kubota (1997)	Rat	Midline	90% PHx	LL, ML, RSL, RIL	Ligation of PV and HA	Piercing ligation
Madrahimov et al. (2006)	Rat	Horizontal laparotomy	90% PHx	LL, MI, RSL, RIL	None	Clamping and piercing suture
Aller et al. (2009)	Rat	Midline	90% PHx	LL, ML, RSL, RIL	Ligation of PV and HA	Selective ligation of HV

LL left lobe; ML median lobe; RL right lobe; CL caudate lobe; RSL Right suprior Lobe; RIL Right inferior lobe

Table 2. Selection of different rodent models of liver resection/partial hepatectomy (PHx). Rodent (liver resection) models impacting on hepatic perfusion (in the context of liver surgery).

Reference	Species	Operation	Surgical technique
Sequential procedures			
Saito et al. (2006)	Rat	Repeat 70% PHx	Impaired regeneration after 2 nd 70% PHx
Sugimoto et al. (2009)	Rat	2-stage PVL**	Two stage PVL more effective than single stage PVÖ
Li et al. (2015)	Rat	BDL followed by + 70% PHx	Impairment of regeneration after BDL
García-Pérez et al. (2015)	Rat	70% PVL + ALPPS	Combined PVL+ ALPPS more effective than PVL alone
Wei et al. (2016)	Rat	70% PVL + ALPPS + 10% PHx	Combined 70% PVL, median lobe transection + caudate lobe resection enhances regeneration of future liver remnant compared to PVL only
Simultaneous procedures			
Dirsch et al. (2008a)	Rat	50% PHx + RMHV ligation	Recovery from pericentral necrosis in outflow obstructed liver by induction of pericentral hepatocyte proliferation
Huang et al. (2014)	Rat	70% PHx + RMHV-ligation	Impaired recovery from focal outflow obstruction due to reduced hepatic arterial flow through inhibition of nitric oxide production
Ren et al. (2015)	Rat	90% PVL + BDL	Faster induction of atrophy/hypertrophy complex by simultaneous bile duct and portal vein ligation compared to PVL alone
Kawaguchi et al. (2019)	Rat	90% PVL + 30% LLHVL	Regeneration of FLR promoted by additional LLHVL
Wei et al. (2020)	Rat	20% PVL + 70% PHx, 70% PVL + 20% PHx	Induction of regeneration in portally deprived liver lobes by additional resection

PHx = partial hepatectomy; PVL = portal vein ligation; ALLPS = associating liver partition with portal vein ligation for staged hepatectomy; RMHVL = right median hepatic vein ligation; LLHVL = Left lateral hepatic vein ligation; BDL = bile duct ligation;

**2-stage PVL: 70% PVL (ML+LLL) as first stage, after 7 days, 20% PVL (RL) as second stage

Table 3. Selection of classical interventional studies exploring molecular pathways. Targeted processes: proliferation, (MSC) angiogenesis inflammation, autophagy.

Reference	Species	Model	Targeted process	Target	Pharmacological intervention	Mechanism
Proliferation						
Adas et al. (2016)	Rat	70% PHx	MSC	Stem cell	MSC + VEGF	Injection of MSCs and VEGF-transfected MSCs into portal vein following liver resection increased bile duct and liver hepatocyte proliferation
Ren et al. (2008)	Rat	70% PHx	Angiogenesis	Oxygenation	Hyperbaric oxygen	Angiogenesis effect of HBO-PC on liver after partial hepatectomy is possibly due to increased HIF-1alpha activity and VEGF expression
Yoshida et al. (2011)	Rat	70% PHx	Angiogenesis	VEGF, eNOS	L-NAME	Endothelial NOS and VEGF coordinately regulate SEC proliferation during liver regeneration.
Moreno-Carranza et al. (2013)	Rats	PRL-KO-mice	Angiogenesis	Pro-angiogenic hormones	Prolactin	PRL stimulates liver regeneration by upregulation of angiogenesis.
von Heesen et al. (2015)	Rat	70% PHx	Inflammation and angiogenesis	TGF, VGF	Cilostazol	Proliferation is promoted via inhibiting TGF- β and up-regulating VEGF
Jepsen et al. (2015)	Rat	70% PHx	Inflammation	Cortisol	Dexamethasone	Low dose dexamethasone targeted to Kupffer cells does not affect histological liver cell regeneration after 70% hepatectomy in rats, but reduces the inflammatory response judged by circulating markers of inflammation.
Lin et al. (2015)	Mouse	70% PHx	Autophagy	mTOR	Amiodarone Chloroquine	Regeneration is promoted via activating autophagy, respectively impaired by inhibition
Lu et al. (2018)	Mouse	PHx-	Autophagy	miRNA	miR-1907	Regeneration is promoted via activating autophagy

³HL: human hepatic cell line; HGF = hepatocyte growth factor; HIF-1 α = hypoxia-inducible factor-1 α ; BAFF = B-cell activating factor

Table 4. Interaction between resection – regeneration and metabolism.

Reference	Species	Model	Treatment		Metabolism change Energy Biomarker	Regeneration
Inhibition of liver regeneration						
Gutiérrez-Salinas et al. (1999)	Rat	70% PHx	ethanol	ATP↓	Redox-Pair↓	Liver wet weight↓
Picard et al. (2004)	Rat	70% PVL	Retrosine		Caspase 3 ↑, TNF-a ↑	Proliferation inhibition and apoptosis activation
Liu et al. (2013)	PPAR β KO Mouse ^a	70% PHx	PPAR β knockout	-	Hexokinase 2 ^b ↓	Ki67↓, Cyclins ↓
Liu et al. (2019)	Sirtuin 6 LKO mouse ^c	70% PHx	Sirtuin 6 knockout	-	Glucose↓	Ki67↓, Cyclins ↓
Induction of liver regeneration						
Liska et al. (2009)	Pig	50% 60% PVL	MSC			Liver regeneration stimulation
Damrauer et al. (2011)	Mouse	78% PHx ^d	A20 ^e	-	PPAR α^f ↑	Ki67 ↑
Kachaylo et al. (2017)	PtenKO Mouse	68% PHx	PTEN knockout		Glycogen ↑, TGs↑	Liver wet weight ↑
Tautenhahn et al. (2016)	Rat	extended liver resection	MSC	Increased lipid oxidation	Impairment of mitochondrial oxidation after resection	Ki67↑, hepatocyte apoptosis ↓
Li et al. (2018b)	Mouse with fatty liver	40% PHx during 60% WIR ^g	ApoA-1 ^h	-	PGC-1 α ↑	PCNA↑, Cyclins↑
Li et al. (2020a)	ARKO Mouse ⁱ	40% PHx during 60% WIR	Aldose reductase knockout	ATP ↑	AMPK ↑	Cyclins ↑
Cheng et al. (2018)	Mouse	70%	PHx	PPAR γ 2	HGF-cMet-ERK1/2 HGF	Hepatocyte proliferation abrogation via inhibiting HGF-cMet-ERK1/2 pathway

MSC: mesenchymal stromal cells; PPAR γ peroxisome proliferator-activated receptor-gamma; HGF = hepatocyte growth factor

^a Peroxisome proliferator-activated receptor β knockout mouse, PPAR β regulates energy homeostasis and cell proliferation

^b Related to glycolysis

^c Sirtuin 6 knockout mouse, Sirtuin 6 is an NAD+-dependent deacetylase

^d Resection of lateral, medial, left and right lobes

^e NF-kB inhibitory protein

^f Peroxisome proliferator-activated receptor α , which promotes mitochondrial ATP

^g Clamping the branch of hepatic artery and portal vein to the right and triangle lobes for 45min and hepatectomy of left and caudate lobes performed during the ischemia duration

^h Phosphatase and tensin homolog (PTEN) knockout mouse. PTEN is an inhibitor of AKT / mTOR axis

ⁱ Aldose reductase (AR) knockout mouse

Table 5. Rodent (liver resection) models impacting on hepatic perfusion (in the context of liver surgery).

Reference	Species	Surgical model	Surgical technique	Treatment and result	Peak of Proliferation (POD)	Alterations in hepatic perfusion
Hossain et al. (2003)	Rat with cirrhotic liver	15 min WIR and 50% PHx ^a	Liver mass ligation and removal	PGE ^b	-	Increase of portal venous flow
Impact of resection on hepatic hemodynamics						
Dahmen et al. (2007)	Rat	stepwise resection (30%, 70%, 90% & 95%)	Piercing sutures for PH	No drug	nd	Stepwise liver resection causes non-linear increase of portal venous flow and pressure
Xie et al. (2016)	Mouse	70% PHx	Piercing sutures for PH	No drug	POD2	70% PHx causes increase of portal venous flow and pressure
Eipel et al. (2010)	Rat	PHx of 30%, 70%, 85% and 90%	Liver mass ligation + removal of spleen	No drug	nd	Splenectomy leads to decrease of portal hyperperfusion and increased arterial blood supply and liver regeneration
Zhuang et al. (2012)	Rabbit	80% PHx	Not indicated	Splenectomy	nd	Splenectomy decreased resection-induced portal vein pressure
Tautenhahn et al. (2017)	Pig	70% PHx	Pringle manoeuvre	MSC		MSC correct hemodynamic dysfunction after liver resection
Impact of focal outflow obstruction on regional hepatic perfusion and microcirculation						
Dirsch et al. (2008b)	Rat	50% PHx (LLL; RSL; RIL; CIL; SL) + RMHVL	Piercing sutures for PH	No drug	PODX	Spontaneous recovery from FOO is associated by formation of sinusoidal vascular canals
Huang et al. (2011)	Rat	Syngeneic Ltx + RMHVL	Piercing sutures for PH	No drug	nd	Spontaneous recovery from FOO and formation of sinusoidal vascular canals is dependent on arterial blood supply
Huang et al. (2014)	Rat	70% PHx (LML; LLL; RSL; RIL; CIL; SL) + RMHVL	Piercing sutures for PH	Molsidomin, L-NAME	POD1	Spontaneous recovery from FOO and formation of sinusoidal vascular canals is impaired by L-NAME
Arlt et al. (2017)	Lew-Rat	70% PHx (LML; LLL; RSL; RIL; CIL; SL) + RMHVL ^c	Piercing sutures for PH	Splenectomy, Carvedilol, ISMN ^d , Sildenafil, Octreotide, Hemin infusion 10 min	POD1	Drugs cause slight reduction of portal pressure and slight increase of HAF, but have no impact on PVF and hepatic damage
Englert et al. (2019)	Rat	Isolated liver		Hemin infusion 10 min		Perfusion pressure of isolated liver increase
Iwasaki et al. (2019)	Rat	BDL5 + 50% PHx	Liver mass ligation and remove	L-NAME	-	Microcirculation of the liver with BDL

^a 50% PHx was performed during 15 min ischemia (occluding hepatoduodenal ligament)^b Prostaglandin E₁^c RMHVL: right median hepatic vein ligation^d ISMN: Nitrovasodilator isosorbide-5-mononitrate

Table 6. Selection of gene expression studies focussing on hepatectomy and liver regeneration.

Reference	Species	Model	Study design	Results
Regeneration after surgery				
Togo et al. (2004)	Mouse	70% PHx	Microarray	Expression of immediate-early gene candidates (IRAK1, KPNA1), candidate genes during the progress of S1 phase (ID2, ID3), inhibiting factor (GADD45G). NFKB is important in the initial stage of liver regeneration.
Lai et al. (2005)	Rat	70% PHx	Microarray	Expression of many proto-oncogenes changes in the remnant liver during liver regeneration measured 2h to 7 days after PHx. 72 different patterns were identified that describe the change of gene expression.
Cimica et al. (2007)	Rat	70% PHx	SAGE	Strong upregulation of CCND1 16h after PHx. CTGF is induced 4h after PHx. Hepatocyte proliferation occurs 16h after PHx.
Chiba et al. (2013)	Mouse	70% PHx	Microarray	APOA4, HP, FGB and FGG are upregulated during liver regeneration
Li et al. (2018a)	Rat	PVL	Microarray	LLL: activation of hypoxia pathways NLL: activation of cell proliferation and cell-cycle pathways
Rib et al. (2018)	Mouse	2/3 PHx, sham ^a	RNA-Seq	After both sham and PHx, cell-division-cycle genes are activated. 20h after PHx the cell-division-cycle genes are still expressed, but 20h after sham they are not.
Comparison of age-dependent changes				
Pibiri et al. (2015)	Mouse	3/4 PHx, sham young, old	Microarray	Similar gene expression in the liver of old and young mice. CCND1 is up-regulated shortly after PHx in young mice, but mostly down-regulated in aged animals. YAP is activated during liver regeneration in elderly, but not in young mice. Other cell cycle genes are expressed similarly in the liver of old and young mice.
Pibiri (2018)	Review	PHx young, old		Age-dependent decrease of BubR1, YAP and SIRT1 associated to dampening of tissue reconstitution and inhibition of cell cycle genes after PHx. Reduced liver perfusion may be related to the ageing of hepatic stellate cells.
Comparison of different surgery models				
Nagano et al. (2004)	Rat	PVL + 90% PHx	Microarray	PVL + 90% PHx vs. sham + 90% PHx: significantly higher survival rate, upregulated gene expression of CCND1.
Borger et al. (2019)	Mouse	ALLPPS, 68% PHx, PVL, transection, sham	RNA-Seq	ALLPPS vs. 68% PHx: Earlier activation of cell cycle-pathway ALLPPS vs. PVL + transection: Enrichment of the IGF1R signaling pathway (cell survival), the ILK pathway (induced cell proliferation), and the IL10 pathway (stability determination), reduced activity of the interferon pathway (transcription).
Colak et al. (2020)	Rat	70% PHx, PVL, ALLPPS, sham	RNA-Seq	PHx/ PVL/ ALLPPS: Enrichment of cell cycle, mitotic cell cycle, M phase, and DNA replication and repair at 24 h; Downregulation of oxidation-reduction, metabolic process and inflammatory response at 96h. PH/ ALLPPS: Downregulation of oxidation-reduction, triglyceride, and steroid metabolic processes PH: Enrichment of cell activation, response to wounding, and immune response
Mechanosensing				
Song et al. (2017)				Shear forces and other mechanical cues influence NO signaling, YAP pathway and actomyosin remodeling

^a placebo surgery (fake operation)

sham = placebo surgery (fake operation); LLL= ligated liver lobes; NLL = non ligated liver lobes; PHx = partial hepatectomy; PVL = portal vein ligation; ALLPPS = associated liver partition and portal vein ligation for staged hepatectomy

Table 7. Selection of computational models on cellular scale.

Reference	Mechano-transduction	Signaling	Metabolism	System	Approach	Geometry	Result
Nikmaneshi et al. (2020)	✓		✓	Mechanotransduction to metabolism (empirical shear stress response).	ODE, FEM	Sinusoid/lobulus	Mechanobiological mathematical model of liver metabolism. Modeling empirically the effect of shear stress on urea and albumin synthesis through mechanotransduction mechanisms.
Peng et al. (2017)	✓	✓		Stiffness sensing, mechanotransduction; signalling (YAP/TAZ);	ODE	Mesenchymal stem cell	Mathematical model of mechanotransduction. Modeling how mechanical memory regulates mesenchymal stem cell fate decisions.
Guberman et al. (2020)	✓	✓		ECM, mechanosensing, YAP, PI3K, AKT, MAPK.	Boolean	Epithelial cell	Boolean regulatory network model that synthesizes mechanosensitive signaling that links anchorage and matrix stiffness to proliferation and migration.
Gérard and Goldbeter (2014)	✓	✓		Mammalian cell cycle integrated with ECM via FAK and contact inhibition via Hippo/YAP pathway.	ODE	Mammalian cell	Model of cyclin-dependent kinases (CDK, cell cycle) with phenomenological effect of ECM via FAK and cell density (contact inhibition mediated via Hippo/YAP pathway).
Meyer et al. (2020)	✓	✓		Modeling (zonated) nuclear YAP levels following mechanical stimulation.	ODE/PDE	Cell/lobule	Mechanistic model for switch-like activation of YAP upon mechanical stimulation during regeneration in the context of bile acid overload.
Sun et al. (2016)	✓	✓		YAP/TAZ signalling and mechanosensing.	ODE	Cell	Model of YAP/TAZ mechanosensing converting extracellular-matrix mechanical properties to biochemical signals via adhesion, and integrating intracellular signalling cascades associated with cytoskeleton dynamics.
Labibi et al. (2020)		✓		YAP/TAZ signalling	ODE	Cell	Model of TGF- β /Smad nuclear accumulation by YAP/TAZ.
Shin and Nguyen (2016)		✓		Hippo signalling (MST1/2, LATS 1/2)	ODE	Cell	Model of Hippo-ERK signalling.)
Scott et al. (2020) (preprint)		✓		YAP/TAZ translocation via stiffness transfer function (RhoA, Fak)	PDE	cell	Spatial modeling of YAP/TAZ nuclear translocation.
Wehling et al. (2021) (abstract)		✓		YAP/TAZ shuttling	PDE	Cell	Mathematical model of YAP and TAZ nuclear/cytoplasmic shuttling in liver cancer cells using 2D reaction diffusion equations.
Aprupe et al. (2020) (abstract)		✓		YAP/TAZ shuttling and Hippo pathway activation	ODE	Cell	Mathematical model of the YAP/TAZ shuttling as a response to cell density, actin dynamics, and liver damaging drugs.
Gille et al. (2010)			✓	HepatoNet1 - Genome scale metabolism.	CB	Hepatocyte	A comprehensive metabolic reconstruction of the human hepatocyte for the analysis of liver physiology.
Mardinoglu et al. (2014)			✓	iHepatocytes2322 - Genome scale metabolism.	CB	Hepatocyte	Genome scale metabolic model of hepatocyte.
Berndt et al. (2018)			✓	Central carbon metabolism	ODE	Hepatocyte	A biochemistry-based model of liver metabolism.
König and Holzhütter (2012); König et al. (2012)			✓	Glucose metabolism	ODE	Hepatocyte/liver	A detailed kinetic model of human hepatic glucose metabolism and application to disease.

ODE: ordinary differential equations; PDE: partial differential equations; ABM: agent-based model; CB: constraint-based approach (flux balance analysis); DCM: deformable cell models;

Table 8. Selection of computational models on lobular scale.

Reference	Perfusion/ Permeability	Function	Modeling approach	Geometry	Result
Debbaut et al. (2014)	Vascular perfusion (Darcy flow), anisotropic permeability	No function	CFD, porous medium approach	Hexagonal liver lobule	This simulation examines the importance of vascular septa for blood perfusion in liver lobules. It takes into account hepatic isotropic and anisotropic permeability.
Rani et al. (2006)	Vascular perfusion (3D-Navier Stokes), shear-thinning model	No function	CFD	Blood vessel, no lobule	Simulation of blood flow in hepatic lobule, distinction between arterial and portal venous blood, pressure values and velocity at different vessels
Bonfiglio et al. (2010)	Newtonian fluid plus shear-thinning model, Darcy flow	No function	Porous medium approach	Hexagonal liver lobule	The model simulates changes in blood perfusion after resection using anisotropy and shear-thinning modification.
Antonov et al. (2017)	Weekly compressible Newtonian fluid, Darcy flow with continuity assumption	No function	Double porosity model, porous medium approach	Hexagonal liver lobule	A model to quantify the pressure distribution in a liver lobule
Hu et al. (2017)	Darcy flow for incompressible Newtonian fluid	No function	Porous medium approach	Hexagonal liver lobule	A mathematical model for flow dynamics in normal, fibrotic and cirrhotic livers. The model illustrates pressure distribution that is validated with experimental data from rats.
Ma et al. (2020)	1D Navier Stokes equation	No function	1D Navier Stokes equation for blood flow	Vascular tree pre- and postoperative	The simulation of preoperative and postoperative perfusion and postoperative hepatic hemodynamics after left hepatectomy
Sluka et al. (2016)	Multicell modeling package CompuCell3D (CC3D)	Acetaminophen metabolism	Multiscale model: (PBPK modeling at whole body scale, Multicell (CC3D) at tissue/ organ scale, reaction kinetics at sub-cellular scale)	Single sinusoid, single hepatocyte	The multiscale model combines all scales as standalone models. Along one sinusoid the APAP plasma concentration is simulated at all scales.
Fu et al. (2018)	Hagen-Poiseuille's law with mass conservation with advective-diffusive transport processes	Xenobiotic metabolism	Transport and metabolism approach in sinusoidal network	Hexagonal shaped lobule as network of compartments based on experiments	This model investigates the spatio-temporal xenobiotic and metabolite concentration with zonation along one hexagonal shaped liver lobule.
Berndt et al. (2018)	Hagen-Poiseuille law for fluid flow through a cylinder	Glucose metabolism	Compartment model with metabolic model	Sinusoidal tissue unit (STU)	Simulation of zoned carbohydrate metabolism, hepatic glucose exchange and hormone clearance. Investigation of metabolic differences due to inhomogeneous blood perfusion in a sinusoid.
Hoehme et al. (2020)	No perfusion	Liver regeneration after PHx / detoxification	Hepatocytes: isotropic, elastic, adhesive object capable of active migration, growth and division cell interaction; JKR-force model	Liver lobe examined from mouse/pigs experiments with hepatocytes as individual modeling units	A predictive computational model shows that biomechanical cell cycle progression control can explain liver regeneration after partial hepatectomy.
Boissier et al. (2020)	Poiseuille law	Detoxification	Modelling microcirculation/blood flow and convection-reaction	Hexagonal liver lobule	A model for the simulation of hemodynamics and advection-reaction transport processes to model the detoxifying organ function.
Diaz Ochoa et al. (2012)	Liquid with a low Reynolds number, Einstein relation	Acetaminophen metabolism	Multiscale model	Hexagonal liver lobule	Simulation of spatial distribution of APAP concentration and cell viability
Ricken et al. (2010, 2015); Ricken and Lambers (2019)	Darcy flow	Glucose and fat metabolism	Theory of Porous Media, Multiscale model (PDE on lobule scale, ODE on cell scale)	Hexagonal liver lobule	Simulation of spatial distribution of glucose and lipid concentration, spatial distribution of blood perfusion, interplay between perfusion and function, accumulation of fat with influence on blood flow and growth processes

CFD: computational fluid dynamics; 3D: three-dimensional; 1D: one-dimensional; PBPK: physiological-based pharmacokinetics model; PDE: partial differential equations; ODE: ordinary differential equations

Table 9. Selection of computational models on organ and body scale-related to hepatectomy.

Reference	Approach	Species	Geometry	Result
Function (pharmacokinetics)				
Köller et al. (2021)	PBPK	Human	Whole-body	PBPK model of ICG pharmacokinetics in hepatectomy. Risk assessment based on pre-operative ICG parameters.
Lu et al. (2006)	PBPK	Rat	Whole-body	PBPK model of hexachlorobenzene pharmacokinetics after partial hepatectomy.
Lagneau et al. (2005)	PBPK	Human	Whole-body	PBPK model of cefazolin pharmacokinetics in (right) hepatectomy) accounting for (i) intraoperative liver pedicular triad clamping; (ii) intraoperative blood loss; (iii) reduction of liver volume after resection.
Thomas et al. (2015)	Linear regression	Human	Whole-body	Linear regression model. Post-resection liver volume could be accurately predicted by the time course of liver inflow, but not by resected liver volume.
Haemodynamics				
Ho et al. (2010, 2012)	CFD	Human	Liver	Hemodynamic model for a patient who received a right donor lobectomy. Hemodynamic equations were solved subject to the sonographically measured inlet velocity and models of portal veins via MRI/CT.
Ma et al. (2020)	CFD	Human	Liver	Hemodynamic model after left hepatectomy (1D Navier-Stokes). Exploration of post-hepatectomy outflow boundary conditions.
Lin et al. (2021)	CFD	Human	Liver	Highly parallel method to simulate blood flows in the liver including hepatic artery, portal vein and hepatic vein from CT data (transient incompressible Navier-Stokes equations). Simulation of pressure, velocity and WSS in hepatectomy.
Debbaut et al. (2012)	Closed loop 0D	Rat	Whole-body	An electrical rat liver model to compare normal with resected liver hemodynamics. Lobe-specific resistive lumped parameter model of the liver. Results demonstrated hyperperfusion effects such as portal hypertension and elevated lobe-specific portal venous flows.
Audebert et al. (2017)	Closed loop 0D	Pig	Whole-body	Closed-loop lumped parameter model for hemodynamics changes observed during hepatectomy in pig. Increase in portal pressure, increase of liver pressure loss, slight decrease of portal flow and major decrease in arterial flow are quantitatively captured.
Golse et al. (2021)	Closed loop 0D	Human	Whole-body	Closed loop 0D model to anticipate postoperative hemodynamics with good correlation between measured and simulated portal vein pressure.

PBPK: physiological-based pharmacokinetics model; CFD: computational fluid dynamics; 0D: zero-dimensional; 1D: one-dimensional

REFERENCES

- 976 Abshagen, K., Eipel, C., and Vollmar, B. (2012a). A critical appraisal of the hemodynamic signal driving
977 liver regeneration. *Langenbecks Arch Surg* 397, 579–590. doi:10.1007/s00423-012-0913-0
- 978 Abshagen, K., Eipel, C., and Vollmar, B. (2012b). A critical appraisal of the hemodynamic signal driving
979 liver regeneration. *Langenbeck's archives of surgery* 397, 579–590. doi:10.1007/s00423-012-0913-0
- 980 Adas, G., Koc, B., Adas, M., Duruksu, G., Subasi, C., Kemik, O., et al. (2016). Effects of mesenchymal
981 stem cells and vegf on liver regeneration following major resection. *Langenbeck's archives of surgery*
982 401, 725–740. doi:10.1007/s00423-016-1380-9
- 983 Ahmadi-Badejani, R., Mosharaf-Dehkordi, M., and Ahmadikia, H. (2020). An image-based geometric
984 model for numerical simulation of blood perfusion within the liver lobules. *Computer methods in
985 biomechanics and biomedical engineering* 23, 987–1004. doi:10.1080/10255842.2020.1782389
- 986 Alexius, B. (1991). [CNS changes can be present in asymptomatic HIV infection]. *Lakartidningen* 88,
987 4004–4005
- 988 Aller, M.-A., Mendez, M., Nava, M.-P., Lopez, L., Arias, J.-L., and Arias, J. (2009). The value of
989 microsurgery in liver research. *Liver International* 29, 1132–1140. doi:10.1111/j.1478-3231.2009.
990 02078.x
- 991 Antonov, M. Y., Grigorev, A. V., and Kolesov, A. E. (2017). Numerical modeling of fluid flow in liver
992 lobule using double porosity model. In *Numerical Analysis and Its Applications*, eds. I. Dimov, I. Faragó,
993 and L. Vulkov (Cham: Springer International Publishing), vol. 10187 of *Lecture Notes in Computer
994 Science*. 187–194. doi:10.1007/978-3-319-57099-0{\textunderscore}18
- 995 Aprupe, L., Schmitt, J., Liu, K., Schirmacher, P., Kummer, U., and Breuhahn, K. (2020). Mathematical
996 modeling of the yap/taz shuttling as a response to cell density, actin dynamics, and liver damaging drugs.
997 *Zeitschrift für Gastroenterologie* 58, 4–21
- 998 Araki, K., Harimoto, N., Kubo, N., Watanabe, A., Igarashi, T., Tsukagoshi, M., et al. (2020). Functional
999 remnant liver volumetry using gd-eob-dtpa-enhanced magnetic resonance imaging (mri) predicts post-
1000 hepatectomy liver failure in resection of more than one segment. *HPB : the official journal of the
1001 International Hepato Pancreato Biliary Association* 22, 318–327. doi:10.1016/j.hpb.2019.08.002
- 1002 Arlt, J., Wei, W., Xie, C., Homeyer, A., Settmacher, U., Dahmen, U., et al. (2017). Modulation of hepatic
1003 perfusion did not improve recovery from hepatic outflow obstruction. *BMC Pharmacol Toxicol* 18, 50.
1004 doi:10.1186/s40360-017-0155-4
- 1005 Armiti-Juber, A. and Ricken, T. (2021). Model order reduction for deformable porous materials
1006 in thin domains via asymptotic analysis. *Archive of Applied Mechanics* 477, 873. doi:10.1007/
1007 s00419-021-01907-3
- 1008 Asenbaum, U., Kaczirek, K., Ba-Ssalamah, A., Ringl, H., Schwarz, C., Waneck, F., et al. (2018). Post-
1009 hepatectomy liver failure after major hepatic surgery: not only size matters. *Eur Radiol* 28, 4748–4756.
1010 doi:10.1007/s00330-018-5487-y
- 1011 Ashburner, M., Ball, C. A., Blake, J. A., Botstein, D., Butler, H., Cherry, J. M., et al. (2000). Gene
1012 ontology: tool for the unification of biology. the gene ontology consortium. *Nature genetics* 25, 25–29.
1013 doi:10.1038/75556
- 1014 Ateshian, G. A. and Ricken, T. (2010). Multigenerational interstitial growth of biological tissues.
1015 *Biomechanics and Modeling in Mechanobiology* 9, 689–702. doi:10.1007/s10237-010-0205-y
- 1016 Audebert, C., Bekheit, M., Bucur, P., Vibert, E., and Vignon-Clementel, I. E. (2017). Partial hepatectomy
1017 hemodynamics changes: Experimental data explained by closed-loop lumped modeling. *J Biomech* 50,
1018 202–208. doi:10.1016/j.jbiomech.2016.11.037

- 1019 Bak-Fredslund, K. P., Lykke Eriksen, P., Munk, O. L., Villadsen, G. E., Keiding, S., and Sørensen,
1020 M. (2017). Metabolic liver function in humans measured by 2-18f-fluoro-2-deoxy-d-galactose pet/ct-
1021 reproducibility and clinical potential. *EJNMMI research* 7, 71. doi:10.1186/s13550-017-0320-1
- 1022 Barth, B. K., Fischer, M. A., Kambakamba, P., Lesurte, M., and Reiner, C. S. (2016). Liver-fat and
1023 liver-function indices derived from gd-eob-dtpa-enhanced liver mri for prediction of future liver remnant
1024 growth after portal vein occlusion. *European journal of radiology* 85, 843–849. doi:10.1016/j.ejrad.
1025 2016.02.008
- 1026 Bartl, M., Pfaff, M., Ghallab, A., Driesch, D., Henkel, S. G., Hengstler, J. G., et al. (2015). Optimality
1027 in the zonation of ammonia detoxification in rodent liver. *Arch Toxicol* 89, 2069–2078. doi:10.1007/
1028 s00204-015-1596-4
- 1029 Bass, L., Robinson, P., and Bracken, A. J. (1978). Hepatic elimination of flowing substrates: the distributed
1030 model. *Journal of theoretical biology* 72, 161–184. doi:10.1016/0022-5193(78)90023-1
- 1031 Bednarsch, J., Menk, M., Malinowski, M., Weber-Carstens, S., Pratschke, J., and Stockmann, M. (2016).
1032 (13) c breath tests are feasible in patients with extracorporeal membrane oxygenation devices. *Artificial
1033 organs* 40, 692–698. doi:10.1111/aor.12634
- 1034 Benfeitas, R., Bidkhor, G., Mukhopadhyay, B., Klevstig, M., Arif, M., Zhang, C., et al. (2019).
1035 Characterization of heterogeneous redox responses in hepatocellular carcinoma patients using network
1036 analysis. *EBioMedicine* 40, 471–487. doi:10.1016/j.ebiom.2018.12.057
- 1037 Bennink, R. J., Dinant, S., Erdogan, D., Heijnen, B. H., Straatsburg, I. H., van Vliet, A. K., et al. (2004).
1038 Preoperative assessment of postoperative remnant liver function using hepatobiliary scintigraphy. *Journal
1039 of nuclear medicine : official publication, Society of Nuclear Medicine* 45, 965–971
- 1040 Berndt, N., Bulik, S., Wallach, I., Wünsch, T., König, M., Stockmann, M., et al. (2018). HEPATOKIN1 is
1041 a biochemistry-based model of liver metabolism for applications in medicine and pharmacology. *Nat
1042 Commun* 9, 2386. doi:10.1038/s41467-018-04720-9
- 1043 Berndt, N., Eckstein, J., Heucke, N., Wuensch, T., Gajowski, R., Stockmann, M., et al. (2021). Metabolic
1044 heterogeneity of human hepatocellular carcinoma: implications for personalized pharmacological
1045 treatment. *The FEBS journal* 288, 2332–2346. doi:10.1111/febs.15587
- 1046 Bidkhor, G., Benfeitas, R., Klevstig, M., Zhang, C., Nielsen, J., Uhlen, M., et al. (2018).
1047 Metabolic network-based stratification of hepatocellular carcinoma reveals three distinct tumor subtypes.
1048 *Proceedings of the National Academy of Sciences of the United States of America* 115, E11874–E11883.
1049 doi:10.1073/pnas.1807305115
- 1050 Björnson, E., Mukhopadhyay, B., Asplund, A., Pristovsek, N., Cinar, R., Romeo, S., et al. (2015).
1051 Stratification of Hepatocellular Carcinoma Patients Based on Acetate Utilization. *Cell Rep* 13, 2014–
1052 2026. doi:10.1016/j.celrep.2015.10.045
- 1053 Blüthner, E., Bednarsch, J., Pape, U.-F., Karber, M., Maasberg, S., Gerlach, U. A., et al. (2020). Advanced
1054 liver function assessment in patients with intestinal failure on long-term parenteral nutrition. *Clinical
1055 nutrition (Edinburgh, Scotland)* 39, 540–547. doi:10.1016/j.clnu.2019.02.039
- 1056 Boissier, N., Drasdo, D., and Vignon-Clementel, I. E. (2020). Simulation of a detoxifying organ function:
1057 Focus on hemodynamics modeling and convection-reaction numerical simulation in microcirculatory
1058 networks. *International Journal for Numerical Methods in Biomedical Engineering*, e3422doi:10.1002/
1059 cmn.3422
- 1060 Boleslawski, E., Petrovai, G., Truant, S., Dharancy, S., Duhamel, A., Salleron, J., et al. (2012). Hepatic
1061 venous pressure gradient in the assessment of portal hypertension before liver resection in patients with
1062 cirrhosis. *Br J Surg* 99, 855–863. doi:10.1002/bjs.8753

- 1063 Bonfiglio, A., Leungchavaphongse, K., Repetto, R., and Siggers, J. H. (2010). Mathematical modeling of
1064 the circulation in the liver lobule. *Journal of biomechanical engineering* 132, 111011. doi:10.1115/1.
1065 4002563
- 1066 Bonfrate, L., Grattagliano, I., Palasciano, G., and Portincasa, P. (2015). Dynamic carbon 13 breath tests for
1067 the study of liver function and gastric emptying. *Gastroenterology report* 3, 12–21. doi:10.1093/gastro/
1068 gou068
- 1069 Borger, P., Schneider, M., Frick, L., Langiewicz, M., Sorokin, M., Buzdin, A., et al. (2019). Exploration
1070 of the Transcriptional Landscape of ALPPS Reveals the Pathways of Accelerated Liver Regeneration.
1071 *Front Oncol* 9, 1206. doi:10.3389/fonc.2019.01206
- 1072 Bracken, M. B. (2009). Why animal studies are often poor predictors of human reactions to exposure.
1073 *Journal of the Royal Society of Medicine* 102, 120–122. doi:10.1258/jrsm.2008.08k033
- 1074 Buckley, C. D., Tan, J., Anderson, K. L., Hanein, D., Volkmann, N., Weis, W. I., et al. (2014). Cell
1075 adhesion. The minimal cadherin-catenin complex binds to actin filaments under force. *Science* 346,
1076 1254211. doi:10.1126/science.1254211
- 1077 Burke, Z. D. and Tosh, D. (2006). The wnt/beta-catenin pathway: master regulator of liver zonation?
1078 *BioEssays : news and reviews in molecular, cellular and developmental biology* 28, 1072–1077. doi:10.
1079 1002/bies.20485
- 1080 Byk, K., Jasinski, K., Bartel, Z., Jasztal, A., Sitek, B., Tomanek, B., et al. (2016). MRI-based assessment of
1081 liver perfusion and hepatocyte injury in the murine model of acute hepatitis. *Magma (New York, N.Y.)*
1082 29, 789–798. doi:10.1007/s10334-016-0563-2
- 1083 Caldez, M. J., van Hul, N., Koh, H. W. L., Teo, X. Q., Fan, J. J., Tan, P. Y., et al. (2018). Metabolic
1084 remodeling during liver regeneration. *Developmental cell* 47, 425–438.e5. doi:10.1016/j.devcel.2018.09.
1085 020
- 1086 Carril, E., Valdecantos, M. P., Lanzón, B., Angulo, S., Valverde, Á. M., Godzien, J., et al. (2020). Metabolic
1087 impact of partial hepatectomy in the non-alcoholic steatohepatitis animal model of methionine-choline
1088 deficient diet. *Journal of pharmaceutical and biomedical analysis* 178, 112958. doi:10.1016/j.jpba.2019.
1089 112958
- 1090 Chen, G., Xia, B., Fu, Q., Huang, X., Wang, F., Chen, Z., et al. (2019). Matrix mechanics as regulatory
1091 factors and therapeutic targets in hepatic fibrosis. *International journal of biological sciences* 15,
1092 2509–2521. doi:10.7150/ijbs.37500
- 1093 Chen, X.-G. and Xu, C.-S. (2014). Proteomic analysis of the regenerating liver following 2/3 partial
1094 hepatectomy in rats. *Biological research* 47, 59. doi:10.1186/0717-6287-47-59
- 1095 Cheng, Z., Liu, L., Zhang, X.-J., Lu, M., Wang, Y., Assfalg, V., et al. (2018). Peroxisome Proliferator-
1096 Activated Receptor gamma negatively regulates liver regeneration after partial hepatectomy via the
1097 HGF/c-Met/ERK1/2 pathways. *Sci Rep* 8, 11894. doi:10.1038/s41598-018-30426-5
- 1098 Chiba, H., Osanai, M., Murata, M., Kojima, T., and Sawada, N. (2008). Transmembrane proteins of tight
1099 junctions. *Biochimica et biophysica acta* 1778, 588–600. doi:10.1016/j.bbamem.2007.08.017
- 1100 Chiba, M., Yasue, H., and Ohkohchi, N. (2013). Gene expression profiling of sense and antisense transcripts
1101 in liver regeneration by microarray analysis. *Biomed Rep* 1, 383–388. doi:10.3892/br.2013.80
- 1102 Cho, A., Chung, Y. E., Choi, J. S., Kim, K. S., Choi, G. H., Park, Y. N., et al. (2017). Feasibility of
1103 preoperative FDG PET/CT total hepatic glycolysis in the remnant liver for the prediction of postoperative
1104 liver function. *AJR. American journal of roentgenology* 208, 624–631. doi:10.2214/AJR.16.16450
- 1105 Choi, S. S., Omenetti, A., Witek, R. P., Moylan, C. A., Syn, W.-K., Jung, Y., et al. (2009). Hedgehog
1106 pathway activation and epithelial-to-mesenchymal transitions during myofibroblastic transformation of

- 1107 rat hepatic cells in culture and cirrhosis. *American journal of physiology. Gastrointestinal and liver*
1108 *physiology* 297, G1093–106. doi:10.1152/ajpgi.00292.2009
- 1109 Chouhan, M. D., Mookerjee, R. P., Bainbridge, A., Punwani, S., Jones, H., Davies, N., et al. (2017).
1110 Caval subtraction 2d phase-contrast mri to measure total liver and hepatic arterial blood flow: Proof-
1111 of-principle, correlation with portal hypertension severity and validation in patients with chronic liver
1112 disease. *Investigative radiology* 52, 170–176. doi:10.1097/RLI.0000000000000328
- 1113 Christ, B., Dahmen, U., Herrmann, K.-H., König, M., Reichenbach, J. R., Ricken, T., et al. (2017).
1114 Computational Modeling in Liver Surgery. *Front. Physiol.* 8, 906. doi:10.3389/fphys.2017.00906
- 1115 Chuang, Y.-H., Ou, H.-Y., Lazo, M. Z., Chen, C.-L., Chen, M.-H., Weng, C.-C., et al. (2018). Predicting
1116 post-hepatectomy liver failure by combined volumetric, functional mr image and laboratory analysis.
1117 *Liver international : official journal of the International Association for the Study of the Liver* 38,
1118 868–874. doi:10.1111/liv.13608
- 1119 Cimica, V., Batusic, D., Haralanova-Ilieva, B., Chen, Y., Holleman, T., Pieler, T., et al. (2007). Serial
1120 analysis of gene expression (SAGE) in rat liver regeneration. *Biochem Biophys Res Commun* 360,
1121 545–552. doi:10.1016/j.bbrc.2007.06.039
- 1122 Colak, D., Al-Harazi, O., Mustafa, O. M., Meng, F., Assiri, A. M., Dhar, D. K., et al. (2020). RNA-
1123 Seq transcriptome profiling in three liver regeneration models in rats: comparative analysis of partial
1124 hepatectomy, ALLPS, and PVL. *Sci Rep* 10, 5213. doi:10.1038/s41598-020-61826-1
- 1125 Cucchetti, A., Cescon, M., Golfieri, R., Piscaglia, F., Renzulli, M., Neri, F., et al. (2016). Hepatic venous
1126 pressure gradient in the preoperative assessment of patients with resectable hepatocellular carcinoma.
1127 *Journal of hepatology* 64, 79–86. doi:10.1016/j.jhep.2015.08.025
- 1128 Dahmen, U., Hall, C. A., Madrahimov, N., Milekhin, V., and Dirsch, O. (2007). Regulation of hepatic
1129 microcirculation in stepwise liver resection. *Acta Gastroenterol Belg* 70, 345–351
- 1130 Damrauer, S. M., Studer, P., da Silva, C. G., Longo, C. R., Ramsey, H. E., Csizmadia, E., et al. (2011). A20
1131 modulates lipid metabolism and energy production to promote liver regeneration. *PLoS One* 6, e17715.
1132 doi:10.1371/journal.pone.0017715
- 1133 d'Assignies, G., Fayard, C., Leitao, H., Alfaiate, T., Tubach, F., Dokmak, S., et al. (2016). Liver steatosis
1134 assessed by preoperative MRI: An independent risk factor for severe complications after major hepatic
1135 resection. *Surgery* 159, 1050–1057. doi:10.1016/j.surg.2015.10.008
- 1136 de Graaf, W., van Lienden, K. P., van Gulik, T. M., and Bennink, R. J. (2010). (99m)tc-mebrofenin
1137 hepatobiliary scintigraphy with spect for the assessment of hepatic function and liver functional volume
1138 before partial hepatectomy. *Journal of nuclear medicine : official publication, Society of Nuclear*
1139 *Medicine* 51, 229–236. doi:10.2967/jnumed.109.069724
- 1140 Deal, R., Frederiks, C., Williams, L., Olthof, P. B., Dirscherl, K., Keutgen, X., et al. (2018). Rapid
1141 Liver Hypertrophy After Portal Vein Occlusion Correlates with the Degree of Collateralization Between
1142 Lobes—a Study in Pigs. *J Gastrointest Surg* 22, 203–213. doi:10.1007/s11605-017-3512-0
- 1143 Debbaut, C., De Wilde, D., Casteleyn, C., Cornillie, P., Van Loo, D., Van Hoorebeke, L., et al. (2012).
1144 Modeling the impact of partial hepatectomy on the hepatic hemodynamics using a rat model. *IEEE*
1145 *Trans Biomed Eng* 59, 3293–3303. doi:10.1109/TBME.2012.2199108
- 1146 Debbaut, C., Vierendeels, J., Siggers, J. H., Repetto, R., Monbalu, D., and Segers, P. (2014). A 3d
1147 porous media liver lobule model: the importance of vascular septa and anisotropic permeability for
1148 homogeneous perfusion. *Computer methods in biomechanics and biomedical engineering* 17, 1295–1310.
1149 doi:10.1080/10255842.2012.744399

- 1150 Degasperi, A., Birtwistle, M. R., Volinsky, N., Rauch, J., Kolch, W., and Kholodenko, B. N. (2014).
1151 Evaluating Strategies to Normalise Biological Replicates of Western Blot Data. *PLoS ONE* 9, e87293.
1152 doi:10.1371/journal.pone.0087293
- 1153 Diaz Ochoa, J. G., Bucher, J., Péry, A. R. R., Zaldivar Comenges, J. M., Niklas, J., and Mauch, K. (2012).
1154 A multi-scale modeling framework for individualized, spatiotemporal prediction of drug effects and
1155 toxicological risk. *Frontiers in pharmacology* 3, 204. doi:10.3389/fphar.2012.00204
- 1156 Dinant, S., de Graaf, W., Verwer, B. J., Bennink, R. J., van Lienden, K. P., Gouma, D. J., et al. (2007).
1157 Risk assessment of posthepatectomy liver failure using hepatobiliary scintigraphy and ct volumetry.
1158 *Journal of nuclear medicine : official publication, Society of Nuclear Medicine* 48, 685–692. doi:10.
1159 2967/jnmed.106.038430
- 1160 Dirsch, O., Madrahimov, N., Chaudri, N., Deng, M., Madrahimova, F., Schenk, A., et al. (2008a).
1161 ERRATUM. *Transplantation* 85, 1866. doi:10.1097/TP.0b013e31816631f9
- 1162 Dirsch, O., Madrahimov, N., Chaudri, N., Deng, M., Madrahimova, F., Schenk, A., et al. (2008b). Recovery
1163 of liver perfusion after focal outflow obstruction and liver resection. *Transplantation* 85, 748–756.
1164 doi:10.1097/TP.0b013e31816631f9
- 1165 Du, K., Hyun, J., Premont, R. T., Choi, S. S., Michelotti, G. A., Swiderska-Syn, M., et al. (2018).
1166 Hedgehog-yap signaling pathway regulates glutaminolysis to control activation of hepatic stellate cells.
1167 *Gastroenterology* 154, 1465–1479.e13. doi:10.1053/j.gastro.2017.12.022
- 1168 Dupont, S., Morsut, L., Aragona, M., Enzo, E., Giulitti, S., Cordenonsi, M., et al. (2011). Role of YAP/TAZ
1169 in mechanotransduction. *Nature* 474, 179–183. doi:10.1038/nature10137
- 1170 Edginton, A. N. and Willmann, S. (2008). Physiology-based simulations of a pathological condition:
1171 prediction of pharmacokinetics in patients with liver cirrhosis. *Clin Pharmacokinet* 47, 743–752.
1172 doi:10.2165/00003088-200847110-00005
- 1173 Eipel, C., Abshagen, K., Ritter, J., Cantré, D., Menger, M. D., and Vollmar, B. (2010). Splenectomy
1174 improves survival by increasing arterial blood supply in a rat model of reduced-size liver. *Transpl Int* 23,
1175 998–1007. doi:10.1111/j.1432-2277.2010.01079.x
- 1176 Elosegui-Artola, A., Trepat, X., and Roca-Cusachs, P. (2018). Control of Mechanotransduction by
1177 Molecular Clutch Dynamics. *Trends Cell Biol* 28, 356–367. doi:10.1016/j.tcb.2018.01.008
- 1178 Englert, F. A., Seidel, R. A., Galler, K., Gouveia, Z., Soares, M. P., Neugebauer, U., et al. (2019). Labile
1179 heme impairs hepatic microcirculation and promotes hepatic injury. *Arch Biochem Biophys* 672, 108075.
1180 doi:10.1016/j.abb.2019.108075
- 1181 Erdogan, D., Heijnen, B. H. M., Bennink, R. J., Kok, M., Dinant, S., Straatsburg, I. H., et al. (2004).
1182 Preoperative assessment of liver function: a comparison of 99mtc-mebrofenin scintigraphy with
1183 indocyanine green clearance test. *Liver international : official journal of the International Association
1184 for the Study of the Liver* 24, 117–123. doi:10.1111/j.1478-3231.2004.00901.x
- 1185 Espié, P., Tytgat, D., Sargentini-Maier, M.-L., Poggesi, I., and Watelet, J.-B. (2009). Physiologically based
1186 pharmacokinetics (pbpk). *Drug metabolism reviews* 41, 391–407. doi:10.1080/10837450902891360
- 1187 Ferraioli, G. (2019). Review of Liver Elastography Guidelines. *J Ultrasound Med* 38, 9–14. doi:10.1002/
1188 jum.14856
- 1189 Filmann, N., Walter, D., Schadde, E., Bruns, C., Keck, T., Lang, H., et al. (2019). Mortality after liver
1190 surgery in Germany. *Br J Surg* 106, 1523–1529. doi:10.1002/bjs.11236
- 1191 Frydrychowicz, A., Roldan-Alzate, A., Winslow, E., Consigny, D., Campo, C. A., Motosugi, U., et al.
1192 (2017). Comparison of radial 4D Flow-MRI with perivascular ultrasound to quantify blood flow in
1193 the abdomen and introduction of a porcine model of pre-hepatic portal hypertension. *Eur Radiol* 27,
1194 5316–5324. doi:10.1007/s00330-017-4862-4

- 1195 Fu, X., Sluka, J. P., Clendenon, S. G., Dunn, K. W., Wang, Z., Klaunig, J. E., et al. (2018). Modeling
1196 of xenobiotic transport and metabolism in virtual hepatic lobule models. *PLoS one* 13, e0198060.
1197 doi:10.1371/journal.pone.0198060
- 1198 García-Pérez, R., Revilla-Nuin, B., Martínez, C. M., Bernabé-García, A., Baroja Mazo, A., and
1199 Parrilla Paricio, P. (2015). Associated Liver Partition and Portal Vein Ligation (ALPPS) vs Selective
1200 Portal Vein Ligation (PVL) for Staged Hepatectomy in a Rat Model. Similar Regenerative Response?
1201 *PLoS ONE* 10, e0144096. doi:10.1371/journal.pone.0144096
- 1202 Gaub, J. and Iversen, J. (1984). Rat Liver Regeneration After 90% Partial Hepatectomy. *Hepatology* 4,
1203 902–904. doi:10.1002/hep.1840040519
- 1204 Gebhardt, R., Baldysiak-Figiel, A., Krügel, V., Ueberham, E., and Gaunitz, F. (2007). Hepatocellular
1205 expression of glutamine synthetase: an indicator of morphogen actions as master regulators of zonation in
1206 adult liver. *Progress in histochemistry and cytochemistry* 41, 201–266. doi:10.1016/j.proghi.2006.12.001
- 1207 Geisel, D., Raabe, P., Lüdemann, L., Malinowski, M., Stockmann, M., Seehofer, D., et al. (2017). Gd-
1208 eob-dtpa-enhanced mri for monitoring future liver remnant function after portal vein embolization and
1209 extended hemihepatectomy: A prospective trial. *European radiology* 27, 3080–3087. doi:10.1007/
1210 s00330-016-4674-y
- 1211 Gérard, C. and Goldbeter, A. (2014). The balance between cell cycle arrest and cell proliferation: control
1212 by the extracellular matrix and by contact inhibition. *Interface Focus* 4, 20130075. doi:10.1098/rsfs.
1213 2013.0075
- 1214 Ghibellini, G., Leslie, E. M., Pollack, G. M., and Brouwer, K. L. R. (2008). Use of tc-99m mebrofenin as a
1215 clinical probe to assess altered hepatobiliary transport: integration of in vitro, pharmacokinetic modeling,
1216 and simulation studies. *Pharmaceutical research* 25, 1851–1860. doi:10.1007/s11095-008-9597-0
- 1217 Gille, C., Bölling, C., Hoppe, A., Bulik, S., Hoffmann, S., Hübner, K., et al. (2010). HepatoNet1: a
1218 comprehensive metabolic reconstruction of the human hepatocyte for the analysis of liver physiology.
1219 *Mol Syst Biol* 6, 411. doi:10.1038/msb.2010.62
- 1220 Golse, N., Joly, F., Combari, P., Lewin, M., Nicolas, Q., Audebert, C., et al. (2021). Predicting the risk of
1221 post-hepatectomy portal hypertension using a digital twin: A clinical proof of concept. *J Hepatol* 74,
1222 661–669. doi:10.1016/j.jhep.2020.10.036
- 1223 Goresky, C. A., Bach, G. G., and Nadeau, B. E. (1973). On the uptake of materials by the intact
1224 liver. the transport and net removal of galactose. *The Journal of clinical investigation* 52, 991–1009.
1225 doi:10.1172/JCI107300
- 1226 Gouya, H., Grabar, S., Vignaux, O., Saade, A., Pol, S., Legmann, P., et al. (2016). Portal hypertension in
1227 patients with cirrhosis: indirect assessment of hepatic venous pressure gradient by measuring azygos
1228 flow with 2d-cine phase-contrast magnetic resonance imaging. *European radiology* 26, 1981–1990.
1229 doi:10.1007/s00330-015-3991-x
- 1230 Gray, M. R. and Tam, Y. K. (1987). The series-compartment model for hepatic elimination. *Drug
1231 metabolism and disposition: the biological fate of chemicals* 15, 27–31
- 1232 Guberman, E., Sherief, H., and Regan, E. R. (2020). Boolean model of anchorage dependence and contact
1233 inhibition points to coordinated inhibition but semi-independent induction of proliferation and migration.
1234 *Comput Struct Biotechnol J* 18, 2145–2165. doi:10.1016/j.csbj.2020.07.016
- 1235 Guo, F., Nian, H., Zhang, H., Huang, L., Tang, Y., Xiao, X., et al. (2006a). Proteomic analysis of
1236 the transition from quiescent to proliferating stages in rat liver hepatectomy model. *Proteomics* 6,
1237 3075–3086. doi:10.1002/pmic.200500322

- 1238 Guo, F., Nian, H., Zhang, H., Huang, L., Tang, Y., Xiao, X., et al. (2006b). Proteomic analysis of
1239 the transition from quiescent to proliferating stages in rat liver hepatectomy model. *Proteomics* 6,
1240 3075–3086. doi:10.1002/pmic.200500322
- 1241 Gupta, M., Choudhury, P. S., Singh, S., and Hazarika, D. (2018). Liver Functional Volumetry by Tc-99m
1242 Mebrofenin Hepatobiliary Scintigraphy before Major Liver Resection: A Game Changer. *Indian J Nucl
1243 Med* 33, 277–283. doi:10.4103/ijnm.IJNM_72_18
- 1244 Gutiérrez-Salinas, J., Miranda-Garduño, L., Trejo-Izquierdo, E., Díaz-Muñoz, M., Vidrio, S., Morales-
1245 González, J. A., et al. (1999). Redox state and energy metabolism during liver regeneration: alterations
1246 produced by acute ethanol administration. *Biochem Pharmacol* 58, 1831–1839. doi:10.1016/
1247 s0006-2952(99)00261-0
- 1248 Haegele, S., Reiter, S., Wanek, D., Offensperger, F., Pereyra, D., Stremitzer, S., et al. (2016). Perioperative
1249 non-invasive indocyanine green-clearance testing to predict postoperative outcome after liver resection.
1250 *PloS one* 11, e0165481. doi:10.1371/journal.pone.0165481
- 1251 Hailfinger, S., Jaworski, M., Braeuning, A., Buchmann, A., and Schwarz, M. (2006). Zonal gene expression
1252 in murine liver: lessons from tumors. *Hepatology (Baltimore, Md.)* 43, 407–414. doi:10.1002/hep.21082
- 1253 Halder, G., Dupont, S., and Piccolo, S. (2012). Transduction of mechanical and cytoskeletal cues by yap
1254 and taz. *Nature reviews. Molecular cell biology* 13, 591–600. doi:10.1038/nrm3416
- 1255 Hemming, A. W., Scudamore, C. H., Shackleton, C. R., Pudek, M., and Erb, S. R. (1992). Indocyanine
1256 green clearance as a predictor of successful hepatic resection in cirrhotic patients. *Am J Surg* 163,
1257 515–518. doi:10.1016/0002-9610(92)90400-1
- 1258 Hendrikse, N. H., Kuipers, F., Meijer, C., Havinga, R., Bijleveld, C. M. A., van der Graaf, W. T. A.,
1259 et al. (2004). In vivo imaging of hepatobiliary transport function mediated by multidrug resistance
1260 associated protein and p-glycoprotein. *Cancer chemotherapy and pharmacology* 54, 131–138. doi:10.
1261 1007/s00280-004-0793-2
- 1262 Heucke, N., Wuensch, T., Mohr, J., Kaffarnik, M., Arsenic, R., Sinn, B., et al. (2019). Non-invasive
1263 structure-function assessment of the liver by 2d time-harmonic elastography and the dynamic liver
1264 maximum capacity (limax) test. *Journal of gastroenterology and hepatology* 34, 1611–1619. doi:10.
1265 1111/jgh.14629
- 1266 Higgins, G. M. (1931). Experimental pathology of the liver. i. restoration of the liver of the white rat
1267 following partial surgical removal. *Arch pathol* 12, 186–202
- 1268 Hintermann, E. and Christen, U. (2019). The many roles of cell adhesion molecules in hepatic fibrosis.
1269 *Cells* 8. doi:10.3390/cells8121503
- 1270 Ho, C.-M., Lin, R.-K., Tsai, S.-F., Hu, R.-H., Liang, P.-C., Sheu, T. W.-H., et al. (2010). Simulation
1271 of portal hemodynamic changes in a donor after right hepatectomy. *J Biomech Eng* 132, 041002.
1272 doi:10.1115/1.4000957
- 1273 Ho, H., Sorrell, K., Bartlett, A., and Hunter, P. (2012). Blood flow simulation for the liver after a virtual
1274 right lobe hepatectomy. *Medical image computing and computer-assisted intervention : MICCAI
1275 ... International Conference on Medical Image Computing and Computer-Assisted Intervention* 15,
1276 525–532. doi:10.1007/978-3-642-33454-2{\textunderscore}65
- 1277 Ho, H. and Zhang, E. (2020). Virtual Lobule Models Are the Key for Multiscale Biomechanical and
1278 Pharmacological Modeling for the Liver. *Front Physiol* 11, 1061. doi:10.3389/fphys.2020.01061
- 1279 [Dataset] Hoehme, S., Gebhardt, R., Hengstler, J. G., and Drasdo, D. (2020). Model predicts fundamental
1280 role of biomechanical control of cell cycle progression during liver regeneration after partial hepatectomy

- 1281 Hossain, M. A., Izuishi, K., and Maeta, H. (2003). Effect of short-term administration of prostaglandin E1
1282 on viability after ischemia/reperfusion injury with extended hepatectomy in cirrhotic rat liver. *World J*
1283 *Surg* 27, 1155–1160. doi:10.1007/s00268-003-6914-y
- 1284 Hou, C.-T., Chen, Y.-L., Lin, C.-C., Chou, C.-T., Lin, K.-H., Lin, P.-Y., et al. (2018). Portal venous
1285 velocity affects liver regeneration after right lobe living donor hepatectomy. *PLoS one* 13, e0204163.
1286 doi:10.1371/journal.pone.0204163
- 1287 Hu, J., Lü, S., Feng, S., and Long, M. (2017). Flow dynamics analyses of pathophysiological liver lobules
1288 using porous media theory. *Acta Mechanica Sinica* 33, 823–832. doi:10.1007/s10409-017-0674-7
- 1289 Huang, H., Deng, M., Jin, H., Liu, A., Dahmen, U., and Dirsch, O. (2014). Reduced Hepatic Arterial
1290 Perfusion Impairs the Recovery From Focal Hepatic Venous Outflow Obstruction in Liver-Resected
1291 Rats. *Transplantation* 97, 1009–1018. doi:10.1097/TP.0000000000000089
- 1292 Huang, H., Deng, M., Jin, H., Liu, A., Dirsch, O., and Dahmen, U. (2011). Hepatic arterial perfusion
1293 is essential for the spontaneous recovery from focal hepatic venous outflow obstruction in rats. *Am J*
1294 *Transplant* 11, 2342–2352. doi:10.1111/j.1600-6143.2011.03682.x
- 1295 Hucka, M., Bergmann, F. T., Chaouiya, C., Dräger, A., Hoops, S., Keating, S. M., et al. (2019). The
1296 systems biology markup language (sbml): Language specification for level 3 version 2 core release 2.
1297 *Journal of integrative bioinformatics* 16. doi:10.1515/jib-2019-0021
- 1298 Hyötyläinen, T., Jerby, L., Petäjä, E. M., Mattila, I., Jäntti, S., Auvinen, P., et al. (2016). Genome-scale
1299 study reveals reduced metabolic adaptability in patients with non-alcoholic fatty liver disease. *Nature*
1300 *communications* 7, 8994. doi:10.1038/ncomms9994
- 1301 Iimuro, Y., Kondo, Y., Suzumura, K., Uyama, N., Asano, Y., Hirano, T., et al. (2013). Regional hepatic
1302 regeneration after liver resection correlates well with preceding changes in the regional portal circulation
1303 in humans. *Digestive diseases and sciences* 58, 3001–3009. doi:10.1007/s10620-013-2756-0
- 1304 Isogai, T., Park, J. S., and Danuser, G. (2017). Cell forces meet cell metabolism. *Nat Cell Biol* 19, 591–593.
1305 doi:10.1038/ncb3542
- 1306 Itoh, S., Yoshizumi, T., Shirabe, K., Kimura, K., Okabe, H., Harimoto, N., et al. (2017). Functional remnant
1307 liver assessment predicts liver-related morbidity after hepatic resection in patients with hepatocellular
1308 carcinoma. *Hepatology research : the official journal of the Japan Society of Hepatology* 47, 398–404.
1309 doi:10.1111/hepr.12761
- 1310 Iwasaki, J., Afify, M., Bleilevens, C., Klinge, U., Weiskirchen, R., Steitz, J., et al. (2019). The Impact of
1311 a Nitric Oxide Synthase Inhibitor (L-NAME) on Ischemia–Reperfusion Injury of Cholestatic Livers
1312 by Pringle Maneuver and Liver Resection after Bile Duct Ligation in Rats. *Int J Mol Sci* 20, E2114.
1313 doi:10.3390/ijms20092114
- 1314 Jahng, G.-H., Li, K.-L., Ostergaard, L., and Calamante, F. (2014). Perfusion magnetic resonance imaging:
1315 a comprehensive update on principles and techniques. *Korean journal of radiology* 15, 554–577.
1316 doi:10.3348/kjr.2014.15.5.554
- 1317 Jang, S., Lee, J. M., Lee, D. H., Joo, I., Yoon, J. H., Chang, W., et al. (2017). Value of mr elastography
1318 for the preoperative estimation of liver regeneration capacity in patients with hepatocellular carcinoma.
1319 *Journal of magnetic resonance imaging : JMRI* 45, 1627–1636. doi:10.1002/jmri.25517
- 1320 Jansen, M., ten Klooster, J. P., Offerhaus, G. J., and Clevers, H. (2009). Lkb1 and ampk family signaling:
1321 the intimate link between cell polarity and energy metabolism. *Physiological reviews* 89, 777–798.
1322 doi:10.1152/physrev.00026.2008
- 1323 Jara, M., Reese, T., Malinowski, M., Valle, E., Seehofer, D., Puhl, G., et al. (2015). Reductions
1324 in post-hepatectomy liver failure and related mortality after implementation of the limax algorithm
1325 in preoperative work-up: a single-centre analysis of 1170 hepatectomies of one or more segments.

- 1326 *HPB : the official journal of the International Hepato Pancreato Biliary Association* 17, 651–658.
1327 doi:10.1111/hpb.12424
- 1328 Jepsen, B. N., Andersen, K. J., Knudsen, A. R., Nyengaard, J. R., Hamilton-Dutoit, S., Svendsen, P., et al.
1329 (2015). Anti-inflammatory liposomes have no impact on liver regeneration in rats. *Annals of medicine
1330 and surgery* (2012) 4, 452–461. doi:10.1016/j.amsu.2015.10.018
- 1331 Johnson, S. P., Ramasawmy, R., Campbell-Washburn, A. E., Wells, J. A., Robson, M., Rajkumar, V., et al.
1332 (2016). Acute changes in liver tumour perfusion measured non-invasively with arterial spin labelling.
1333 *British journal of cancer* 114, 897–904. doi:10.1038/bjc.2016.51
- 1334 Jones, H. and Rowland-Yeo, K. (2013). Basic concepts in physiologically based pharmacokinetic modeling
1335 in drug discovery and development. *CPT: pharmacometrics & systems pharmacology* 2, e63. doi:10.
1336 1038/psp.2013.41
- 1337 Jung, Y. S., Kim, S. J., Kwon, D. Y., Jun, D. S., and Kim, Y. C. (2013). Significance of alterations in the
1338 metabolomics of sulfur-containing amino acids during liver regeneration. *Biochimie* 95, 1605–1610.
1339 doi:10.1016/j.biochi.2013.04.015
- 1340 Kachaylo, E., Tschor, C., Calo, N., Borgeaud, N., Ungethüm, U., Limani, P., et al. (2017). PTEN
1341 Down-Regulation Promotes β -Oxidation to Fuel Hypertrophic Liver Growth After Hepatectomy in Mice.
1342 *Hepatology* 66, 908–921. doi:10.1002/hep.29226
- 1343 Kahn, D., van Hoorn-Hickman, R., and Terblanche, J. (1984). Liver blood flow after partial hepatectomy
1344 in the pig. *J Surg Res* 37, 290–294. doi:10.1016/0022-4804(84)90191-4
- 1345 Kanehisa, M. and Goto, S. (2000). Kegg: kyoto encyclopedia of genes and genomes. *Nucleic acids
1346 research* 28, 27–30. doi:10.1093/nar/28.1.27
- 1347 Kang, N. (2020). Mechanotransduction in Liver Diseases. *Semin Liver Dis* 40, 84–90. doi:10.1055/
1348 s-0039-3399502
- 1349 Kawaguchi, D., Hiroshima, Y., Kumamoto, T., Mori, R., Matsuyama, R., Ichikawa, Y., et al. (2019). Effect
1350 of portal vein ligation plus venous congestion on liver regeneration in rats. *Annals of hepatology* 18,
1351 89–100. doi:10.5604/01.3001.0012.7866
- 1352 Kawasaki, T., Moriyasu, F., Kimura, T., Someda, H., Fukuda, Y., and Ozawa, K. (1991). Changes in
1353 portal blood flow consequent to partial hepatectomy: Doppler estimation. *Radiology* 180, 373–377.
1354 doi:10.1148/radiology.180.2.2068298
- 1355 Keating, S. M., Waltemath, D., König, M., Zhang, F., Dräger, A., Chaouiya, C., et al. (2020). SBML
1356 Level 3: an extensible format for the exchange and reuse of biological models. *Mol Syst Biol* 16, e9110.
1357 doi:10.15252/msb.20199110
- 1358 Keiding, S., Sørensen, M., Frisch, K., Gormsen, L. C., and Munk, O. L. (2018). Quantitative PET of liver
1359 functions. *Am J Nucl Med Mol Imaging* 8, 73–85
- 1360 Kim, D. K., Choi, J.-I., Choi, M. H., Park, M. Y., Lee, Y. J., Rha, S. E., et al. (2018). Prediction of
1361 posthepatectomy liver failure: MRI with hepatocyte-specific contrast agent versus indocyanine green
1362 clearance test. *AJR. American journal of roentgenology* 211, 580–587. doi:10.2214/AJR.17.19206
- 1363 Kin, Y., Nimura, Y., Hayakawa, N., Kamiya, J., Kondo, S., Nagino, M., et al. (1994). Doppler analysis
1364 of hepatic blood flow predicts liver dysfunction after major hepatectomy. *World journal of surgery* 18,
1365 143–149. doi:10.1007/BF00348207
- 1366 Kirch, J., Thomaseth, C., Jensch, A., and Radde, N. E. (2016). The effect of model rescaling and
1367 normalization on sensitivity analysis on an example of a mapk pathway model. *EPJ Nonlinear
1368 Biomedical Physics* 4, e107165. doi:10.1140/epjnbp/s40366-016-0030-z

- 1369 Köller, A., Grzegorzewski, J., Tautenhahn, H.-M., and König, M. (2021). Prediction of survival after
1370 partial hepatectomy using a physiologically based pharmacokinetic model of indocyanine green liver
1371 function tests. *bioRxiv* doi:10.1101/2021.06.15.448411
- 1372 König, M., Bulik, S., and Holzhütter, H.-G. (2012). Quantifying the contribution of the liver to glucose
1373 homeostasis: a detailed kinetic model of human hepatic glucose metabolism. *PLoS Comput Biol* 8,
1374 e1002577. doi:10.1371/journal.pcbi.1002577
- 1375 König, M. and Holzhütter, H.-G. (2012). Kinetic modeling of human hepatic glucose metabolism in type 2
1376 diabetes mellitus predicts higher risk of hypoglycemic events in rigorous insulin therapy. *J Biol Chem*
1377 287, 36978–36989. doi:10.1074/jbc.M112.382069
- 1378 Kreutz, C., Bartolome Rodriguez, M. M., Maiwald, T., Seidl, M., Blum, H. E., Mohr, L., et al. (2007).
1379 An error model for protein quantification. *Bioinformatics* 23, 2747–2753. doi:10.1093/bioinformatics/
1380 btm397
- 1381 Kruepunga, N., Hakvoort, T. B. M., Hikspoors, J. P. J. M., Köhler, S. E., and Lamers, W. H. (2019).
1382 Anatomy of rodent and human livers: What are the differences? *Biochimica et biophysica acta. Molecular*
1383 *basis of disease* 1865, 869–878. doi:10.1016/j.bbadi.2018.05.019
- 1384 Kubota, K. (1997). Measurement of liver volume and hepatic functional reserve as a guide to decision-
1385 making in resectional surgery for hepatic tumors. *Hepatology* 26, 1176–1181. doi:10.1053/jhep.1997.
1386 v26.pm0009362359
- 1387 Kumar, S., Zou, Y., Bao, Q., Wang, M., and Dai, G. (2013). Proteomic analysis of immediate-early
1388 response plasma proteins after 70% and 90% partial hepatectomy. *Hepatology research : the official*
1389 *journal of the Japan Society of Hepatology* 43, 876–889. doi:10.1111/hepr.12030
- 1390 Labibi, B., Bashkurov, M., Wrana, J. L., and Attisano, L. (2020). Modeling the Control of TGF- β /Smad
1391 Nuclear Accumulation by the Hippo Pathway Effectors, Taz/Yap. *iScience* 23, 101416. doi:10.1016/j.
1392isci.2020.101416
- 1393 Lagneau, F., Marty, J., Beyne, P., and Tod, M. (2005). Physiological modeling for indirect evaluation of drug
1394 tissular pharmacokinetics under non-steady-state conditions: an example of antimicrobial prophylaxis
1395 during liver surgery. *J Pharmacokinet Pharmacodyn* 32, 1–32. doi:10.1007/s10928-005-2101-0
- 1396 Lai, H.-S., Chen, Y., Lin, W.-H., Chen, C.-N., Wu, H.-C., Chang, C.-J., et al. (2005). Quantitative gene
1397 expression analysis by cDNA microarray during liver regeneration after partial hepatectomy in rats. *Surg*
1398 *Today* 35, 396–403. doi:10.1007/s00595-004-2962-7
- 1399 Lee, D. H., Lee, J. M., Yi, N.-J., Lee, K.-W., Suh, K.-S., Lee, J.-H., et al. (2017). Hepatic stiffness
1400 measurement by using mr elastography: prognostic values after hepatic resection for hepatocellular
1401 carcinoma. *European radiology* 27, 1713–1721. doi:10.1007/s00330-016-4499-8
- 1402 Leporq, B., Daire, J.-L., Pastor, C. M., Deltenre, P., Sempoux, C., Schmidt, S., et al. (2018). Quantification
1403 of hepatic perfusion and hepatocyte function with dynamic gadoteric acid-enhanced mri in patients
1404 with chronic liver disease. *Clinical science (London, England : 1979)* 132, 813–824. doi:10.1042/
1405 CS20171131
- 1406 Leung, J. C.-F., Loong, T. C.-W., Pang, J., Wei, J. L., and Wong, V. W.-S. (2018). Invasive and non-invasive
1407 assessment of portal hypertension. *Hepatol Int* 12, 44–55. doi:10.1007/s12072-017-9795-0
- 1408 Li, B., Zhu, Y., Xie, L., Hu, S., Liu, S., and Jiang, X. (2018a). Portal vein ligation alters coding and
1409 noncoding gene expression in rat livers. *Biochem Cell Biol* 96, 1–10. doi:10.1139/bcb-2017-0070
- 1410 Li, C. X., Chen, L. L., Li, X. C., Ng, K. T.-P., Yang, X. X., Lo, C. M., et al. (2018b). ApoA-1
1411 accelerates regeneration of small-for-size fatty liver graft after transplantation. *Life Sci* 215, 128–135.
1412 doi:10.1016/j.lfs.2018.10.053

- 1413 Li, C. X., Wang, H. W., Jiang, W. J., Li, G. C., Zhang, Y. D., Luo, C. H., et al. (2020a). The Inhibition of
1414 Aldose Reductase Accelerates Liver Regeneration through Regulating Energy Metabolism. *Oxid Med
1415 Cell Longev* 2020, 3076131. doi:10.1155/2020/3076131
- 1416 Li, J., Li, X., Xu, W., Wang, S., Hu, Z., Zhang, Q., et al. (2015). Antifibrotic effects of luteolin on hepatic
1417 stellate cells and liver fibrosis by targeting AKT/mTOR/p70S6K and TGF β /Smad signalling pathways.
1418 *Liver Int* 35, 1222–1233. doi:10.1111/liv.12638
- 1419 Li, W., Li, P., Li, N., Du, Y., Lü, S., Elad, D., et al. (2020b). Matrix stiffness and shear stresses
1420 modulate hepatocyte functions in a fibrotic liver sinusoidal model. *American journal of physiology.
1421 Gastrointestinal and liver physiology* doi:10.1152/ajpgi.00379.2019
- 1422 Lin, C.-W., Chen, Y.-S., Lin, C.-C., Chen, Y.-J., Lo, G.-H., Lee, P.-H., et al. (2015). Amiodarone as
1423 an autophagy promoter reduces liver injury and enhances liver regeneration and survival in mice after
1424 partial hepatectomy. *Sci Rep* 5, 15807. doi:10.1038/srep15807
- 1425 Lin, Z., Chen, R., Gao, B., Qin, S., Wu, B., Liu, J., et al. (2021). A highly parallel simulation of
1426 patient-specific hepatic flows. *Int J Numer Method Biomed Eng*, e3451doi:10.1002/cnm.3451
- 1427 Liska, V., Slowik, P., Eggenhofer, E., Treska, V., Renner, P., Popp, F. C., et al. (2009). Intraportal
1428 injection of porcine multipotent mesenchymal stromal cells augments liver regeneration after portal vein
1429 embolization. *In Vivo* 23, 229–235
- 1430 Liu, H.-X., Fang, Y., Hu, Y., Gonzalez, F. J., Fang, J., and Wan, Y.-J. Y. (2013). PPAR β Regulates Liver
1431 Regeneration by Modulating Akt and E2f Signaling. *PLoS One* 8, e65644. doi:10.1371/journal.pone.
1432 0065644
- 1433 Liu, Q., Pu, S., Chen, L., Shen, J., Cheng, S., Kuang, J., et al. (2019). Liver-specific Sirtuin6 ablation
1434 impairs liver regeneration after 2/3 partial hepatectomy. *Wound Repair Regen* 27, 366–374. doi:10.1111/
1435 wrw.12703
- 1436 Liu, X., Jiang, H., Chen, J., Zhou, Y., Huang, Z., and Song, B. (2017). Gadoxetic acid disodium-enhanced
1437 magnetic resonance imaging outperformed multidetector computed tomography in diagnosing small
1438 hepatocellular carcinoma: A meta-analysis. *Liver Transpl* 23, 1505–1518. doi:10.1002/lt.24867
- 1439 Lock, J. F., Malinowski, M., Seehofer, D., Hoppe, S., Röhl, R. I., Niehues, S. M., et al. (2012). Function and
1440 volume recovery after partial hepatectomy: influence of preoperative liver function, residual liver volume,
1441 and obesity. *Langenbeck's archives of surgery* 397, 1297–1304. doi:10.1007/s00423-012-0972-2
- 1442 Love, M. I., Huber, W., and Anders, S. (2014). Moderated estimation of fold change and dispersion for
1443 rna-seq data with deseq2. *Genome biology* 15, 550. doi:10.1186/s13059-014-0550-8
- 1444 Lu, T., Hao, J., Shen, C., Gu, G., Zhang, J., and Xu, N. (2018). Partial Hepatectomy-Induced Upregulation
1445 of miR-1907 Accelerates Liver Regeneration by Activation Autophagy. *Biomed Res Int* 2018, 3817057.
1446 doi:10.1155/2018/3817057
- 1447 Lu, Y., Liu, P., Fu, P., Chen, Y., Nan, D., and Yang, X. (2017). Comparison of the dwi and gd-eob-
1448 dtpa-enhanced mri on assessing the hepatic ischemia and reperfusion injury after partial hepatectomy.
1449 *Biomedicine & pharmacotherapy = Biomedecine & pharmacotherapie* 86, 118–126. doi:10.1016/j.
1450 biopha.2016.11.123
- 1451 Lu, Y., Lohitnavy, M., Reddy, M. B., Lohitnavy, O., Ashley, A., and Yang, R. S. H. (2006). An updated physiologically based pharmacokinetic model for hexachlorobenzene: incorporation of
1452 pathophysiological states following partial hepatectomy and hexachlorobenzene treatment. *Toxicol Sci*
1453 91, 29–41. doi:10.1093/toxsci/kfj133
- 1455 Ma, R., Hunter, P., Cousins, W., Ho, H., Bartlett, A., and Safaei, S. (2020). Modeling the hepatic arterial
1456 flow in living liver donor after left hepatectomy and postoperative boundary condition exploration. *Int J
1457 Numer Method Biomed Eng* 36, e3268. doi:10.1002/cnm.3268

- 1458 Madrahimov, N., Dirsch, O., Broelsch, C., and Dahmen, U. (2006). Marginal hepatectomy in the rat: from
1459 anatomy to surgery. *Ann Surg* 244, 89–98. doi:10.1097/01.sla.0000218093.12408.0f
- 1460 Mann, F. C., Fishback, F. C., Gay, J. S., and Green, G. F. (1931). Experimental pathology of the liver.
1461 *A.M.A. Arch Pathol* 12, 787–793
- 1462 Mardinoglu, A., Agren, R., Kampf, C., Asplund, A., Uhlen, M., and Nielsen, J. (2014). Genome-scale
1463 metabolic modelling of hepatocytes reveals serine deficiency in patients with non-alcoholic fatty liver
1464 disease. *Nat Commun* 5, 3083. doi:10.1038/ncomms4083
- 1465 Mardinoglu, A., Wu, H., Bjornson, E., Zhang, C., Hakkarainen, A., Räsänen, S. M., et al. (2018). An
1466 integrated understanding of the rapid metabolic benefits of a carbohydrate-restricted diet on hepatic
1467 steatosis in humans. *Cell metabolism* 27, 559–571.e5. doi:10.1016/j.cmet.2018.01.005
- 1468 Martirosian, P., Pohmann, R., Schraml, C., Schwartz, M., Kuestner, T., Schwenzer, N. F., et al. (2019).
1469 Spatial-temporal perfusion patterns of the human liver assessed by pseudo-continuous arterial spin
1470 labeling mri. *Zeitschrift fur medizinische Physik* 29, 173–183. doi:10.1016/j.zemedi.2018.08.004
- 1471 Means, S. A. and Ho, H. (2019). A spatial-temporal model for zonal hepatotoxicity of acetaminophen.
1472 *Drug metabolism and pharmacokinetics* 34, 71–77. doi:10.1016/j.dmpk.2018.09.266
- 1473 Meyer, K., Morales-Navarrete, H., Seifert, S., Wilsch-Braeuninger, M., Dahmen, U., Tanaka, E. M., et al.
1474 (2020). Bile canaliculi remodeling activates YAP via the actin cytoskeleton during liver regeneration.
1475 *Mol Syst Biol* 16, e8985. doi:10.15252/msb.20198985
- 1476 Michalopoulos, G. K. (2017). Hepatostat: Liver regeneration and normal liver tissue maintenance.
1477 *Hepatology* 65, 1384–1392. doi:10.1002/hep.28988
- 1478 Mihaylova, M. M. and Shaw, R. J. (2011). The ampk signalling pathway coordinates cell growth, autophagy
1479 and metabolism. *Nature cell biology* 13, 1016–1023. doi:10.1038/ncb2329
- 1480 Monga, S. P. S. (2014). Role and regulation of β -catenin signaling during physiological liver growth. *Gene
1481 Expr* 16, 51–62. doi:10.3727/105221614X13919976902138
- 1482 Moreno-Carranza, B., Goya-Arce, M., Vega, C., Adán, N., Triebel, J., López-Barrera, F., et al. (2013).
1483 Prolactin promotes normal liver growth, survival, and regeneration in rodents: effects on hepatic il-6,
1484 suppressor of cytokine signaling-3, and angiogenesis. *American journal of physiology. Regulatory,
1485 integrative and comparative physiology* 305, R720–6. doi:10.1152/ajpregu.00282.2013
- 1486 Muhi, A., Ichikawa, T., Motosugi, U., Sano, K., Fatima, Z., Matsuda, M., et al. (2013). Diffusion-weighted
1487 imaging of hepatocellular carcinoma for predicting early recurrence and survival after hepatectomy.
1488 *Hepatology international* 7, 662–668. doi:10.1007/s12072-012-9383-2
- 1489 Müsch, A. (2014). The unique polarity phenotype of hepatocytes. *Experimental cell research* 328, 276–283.
1490 doi:10.1016/j.yexcr.2014.06.006
- 1491 Nagano, Y., Nagahori, K., Yoshiro, F., Hamaguchi, Y., Ishikawa, T., Ichikawa, Y., et al. (2004). Gene
1492 expression profile analysis of regenerating liver after portal vein ligation in rats by a cDNA microarray
1493 system. *Liver Int* 24, 253–258. doi:10.1111/j.1478-3231.2004.0912.x
- 1494 Neal, M. L., König, M., Nickerson, D., Misirlı, G., Kalbasi, R., Dräger, A., et al. (2019). Harmonizing
1495 semantic annotations for computational models in biology. *Briefings in bioinformatics* 20, 540–550.
1496 doi:10.1093/bib/bby087
- 1497 Niiya, T., Murakami, M., Aoki, T., Murai, N., Shimizu, Y., and Kusano, M. (1999). Immediate increase of
1498 portal pressure, reflecting sinusoidal shear stress, induced liver regeneration after partial hepatectomy.
1499 *Journal of hepato-biliary-pancreatic surgery* 6, 275–280. doi:10.1007/s005340050118
- 1500 Nikmaneshi, M. R., Firoozabadi, B., and Munn, L. L. (2020). A mechanobiological mathematical model
1501 of liver metabolism. *Biotechnol Bioeng* 117, 2861–2874. doi:10.1002/bit.27451

- 1502 Nishii, K., Brodin, E., Renshaw, T., Weesner, R., Moran, E., Soker, S., et al. (2018). Shear stress upregulates
1503 regeneration-related immediate early genes in liver progenitors in 3d ecm-like microenvironments.
1504 *Journal of cellular physiology* 233, 4272–4281. doi:10.1002/jcp.26246
- 1505 Nista, E. C., Fini, L., Armuzzi, A., Candelli, M., Zocco, M. A., Cazzato, I. A., et al. (2004). 13C-breath
1506 tests in the study of microsomal liver function. *Eur Rev Med Pharmacol Sci* 8, 33–46
- 1507 Nobuoka, T., Mizuguchi, T., Oshima, H., Shibata, T., Kimura, Y., Mitaka, T., et al. (2006). Portal
1508 blood flow regulates volume recovery of the rat liver after partial hepatectomy: molecular evaluation.
1509 *European surgical research. Europaische chirurgische Forschung. Recherches chirurgicales europeennes*
1510 38, 522–532. doi:10.1159/000096292
- 1511 Nonami, T., Nakao, A., Kurokawa, T., Inagaki, H., Matsushita, Y., Sakamoto, J., et al. (1999). Blood loss
1512 and icg clearance as best prognostic markers of post-hepatectomy liver failure. *Hepato-gastroenterology*
1513 46, 1669–1672
- 1514 Palaniyappan, N., Cox, E., Bradley, C., Scott, R., Austin, A., O'Neill, R., et al. (2016). Non-invasive
1515 assessment of portal hypertension using quantitative magnetic resonance imaging. *J. Hepatol.* 65,
1516 1131–1139. doi:10.1016/j.jhep.2016.07.021
- 1517 Pang, K. S. and Rowland, M. (1977). Hepatic clearance of drugs. i. theoretical considerations of a "well-
1518 stirred" model and a "parallel tube" model. influence of hepatic blood flow, plasma and blood cell binding,
1519 and the hepatocellular enzymatic activity on hepatic drug clearance. *Journal of pharmacokinetics and*
1520 *biopharmaceutics* 5, 625–653. doi:10.1007/BF01059688
- 1521 Papatheodorou, I., Moreno, P., Manning, J., Fuentes, A. M.-P., George, N., Fexova, S., et al. (2020).
1522 Expression Atlas update: from tissues to single cells. *Nucleic Acids Res* 48, D77–D83. doi:10.1093/nar/
1523 gkz947
- 1524 Peng, T., Liu, L., MacLean, A. L., Wong, C. W., Zhao, W., and Nie, Q. (2017). A mathematical model of
1525 mechanotransduction reveals how mechanical memory regulates mesenchymal stem cell fate decisions.
1526 *BMC Syst Biol* 11, 55. doi:10.1186/s12918-017-0429-x
- 1527 Perel, P., Roberts, I., Sena, E., Wheble, P., Briscoe, C., Sandercock, P., et al. (2007). Comparison of
1528 treatment effects between animal experiments and clinical trials: systematic review. *BMJ (Clinical*
1529 *research ed.)* 334, 197. doi:10.1136/bmj.39048.407928.BE
- 1530 Periwal, V., Gaillard, J. R., Needleman, L., and Doria, C. (2014). Mathematical model of liver regeneration
1531 in human live donors. *Journal of cellular physiology* 229, 599–606. doi:10.1002/jcp.24482
- 1532 Pibiri, M. (2018). Liver regeneration in aged mice: new insights. *Aging (Albany NY)* 10, 1801–1824.
1533 doi:10.18632/aging.101524
- 1534 Pibiri, M., Sulas, P., Leoni, V. P., Perra, A., Kowalik, M. A., Cordella, A., et al. (2015). Global gene
1535 expression profile of normal and regenerating liver in young and old mice. *Age (Dordr)* 37, 9796.
1536 doi:10.1007/s11357-015-9796-7
- 1537 Picard, C., Starkel, P., Sempoux, C., Saliez, A., Lebrun, V., and Horsmans, Y. (2004). Molecular
1538 mechanisms of apoptosis in the liver of rats after portal branch ligation with and without retrorsine. *Lab*
1539 *Invest* 84, 618–628. doi:10.1038/labinvest.3700085
- 1540 Pivovarov, D., Willner, K., Steinmann, P., Brumme, S., Müller, M., Srisupattarawanit, T., et al. (2019).
1541 Challenges of order reduction techniques for problems involving polymorphic uncertainty. *GAMM-*
1542 *Mitteilungen* 42, e201900011. doi:10.1002/gamm.201900011
- 1543 Pocaterra, A., Romani, P., and Dupont, S. (2020). Yap/taz functions and their regulation at a glance.
1544 *Journal of cell science* 133. doi:10.1242/jcs.230425

- 1545 Puhl, G., Schaser, K. D., Vollmar, B., Menger, M. D., and Settmacher, U. (2003). Noninvasive in
1546 vivo analysis of the human hepatic microcirculation using orthogonal polarization spectral imaging.
1547 *Transplantation* 75, 756–761. doi:10.1097/01.TP.0000056634.18191.1A
- 1548 Rani, H. P., Sheu, T. W. H., Chang, T. M., and Liang, P. C. (2006). Numerical investigation of non-
1549 newtonian microcirculatory blood flow in hepatic lobule. *Journal of biomechanics* 39, 551–563.
1550 doi:10.1016/j.jbiomech.2004.11.029
- 1551 Ray, S., Mehta, N. N., Golhar, A., and Nundy, S. (2018). Post hepatectomy liver failure - A comprehensive
1552 review of current concepts and controversies. *Ann Med Surg (Lond)* 34, 4–10. doi:10.1016/j.amsu.2018.
1553 08.012
- 1554 Ren, P., Kang, Z., Gu, G., Liu, Y., Xu, W., Tao, H., et al. (2008). Hyperbaric oxygen preconditioning
1555 promotes angiogenesis in rat liver after partial hepatectomy. *Life sciences* 83, 236–241. doi:10.1016/j.lfs.2008.06.011
- 1557 Ren, W., Chen, G., Wang, X., Zhang, A., Li, C., Lv, W., et al. (2015). Simultaneous bile duct and portal
1558 vein ligation induces faster atrophy/hypertrophy complex than portal vein ligation: role of bile acids. *Sci
1559 Rep* 5, 8455. doi:10.1038/srep08455
- 1560 Rib, L., Villeneuve, D., Minocha, S., Praz, V., Hernandez, N., Guex, N., et al. (2018). Cycles of gene
1561 expression and genome response during mammalian tissue regeneration. *Epigenetics Chromatin* 11, 52.
1562 doi:10.1186/s13072-018-0222-0
- 1563 Ricken, T. and Bluhm, J. (2010). Remodeling and growth of living tissue: a multiphase theory. *Archive of
1564 Applied Mechanics* 80, 453–465
- 1565 Ricken, T., Dahmen, U., and Dirsch, O. (2010). A biphasic model for sinusoidal liver perfusion remodeling
1566 after outflow obstruction. *Biomechanics and modeling in mechanobiology* 9, 435–450. doi:10.1007/
1567 s10237-009-0186-x
- 1568 Ricken, T. and Lambers, L. (2019). On computational approaches of liver lobule function and perfusion
1569 simulation. *GAMM-Mitteilungen* 42, e0198060. doi:10.1002/gamm.201900016
- 1570 Ricken, T., Schwarz, A., and Bluhm, J. (2007). A triphasic model of transversely isotropic biological
1571 tissue with applications to stress and biologically induced growth. *Computational Materials Science* 39,
1572 124–136. doi:10.1016/j.commatsci.2006.03.025
- 1573 Ricken, T., Werner, D., Holzhütter, H. G., König, M., Dahmen, U., and Dirsch, O. (2015). Modeling
1574 function-perfusion behavior in liver lobules including tissue, blood, glucose, lactate and glycogen by use
1575 of a coupled two-scale pde-ode approach. *Biomechanics and modeling in mechanobiology* 14, 515–536.
1576 doi:10.1007/s10237-014-0619-z
- 1577 Rinck, P. A., Petersen, S. B., and Lauterbur, P. C. (1984). [NMR imaging of fluorine-containing substances.
1578 19-Fluorine ventilation and perfusion studies]. *Rofo* 140, 239–243. doi:10.1055/s-2008-1052964
- 1579 Roldán-Alzate, A., Frydrychowicz, A., Said, A., Johnson, K. M., Francois, C. J., Wieben, O., et al. (2015).
1580 Impaired regulation of portal venous flow in response to a meal challenge as quantified by 4D flow MRI.
1581 *J Magn Reson Imaging* 42, 1009–1017. doi:10.1002/jmri.24886
- 1582 Rosen, B. R., Belliveau, J. W., Vevea, J. M., and Brady, T. J. (1990). Perfusion imaging with nmr contrast
1583 agents. *Magnetic resonance in medicine* 14, 249–265. doi:10.1002/mrm.1910140211
- 1584 Rous, P. and Larimore, L. D. (1920). RELATION OF THE PORTAL BLOOD TO LIVER MAINTENANCE
1585 : A DEMONSTRATION OF LIVER ATROPHY CONDITIONAL ON COMPENSATION. *J Exp Med*
1586 31, 609–632. doi:10.1084/jem.31.5.609
- 1587 Rowland, M., Benet, L. Z., and Graham, G. G. (1973). Clearance concepts in pharmacokinetics. *Journal
1588 of pharmacokinetics and biopharmaceutics* 1, 123–136. doi:10.1007/BF01059626

- 1589 Rozga, J., Jeppsson, B., and Bengmark, S. (1986). Portal branch ligation in the rat. Reevaluation of a
1590 model. *Am J Pathol* 125, 300–308
- 1591 Rubin, T. M., Heyne, K., Luchterhand, A., Jan Bednarsch, n., W R Vondran, F., Polychronidis, G., et al.
1592 (2017). Kinetic validation of the LiMAX test during 10 000 intravenous 13C-methacetin breath tests. *J
1593 Breath Res* 12, 016005. doi:10.1088/1752-7163/aa820b
- 1594 Rui, L. (2014). Energy metabolism in the liver. *Compr Physiol* 4, 177–197. doi:10.1002/cphy.c130024
- 1595 Saito, S., Togo, S., Morioka, D., Matsuo, K.-i., Yoshimoto, N., Nagano, Y., et al. (2006). A rat model of a
1596 repeat 70% major hepatectomy. *The Journal of surgical research* 134, 322–326. doi:10.1016/j.jss.2006.
1597 01.008
- 1598 Saito, Y., Morine, Y., Iwahashi, S., Ikemoto, T., Imura, S., Yamanaka-Okumura, H., et al. (2018). Changes
1599 of liver metabolites following hepatectomy with ischemia reperfusion towards liver regeneration. *Annals
1600 of gastroenterological surgery* 2, 204–211. doi:10.1002/ags3.12058
- 1601 Saltelli, A., Bammer, G., Bruno, I., Charters, E., Di Fiore, M., Didier, E., et al. (2020). Five ways to ensure
1602 that models serve society: a manifesto. *Nature* 582, 482–484. doi:10.1038/d41586-020-01812-9
- 1603 Salvi, A. M. and DeMali, K. A. (2018). Mechanisms linking mechanotransduction and cell metabolism.
1604 *Curr Opin Cell Biol* 54, 114–120. doi:10.1016/j.ceb.2018.05.004
- 1605 Samino, S., Revuelta-Cervantes, J., Vinaixa, M., Rodríguez, M. Á., Valverde, A. M., and Correig, X.
1606 (2013). A (1)h nmr metabolic profiling to the assessment of protein tyrosine phosphatase 1b role in liver
1607 regeneration after partial hepatectomy. *Biochimie* 95, 808–816. doi:10.1016/j.biochi.2012.11.015
- 1608 Sato, N., Kenjo, A., Kimura, T., Okada, R., Ishigame, T., Kofunato, Y., et al. (2018). Prediction of
1609 major complications after hepatectomy using liver stiffness values determined by magnetic resonance
1610 elastography. *The British journal of surgery* 105, 1192–1199. doi:10.1002/bjs.10831
- 1611 Sato, Y., Koyama, S., Tsukada, K., and Hatakeyama, K. (1997). Acute portal hypertension reflecting
1612 shear stress as a trigger of liver regeneration following partial hepatectomy. *Surg Today* 27, 518–526.
1613 doi:10.1007/BF02385805
- 1614 Sato, Y., Tsukada, K., and Hatakeyama, K. (1999). Role of shear stress and immune responses in liver
1615 regeneration after a partial hepatectomy. *Surgery today* 29, 1–9. doi:10.1007/BF02482962
- 1616 Schnitzbauer, A. A., Lang, S. A., Goessmann, H., Nadalin, S., Baumgart, J., Farkas, S. A., et al. (2012).
1617 Right portal vein ligation combined with in situ splitting induces rapid left lateral liver lobe hypertrophy
1618 enabling 2-staged extended right hepatic resection in small-for-size settings. *Annals of surgery* 255,
1619 405–414. doi:10.1097/SLA.0b013e31824856f5
- 1620 Schoen, J. M., Wang, H. H., Minuk, G. Y., and Lautt, W. W. (2001). Shear stress-induced nitric oxide
1621 release triggers the liver regeneration cascade. *Nitric oxide : biology and chemistry* 5, 453–464.
1622 doi:10.1006/niox.2001.0373
- 1623 Schoenheimer, R. (1942). The dynamic state of body constituents. *Harvard University Press, Cambridge,
1624 MA*
- 1625 Scott, K. E., Fraley, S. I., and Rangamani, P. (2020). *Transfer function for YAP/TAZ nuclear translocation
1626 revealed through spatial systems modeling*, vol. 18. doi:10.1101/2020.10.14.340349
- 1627 Sebagh, M., Santoni, M.-J., Hall, B., Borg, J.-P., and Schwartz, M. A. (2009). Regulation of lkb1/strad
1628 localization and function by e-cadherin. *Current biology : CB* 19, 37–42. doi:10.1016/j.cub.2008.11.033
- 1629 Sekine, S., Lan, B. Y.-A., Bedolli, M., Feng, S., and Hebrok, M. (2006). Liver-specific loss of beta-catenin
1630 blocks glutamine synthesis pathway activity and cytochrome p450 expression in mice. *Hepatology
(Baltimore, Md.)* 43, 817–825. doi:10.1002/hep.21131

- 1632 Sheng, R.-F., Yang, L., Jin, K.-P., Wang, H.-Q., Liu, H., Ji, Y., et al. (2018). Assessment of liver regeneration
1633 after associating liver partition and portal vein ligation for staged hepatectomy: a comparative study with
1634 portal vein ligation. *HPB (Oxford)* 20, 305–312. doi:10.1016/j.hpb.2017.09.004
- 1635 Shi, Y., Lawford, P., and Hose, R. (2011). Review of zero-d and 1-d models of blood flow in the
1636 cardiovascular system. *Biomedical engineering online* 10, 33. doi:10.1186/1475-925X-10-33
- 1637 Shin, S.-Y. and Nguyen, L. K. (2016). Unveiling Hidden Dynamics of Hippo Signalling: A Systems
1638 Analysis. *Genes (Basel)* 7. doi:10.3390/genes7080044
- 1639 Shu, X., Li, N., Wu, Y., Li, W., Zhang, X., Li, P., et al. (2021). Mechanotransduction of liver sinusoidal
1640 endothelial cells under varied mechanical stimuli. *Acta Mechanica Sinica* 37, 201–217. doi:10.1007/
1641 s10409-021-01057-3
- 1642 Sluka, J. P., Fu, X., Swat, M., Belmonte, J. M., Cosmanescu, A., Clendenon, S. G., et al. (2016). A
1643 Liver-Centric Multiscale Modeling Framework for Xenobiotics. *PLoS ONE* 11, e0162428. doi:10.1371/
1644 journal.pone.0162428
- 1645 Smith, L. P., Hucka, M., Hoops, S., Finney, A., Ginkel, M., Myers, C. J., et al. (2015). Sbml level 3
1646 package: Hierarchical model composition, version 1 release 3. *Journal of Integrative Bioinformatics*
1647 doi:10.2390/biecoll-jib-2015-268
- 1648 Smith, L. P., Moodie, S. L., Bergmann, F. T., Gillespie, C., Keating, S. M., König, M., et al. (2020).
1649 Systems biology markup language (sbml) level 3 package: Distributions, version 1, release 1. *Journal of*
1650 *integrative bioinformatics* 17. doi:10.1515/jib-2020-0018
- 1651 Song, Z., Gupta, K., Ng, I. C., Xing, J., Yang, Y. A., and Yu, H. (2017). Mechanosensing in liver
1652 regeneration. *Semin Cell Dev Biol* 71, 153–167. doi:10.1016/j.semcd.2017.07.041
- 1653 Stockmann, M., Lock, J. F., Riecke, B., Heyne, K., Martus, P., Fricke, M., et al. (2009). Prediction of
1654 postoperative outcome after hepatectomy with a new bedside test for maximal liver function capacity.
1655 *Annals of surgery* 250, 119–125. doi:10.1097/SLA.0b013e3181ad85b5
- 1656 Strey, C. W., Winters, M. S., Markiewski, M. M., and Lambris, J. D. (2005). Partial hepatectomy induced
1657 liver proteome changes in mice. *Proteomics* 5, 318–325. doi:10.1002/pmic.200400913
- 1658 Sugimoto, T., Yamada, T., Iwata, H., Sekino, T., Matsumoto, S., Ishida, N., et al. (2009). Two-stage portal
1659 vein ligation facilitates liver regeneration in rats. *Eur Surg Res* 42, 181–188. doi:10.1159/000203406
- 1660 Sugiura, R., Kuwatani, M., Nishida, M., Hirata, K., Sano, I., Kato, S., et al. (2019). Correlation between
1661 Liver Elasticity by Ultrasound Elastography and Liver Functional Reserve. *Ultrasound Med Biol* 45,
1662 2704–2712. doi:10.1016/j.ultrasmedbio.2019.06.407
- 1663 Sun, M., Spill, F., and Zaman, M. H. (2016). A Computational Model of YAP/TAZ Mechanosensing.
1664 *Biophys J* 110, 2540–2550. doi:10.1016/j.bpj.2016.04.040
- 1665 Sun, Y., Deng, X., Li, W., Yan, Y., Wei, H., Jiang, Y., et al. (2007). Liver proteome analysis of adaptive
1666 response in rat immediately after partial hepatectomy. *Proteomics* 7, 4398–4407. doi:10.1002/pmic.
1667 200600913
- 1668 Swiderska-Syn, M., Xie, G., Michelotti, G. A., Jewell, M. L., Premont, R. T., Syn, W.-K., et al. (2016).
1669 Hedgehog regulates yes-associated protein 1 in regenerating mouse liver. *Hepatology (Baltimore, Md.)*
1670 64, 232–244. doi:10.1002/hep.28542
- 1671 Takahashi, H., Shigefuku, R., Yoshida, Y., Ikeda, H., Matsunaga, K., Matsumoto, N., et al. (2014).
1672 Correlation between hepatic blood flow and liver function in alcoholic liver cirrhosis. *World J*
1673 *Gastroenterol* 20, 17065–17074. doi:10.3748/wjg.v20.i45.17065
- 1674 Tautenhahn, H.-M., Brückner, S., Baumann, S., Winkler, S., Otto, W., von Bergen, M., et al. (2016).
1675 Attenuation of Postoperative Acute Liver Failure by Mesenchymal Stem Cell Treatment Due to Metabolic
1676 Implications. *Annals of Surgery* 263, 546–556. doi:10.1097/SLA.0000000000001155

- 1677 Tautenhahn, H.-M., Brückner, S., Uder, C., Erler, S., Hempel, M., von Bergen, M., et al. (2017).
1678 Mesenchymal stem cells correct haemodynamic dysfunction associated with liver injury after extended
1679 resection in a pig model. *Sci Rep* 7, 2617. doi:10.1038/s41598-017-02670-8
- 1680 Tchirikov, M., Kertschanska, S., Stürenberg, H. J., and Schröder, H. J. (2002). Liver blood perfusion as a
1681 possible instrument for fetal growth regulation. *Placenta* 23 Suppl A, S153–8. doi:10.1053/plac.2002.
1682 0810
- 1683 Thng, C. H., Koh, T. S., Collins, D. J., and Koh, D. M. (2010). Perfusion magnetic resonance imaging of
1684 the liver. *World journal of gastroenterology* 16, 1598–1609. doi:10.3748/wjg.v16.i13.1598
- 1685 Thomas, M. N., Weninger, E., Angele, M., Bösch, F., Pratschke, S., Andrassy, J., et al. (2015).
1686 Intraoperative simulation of remnant liver function during anatomic liver resection with indocyanine
1687 green clearance (LiMON) measurements. *HPB (Oxford)* 17, 471–476. doi:10.1111/hpb.12380
- 1688 Thomaseth, C. and Radde, N. (2016). Normalization of western blot data affects the statistics of
1689 estimators**this work was supported by the german federal ministry of education and research (bmbf)
1690 within the e:bio-innovationswettbewerb systembiologie project predict (grant number fkz0316186a) and
1691 the german research foundation (dfg) within the cluster of excellence in simulation technology (exc
1692 310/2) at the university of stuttgart. *IFAC-PapersOnLine* 49, 56–62. doi:<https://doi.org/10.1016/j.ifacol.2016.12.103>. Foundations of Systems Biology in Engineering - FOSBE 2016
- 1694 Togo, S., Makino, H., Kobayashi, T., Morita, T., Shimizu, T., Kubota, T., et al. (2004). Mechanism of
1695 liver regeneration after partial hepatectomy using mouse cDNA microarray. *J Hepatol* 40, 464–471.
1696 doi:10.1016/j.jhep.2003.11.005
- 1697 Torre, C., Perret, C., and Colnot, S. (2011). Transcription dynamics in a physiological process: β -catenin
1698 signaling directs liver metabolic zonation. *The international journal of biochemistry & cell biology* 43,
1699 271–278. doi:10.1016/j.biocel.2009.11.004
- 1700 Troelstra, M. A., Witjes, J. J., van Dijk, A.-M., Mak, A. L., Gurney-Champion, O., Runge, J. H., et al.
1701 (2021). Assessment of imaging modalities against liver biopsy in nonalcoholic fatty liver disease: The
1702 amsterdam nafld-nash cohort. *Journal of magnetic resonance imaging : JMRI* doi:10.1002/jmri.27703
- 1703 von Heesen, M., Dold, S., Müller, S., Scheuer, C., Kollmar, O., Schilling, M. K., et al. (2015). Cilostazol
1704 improves hepatic blood perfusion, microcirculation, and liver regeneration after major hepatectomy
1705 in rats. *Liver transplantation : official publication of the American Association for the Study of Liver
1706 Diseases and the International Liver Transplantation Society* 21, 792–800. doi:10.1002/lt.24114.
- 1707 Wan, S., Liu, X., Jiang, H., Teng, Z., and Song, B. (2021). Noninvasive imaging assessment of portal
1708 hypertension: where are we now and where does the future lie? *Expert review of molecular diagnostics*
1709 21, 343–345. doi:10.1080/14737159.2021.1904897
- 1710 Wang, Y., Zhang, L., Ning, J., Zhang, X., Li, X., Zhang, L., et al. (2021a). Preoperative
1711 Remnant Liver Function Evaluation Using a Routine Clinical Dynamic Gd-EOB-DTPA-Enhanced
1712 MRI Protocol in Patients with Hepatocellular Carcinoma. *Ann Surg Oncol* 28, 3672–3682. doi:10.1245/
1713 s10434-020-09361-1
- 1714 Wang, Y., Zhang, L., Ning, J., Zhang, X., Li, X., Zhang, L., et al. (2021b). Preoperative remnant
1715 liver function evaluation using a routine clinical dynamic gd-eob-dtpa-enhanced mri protocol in
1716 patients with hepatocellular carcinoma. *Annals of surgical oncology* 28, 3672–3682. doi:10.1245/
1717 s10434-020-09361-1
- 1718 Wehling, L., Keegan, L., Schmitt, J., Sahle, S., Schirmacher, P., Kummer, U., et al. (2021).
1719 Mathematical modeling of yap and taz nuclear/cytoplasmic shuttling in liver cancer cells. *Zeitschrift für
1720 Gastroenterologie* 59, 4–15

- 1721 Wei, W., Hua, C., Zhang, T., Dirsch, O., Gremse, F., Homeyer, A., et al. (2020). Size of portally deprived
1722 liver lobe after portal vein ligation and additional partial hepatectomy: Result of balancing proliferation
1723 and apoptosis. *Sci Rep* 10, 4893. doi:10.1038/s41598-020-60310-0
- 1724 Wei, W., Zhang, T., Zafarnia, S., Schenk, A., Xie, C., Kan, C., et al. (2016). Establishment of a rat model:
1725 Associating liver partition with portal vein ligation for staged hepatectomy. *Surgery* 159, 1299–1307.
1726 doi:10.1016/j.surg.2015.12.005
- 1727 Weinbren, K. (1955). The portal blood supply and regeneration of the rat liver. *British journal of*
1728 *experimental pathology* 36, 583–591
- 1729 Weinbren, K. and Woodward, E. (1964). DELAYED INCORPORATION OF 32P FROM
1730 ORTHOPHOSPHATE INTO DEOXYRIBONUCLEIC ACID OF RAT LIVER AFTER SUBTOTAL
1731 HEPATECTOMY. *Br J Exp Pathol* 45, 442–449
- 1732 Weiss, J., Ruff, C., Grosse, U., Grözinger, G., Horger, M., Nikolaou, K., et al. (2019). Assessment of
1733 hepatic perfusion using grasp mri: Bringing liver mri on a new level. *Investigative radiology* 54, 737–743.
1734 doi:10.1097/RLI.0000000000000586
- 1735 Wells, R. G. (2005). The role of matrix stiffness in hepatic stellate cell activation and liver fibrosis. *J Clin*
1736 *Gastroenterol* 39, S158–161. doi:10.1097/01.mcg.0000155516.02468.0f
- 1737 Williams, D. S., Detre, J. A., Leigh, J. S., and Koretsky, A. P. (1992). Magnetic resonance imaging of
1738 perfusion using spin inversion of arterial water. *Proceedings of the National Academy of Sciences of the*
1739 *United States of America* 89, 212–216. doi:10.1073/pnas.89.1.212
- 1740 Willmann, S., Schmitt, W., Keldenich, J., and Dressman, J. B. (2003). A physiologic model for simulating
1741 gastrointestinal flow and drug absorption in rats. *Pharm Res* 20, 1766–1771. doi:10.1023/b:pham.
1742 0000003373.72652.c0
- 1743 [Dataset] Winkler, K., Keiding, S., and Tygstrup, N. (1973). Clearance as a quantitative measure of liver
1744 function
- 1745 Xie, C., Wei, W., Schenk, A., Schwen, L. O., Zafarnia, S., Schwier, M., et al. (2016). Visualization
1746 of Vascular and Parenchymal Regeneration after 70% Partial Hepatectomy in Normal Mice. *JoVE*,
1747 53935doi:10.3791/53935
- 1748 Yin, M., Glaser, K. J., Manduca, A., Mounajed, T., Malhi, H., Simonetto, D. A., et al. (2017).
1749 Distinguishing between Hepatic Inflammation and Fibrosis with MR Elastography. *Radiology* 284,
1750 694–705. doi:10.1148/radiol.2017160622
- 1751 Yin, M. and Venkatesh, S. K. (2018). Ultrasound or MR elastography of liver: which one shall I use?
1752 *Abdom Radiol (NY)* 43, 1546–1551. doi:10.1007/s00261-017-1340-z
- 1753 Yoon, J. H., Choi, J.-I., Jeong, Y. Y., Schenk, A., Chen, L., Laue, H., et al. (2016). Pre-treatment estimation
1754 of future remnant liver function using gadoxetic acid mri in patients with hcc. *Journal of hepatology* 65,
1755 1155–1162. doi:10.1016/j.jhep.2016.07.024
- 1756 Yoshida, D., Akahoshi, T., Kawanaka, H., Yamaguchi, S., Kinjo, N., Taketomi, A., et al. (2011). Roles of
1757 vascular endothelial growth factor and endothelial nitric oxide synthase during revascularization and
1758 regeneration after partial hepatectomy in a rat model. *Surgery today* 41, 1622–1629. doi:10.1007/
1759 s00595-010-4484-9
- 1760 Yzet, T., Bouzerar, R., Baledent, O., Renard, C., Lumbala, D. M., Nguyen-Khac, E., et al. (2010).
1761 Dynamic measurements of total hepatic blood flow with Phase Contrast MRI. *Eur J Radiol* 73, 119–124.
1762 doi:10.1016/j.ejrad.2008.09.032
- 1763 Zhang, Y. N., Fowler, K. J., Hamilton, G., Cui, J. Y., Sy, E. Z., Balanay, M., et al. (2018). Liver
1764 fat imaging-a clinical overview of ultrasound, CT, and MR imaging. *Br J Radiol* 91, 20170959.
1765 doi:10.1259/bjr.20170959

- 1766 Zhao, Y., Chen, E., Huang, K., Xie, Z., Zhang, S., Wu, D., et al. (2020). Dynamic alterations of plasma
1767 metabolites in the progression of liver regeneration after partial hepatectomy. *Journal of proteome*
1768 *research* 19, 174–185. doi:10.1021/acs.jproteome.9b00493
- 1769 Zhuang, Z.-G., Xu, J.-R., Qian, L.-J., Xia, Q., and Chi, J.-C. (2012). Computed tomography perfusion
1770 study of hemodynamic changes and portal hyperperfusion in a rabbit model of small-for-size liver.
1771 *Hepatobiliary Pancreat Dis Int* 11, 74–80. doi:10.1016/s1499-3872(11)60128-8